

# Supramolecular Mimics of Heme-Protein Binding Sites

Roberto Fiammengo

2002

Ph.D. thesis  
University of Twente



Twente University Press

Also available in print:

<http://www.tup.utwente.nl/catalogue/book/index.jsp?isbn=9036518040>

**SUPRAMOLECULAR MIMICS OF HEME-PROTEIN  
BINDING SITES**



This work was supported by the Netherlands Research Council for Chemical Sciences (CW) with financial aid from the Technology Foundation STW, project nr. 349-3985.



Twente University Press

**Publisher:**

Twente University Press, P.O. Box 217, 7500AE Enschede, the Netherlands

[www.tup.utwente.nl](http://www.tup.utwente.nl)

Print: Ocè Facility Services, Enschede

© R. Fiammengo, Enschede, 2002

No part of this work may be reproduced by print, photocopy or any other means without the permission in writing from the publisher.

ISBN 9036518040

# **SUPRAMOLECULAR MIMICS OF HEME-PROTEIN BINDING SITES**

PROEFSCHRIFT

ter verkrijging van  
de graad van doctor aan de Universiteit Twente,  
op gezag van de rector magnificus,  
prof. dr. F. A. van Vught,  
volgens besluit van het College voor Promoties  
in het openbaar te verdedigen  
op vrijdag 27 september 2002 te 13.15 uur.

door

Roberto Fiammengo

geboren op 19 september 1971  
te Torino, Italië

Dit proefschrift is goedgekeurd door:

Promotor: Prof. dr. ir. D. N. Reinhoudt

assistent-promotor: Dr. M. Crego Calama

*Ai miei genitori*



# Table of contents

## CHAPTER 1

<b>GENERAL INTRODUCTION</b>	<b>1</b>
-----------------------------	----------

## CHAPTER 2

<b>SYNTHETIC SELF-ASSEMBLED MODELS WITH BIOMIMETIC FUNCTIONS</b>	<b>7</b>
--	----------

2.1 Introduction	7
2.2 Electron and energy transfer processes	8
2.2.1 Photosynthesis	9
2.2.2 Aspecific models for electron transfer processes	15
2.2.3 Cytochrome and redox cofactor activity mimics	17
2.3 Catalysis and enzyme mimics	18
2.4 Allosterism	21
2.5 Membrane Transport	22
2.6 Artificial Molecular Machines	24
2.7 Synthetic models for hemoglobin (Hb) and myoglobin (Mb)	26
2.7.1 Hemoglobin and myoglobin: cooperativity in O <sub>2</sub> -binding makes the difference	26
2.7.2 Synthetic models: stability and understanding of the O <sub>2</sub> adduct	29
2.7.3 Synthetic systems having Co <sup>II</sup> in the active site: the stability issue	34
2.8 Concluding remarks	35
2.9 References and notes	36

## CHAPTER 3

<b>NONCOVALENT SYNTHESIS OF CALIX[4]ARENE-CAPPED PORPHYRINS IN POLAR SOLVENTS VIA IONIC INTERACTIONS</b>	<b>43</b>
--	-----------

3.1 Introduction	43
3.2 Results and discussion	45
3.2.1 Synthesis	45
3.2.2 Self-assembly Studies	46
3.2.3 Ligand Binding Studies	56
3.3 Summary and Outlook	59
3.4 Experimental	59
3.4.1 General information and instrumentation	59
3.4.2 Binding studies	60



3.4.3 Synthesis	60
3.5 References	63
<b>CHAPTER 4</b>	
<b>STRUCTURAL WATER SOLUBLE MODELS OF THE HEME-PROTEIN ACTIVE SITE</b>	
<b>VIA SELF-ASSEMBLY</b>	<b>67</b>
4.1 Introduction	67
4.2 Results and discussion	70
4.2.1 Synthesis	70
4.2.2 Assembly formation	70
4.2.3 Selective binding of nitrogenous ligands <sup>32</sup>	75
4.3 Conclusions	79
4.4 Experimental part	80
4.4.1 General information and instrumentation	80
4.4.2 Binding studies	80
4.5 References and notes	81
<b>APPENDIX</b>	<b>88</b>
<b>CHAPTER 5</b>	
<b>TOWARDS WATER SOLUBLE FUNCTIONAL MODELS OF O<sub>2</sub> BINDING HEME-PROTEINS</b>	
<b>VIA SELF-ASSEMBLY</b>	<b>91</b>
5.1 Introduction	91
5.2 Results and discussion	92
5.2.1 Synthesis	92
5.2.2 Assembly formation	92
5.2.3 O <sub>2</sub> binding	93
5.2.4 Facilitated O <sub>2</sub> transport across supported liquid membranes	100
5.3 Conclusions	101
5.4 Experimental part	102
5.5 References and notes	103
<b>CHAPTER 6</b>	
<b>NONCOVALENT SECONDARY INTERACTIONS IN CO(II)SALEN COMPLEXES:</b>	
<b>O<sub>2</sub> BINDING AND CATALYTIC ACTIVITY IN CYCLOHEXENE OXYGENATION</b>	<b>107</b>
6.1 Introduction	107
6.2 Results and discussion	109

6.3	Conclusions	116
6.4	Experimental part	116
6.5	References and notes	121
<b>CHAPTER 7</b>		
<b>RECOGNITION OF CAFFEINE IN AQUEOUS SOLUTIONS</b>		<b>125</b>
7.1	Introduction	125
7.2	Results and discussion	127
7.2.1	Synthesis.	127
7.2.2	Caffeine binding studies	127
7.2.3	Selectivity towards other ligands structurally related to caffeine	136
7.3	Conclusions and outlook	139
7.4	Experimental part	140
7.4.1	General information and instrumentation	140
7.4.2	Buffers	140
7.4.3	Binding studies	140
7.4.4	Synthesis	142
7.5	References and notes	145
<b>SUMMARY</b>		<b>151</b>
<b>SAMENVATTING</b>		<b>155</b>
<b>ACKNOWLEDGEMENTS</b>		<b>159</b>
<b>THE AUTHOR</b>		<b>163</b>



# Chapter 1

## GENERAL INTRODUCTION

What does “supramolecular chemistry” mean currently? And what is the impact of this relatively recent field of science on the chemical community compared to more traditional fields such as organic or inorganic chemistry? These and several other closely related questions were addressed in March 2002 in a special issue of the renowned international journal *Science*.\*

The term Supramolecular Chemistry was coined by Jean-Marie Lehn, who was awarded the 1987 Nobel Prize in Chemistry together with Donald Cram and Charles Pederson. His definition of “chemistry beyond the molecule” implied a direct interest towards noncovalent interactions between molecules.<sup>1</sup> It also introduced a new way of thinking about interactions that had previously been studied in the fields of coordination chemistry and biochemistry. As a matter of fact, chemists, possessing already more than 150 years of experience with noncovalent interactions between molecules, have started to use these interactions as tools for the construction of functional systems.

However, Reinhoudt and Crego-Calama have recently defined a supramolecular system or a supramolecule as “a collection of atoms held together by covalent and noncovalent bonds”<sup>2</sup> stressing that covalent and noncovalent synthesis must be efficiently integrated in order to obtain specific connectivity between atoms. This is an approach that Nature has exploited for billions of years!

The first field of application for supramolecular chemistry was the creation of synthetic receptors and molecular recognition systems.<sup>3,4</sup> The high selectivity expressed by some

---

\* “Supramolecular chemistry and self-assembly” in *Science* **2002**, 295, 2395-2421.

crown ether based receptors towards  $\text{Na}^+$  and  $\text{K}^+$  (rivaling the selectivity of the natural antibiotic valinomycin) serves as an example of the level of control that has been achieved.<sup>5</sup>

Soon after the introduction of supramolecular chemistry another term became frequently used: self-assembly. According to Whitesides, self-assembly is not a formalized subject and the term has been often overused.<sup>6</sup> In principle, the definition of self-assembly refers only to reversible processes that involve pre-existing components (separate or distinct parts of a disordered structure), which can be controlled by proper design of the components. The author believes that the attraction that humans have for “the appearance of order from disorder” is one of the reasons for the attention that the self-assembly concept generates. Despite the very philosophical nature of this statement, the true scientific reasons remain also of very fundamental importance and concern, such as the understanding of the emergence of life from a system of chemical reactions.

Furthermore, scientists are also very practical and have devoted their attention to the possibility of building complex structures in a designed way in order to perform a particular function.

In the context of supramolecular chemistry, functional devices are all those entities able to perform actions such as energy, electron, and ion exchange (or transfer),<sup>7,8</sup> and even mechanical motion.<sup>9</sup> Currently, the fabrication of molecular electronic systems is the application field that perhaps attracts more consideration. In 2001, the first molecular-scale logic and memory circuits were achieved by several research groups. This great accomplishment has earned them *Science's Breakthrough of the Year*.<sup>10</sup>

Besides the technological applications of self-assembled molecular devices there are other motivations for the interest in this field. Self-assembly processes are omnipresent in the biological world. One major advantage lent by self-assembly is the possibility of having repair mechanisms that are normally impossible for systems created solely by covalent synthesis. Furthermore, it is the most economical way to obtain highly structured systems with specific functions. In fact, from quite a limited number of building blocks (such as the four DNA nucleotides or the twenty natural amino acids), Nature is able to assemble an almost infinite number of complex structures having the desired biological roles. Some remarkable examples are the transfer and storage of

genetic information in nucleic acids, the formation of cell membranes and the metabolic activity of some enzymes.

However, considering the implementation of biomimetic functions into synthetic systems, it should be emphasized that the most common approach to the problem has been via covalent chemistry. The preparation of oxygenation catalysts (mimics of cytochrome P450)<sup>11</sup> and more generally of functional analogues of heme protein active sites,<sup>12</sup> illustrate well the degree of sophistication reached using covalent models. Only recently has the Nature-inspired self-assembly approach gained more credit.<sup>13</sup> Nevertheless, many biological functions have not yet been targeted in synthetic systems via self-assembly. For instance, surprisingly there are no reports about synthetic model systems for O<sub>2</sub> binding heme proteins based on self-assembly.

The main focus of this thesis is aimed at the preparation of simple self-assembled mimics of O<sub>2</sub> binding heme protein active sites. Moreover, we have considered as a major target the development of a model system that could be used in aqueous solution. The two main reasons for this choice are that water is the most biologically relevant solvent, and the possible use of these synthetic O<sub>2</sub> carriers for biomedical applications (i.e. production of O<sub>2</sub>-enriched air for patients that suffer from shortness of breath).

Chapter 2 reviews the most recent efforts in the field of self-assembled systems with biomimetic functions (sections 2.2 – 2.6). There are contributions spanning from the mimicry of photosynthetic systems to the preparation of artificial molecular machines. Section 2.7 summarizes the most important biological aspects connected to the field of O<sub>2</sub> carriers and gives an overview of synthetic models obtained via classical covalent synthesis.

Chapters 3 and 4 describe the results of designing and studying a self-assembly system based on cationic porphyrins and anionic calix[4]arenes, both in polar organic solvents and in aqueous solutions.

Chapter 5 deals with the O<sub>2</sub> binding properties and the stability of these self-assembled systems.

The work described in Chapters 6 and 7 is not strictly based on self-assembled systems but shares with the preceding work the strategic use of noncovalent interactions which

have been applied in the design of salen based O<sub>2</sub> carriers or porphyrin based caffeine receptors.

Chapter 6 describes the use of noncovalent interactions viz. hydrogen bonds, to induce stabilization of the O<sub>2</sub> adducts of Co<sup>II</sup>-salen complexes. Simple variations in the structure of the complexes afford O<sub>2</sub> adducts of different stability that have been used in the development of a novel method (based on the observation of catalytic activity in the oxygenation reaction of cyclohexene) for testing their robustness.

Chapter 7 reports the combination of several noncovalent interactions, like hydrophobic interactions, stacking, and metal coordination, for the design of the first water soluble synthetic receptor for caffeine (a natural constituent of tea, coffee, guarana paste, cola nuts, and cacao beans).

## References

1. Lehn, J.-M. *Angew. Chem. Int. Ed. Engl.* **1988**, *27*, 89-112.
2. Reinhoudt, D. N.; Crego-Calama, M. *Science* **2002**, *295*, 2403-2407.
3. Lehn, J.-M. *Supramolecular Chemistry: Concepts and Perspectives.*; VCH: Weinheim, Germany, 1995.
4. *Comprehensive Supramolecular Chemistry*; Atwood, J. L.; Davies, J. E. D.; MacNicol, D. D.; Vögtle, F., Eds; Pergamon: Oxford, 1996.
5. Ungaro, R.; Arduini, A.; Casnati, A.; Pochini, A.; Ugozzoli, F. *Pure Appl. Chem.* **1996**, *68*, 1213-1218.
6. Whitesides, G. M.; Grzybowski, B. *Science* **2002**, *295*, 2418-2421.
7. Balzani, V.; Scandola, F. *Supramolecular Photochemistry*; Ellis Horwood: Chichester, UK, 1991.
8. Gokel, G. W.; Mukhopadhyay, A. *Chem. Soc. Rev.* **2001**, *30*, 274-286.
9. Balzani, V.; Credi, A.; Raymo, F. M.; Stoddart, F. J. *Angew. Chem. Int. Ed.* **2000**,

- 39, 3348-3391.
10. Service, R. F. *Science* **2001**, *294*, 2442-2443.
  11. Feiters, M. C.; Rowan, A. E.; Nolte, R. J. M. *Chem. Soc. Rev.* **2000**, *29*, 375-384.
  12. Collman, J. P. *Inorg. Chem.* **1997**, *36*, 5145-5155.
  13. Fiammengo, R.; Crego-Calama, M.; Reinhoudt, D. N. *Curr. Opin. Chem. Biol.* **2001**, *5*, 660-673.





### **SYNTHETIC SELF-ASSEMBLED MODELS WITH BIOMIMETIC FUNCTIONS\***

*Synthetic systems prepared via self-assembly are becoming more frequently studied in the field of biomimetic models. The implementation of biomimetic functions in these systems may help to clarify natural processes and result in technological applications such as artificial photosynthetic systems for solar energy collection. The first part of this chapter is focused on self-assembled model systems (obtained from synthetic subunits) with biomimetic function that have appeared in the literature since 1996. The second part of the chapter focuses on O<sub>2</sub> binding heme proteins, which is the target function of the biomimetic self-assembly strategy outlined in the following Chapters. Porphyrin based O<sub>2</sub> carriers are mainly considered.*

#### **2.1 Introduction**

Self-assembly processes are of paramount importance in biology. Nature uses self-assembly to build up highly structured systems with specific functions. Astonishing examples of this strategy are the transfer and storage of genetic information in nucleic acids, the conversion of solar energy into biochemical energy by the photosynthetic reaction center of plants and bacteria and the organization of proteins into efficient molecular machines (DNA polymerase III holoenzyme).<sup>1</sup> Complexity in biological systems is required to promote energetically demanding processes under physiological

---

\* Part of this chapter has been published as review: Fiammengo R., Crego-Calama M., Reinhoudt, D. N. *Curr. Opin. Chem. Biol.* **2001**, 5, 660-673.

conditions. Self-assembly is the key to arrive at such systems in the most economic and reliable way, minimizing the occurrence of errors and/or correcting them.

The use of self-assembly in synthetic model systems is thus a very powerful tool to uncover some of the basic principles of the biological world. A better understanding of the principles behind functioning natural systems provides also a strong motivation for research towards possible technological applications in material science or in molecular electronics. All of these applications that require rather large functional molecular systems (nanodevices) are expected to benefit greatly from advances in the field of nanotechnology.

Only examples in which the self-assembly process takes place in solution are relevant for the experimental work described in the following chapters. Moreover, in agreement with the aim of this thesis, systems that mimic only the structural features of natural systems but not their activity (protein folding, membrane and bilayer formation, molecular recognition) are not reviewed.

In sections 2.2-2.6 are described examples of electron and energy transfer processes, enzyme mimics, allosteric systems, and artificial molecular machines implementing self-assembly as the key feature. In section 2.7 the attention is focused on synthetic models for hemoglobin and myoglobin, two O<sub>2</sub> binding heme proteins. Surprisingly there are no examples reported so far of biomimetic O<sub>2</sub> binders and transporters obtained via self-assembly.

## **2.2 Electron and energy transfer processes**

Much attention has been devoted to the mimicry and understanding of electron transfer processes since they occur in a wide variety of biological systems. The efforts of the scientific community have been mainly focused on photosynthetic systems and on electron carriers such as cytochromes. The self-assembly approach has also been used to study models for redox cofactor activity.

### 2.2.1 Photosynthesis

One of the most impressive series of chemical reactions that takes place in nature is the conversion of water and carbon dioxide into carbohydrates using sunlight energy. Biological light-harvesting systems such as photosystem I and II mediate this chain of events: solar energy is absorbed by natural pigments (chromophoric units) and efficiently transformed into chemical energy. Since the structural elucidation of Photosystem I and II, the importance of the spatial arrangement of different chromophoric units in the so-called light-harvesting system of the photosynthetic center has been recognized. For instance, an intact Photosystem II complex in green plants contains up to 200 chlorophyll molecules, absorbing and transferring the energy coming from sunlight. Green photosynthetic bacteria also display large aggregates of chromophoric units (bacteriochlorophylls-*c*, *d*, *e*) not supported by any protein. Therefore many model systems consist of multiporphyrin systems (more general tetrapyrrole macrocycles) or arrays in which the chromophoric units are placed in a predefined spatial arrangement and are able to undergo photoinduced electron and energy transfer.

One of the most used approaches to the mimicry of the light-harvesting system of bacteria is to synthesize porphyrin arrays by metal coordination chemistry. A very detailed review on the construction of multiporphyrin systems using metal coordination interactions covers most of the literature through 1999.<sup>2</sup> The research in this field is still very active and some interesting papers that appeared after this date are discussed. Hunter and coworkers have used coordination chemistry to build relatively large light-harvesting complexes making use of pyridine coordination to metal porphyrins. The formation of a stable pentameric assembly constituted of one free-base porphyrin **H<sub>2</sub>P** (bearing four pyridyl groups) with two molecules of a covalently linked Zn porphyrin dimer **Zn<sub>2</sub>PD** was reported.<sup>3</sup> The process is highly cooperative and gives rise to a well-defined three dimensional structure. The two **Zn<sub>2</sub>PD** molecules act as antennas and efficiently transfer energy to **H<sub>2</sub>P**. The same concept of cooperativity operates for the construction of an unusually stable complex with approximately 12 Co<sup>II</sup>-porphyrin units.<sup>4</sup> In a third example a shape persistent cyclic array of six zinc porphyrins (*cyclo*-Zn<sub>6</sub>U) was used to study the energy transfer process between porphyrins which differ only slightly in energy. In fact it was possible to show quantitative energy transfer from uncoordinated zinc porphyrins to

the pyridyl coordinated zinc porphyrins.<sup>5</sup> Other groups have also used the interaction between pyridyl moieties and zinc porphyrins for the preparation of photoactive complexes. In particular, using picosecond time-resolved transient absorption spectroscopy it was shown that intramolecular photoinduced charge separation and recombination occur in a system constituted of two covalently linked zinc porphyrins and a pyromellitimide acceptor.<sup>6</sup>

Very recently the first example of axial coordination of pyridyl porphyrins to zinc phthalocyanines in edge-to-face arrays has been reported.<sup>7</sup> The system has been characterized using <sup>1</sup>H NMR, UV and fluorescence spectroscopy. Photoinduced electron transfer has been deduced from the fluorescence quenching of the tetrapyrrolyl porphyrin as a function of the zinc phthalocyanine concentration. Moreover, it was possible to show that an energy transfer pathway was not operative in the system since no phthalocyanine emission was detected upon porphyrin excitation. The self-assembly strategy involving metal coordination has been used to promote self-organization in a flexible photoactive Zn-porphyrin/fullerene/Zn-porphyrin triad.<sup>8</sup> Addition of DABCO to a solution of the triad brings the two Zn porphyrins in a cofacial position and converts the system into a more rigid tetrad that undergoes efficient energy and electron transfer. Considerably longer charge-separated states were observed for the system upon photoexcitation.

Other interesting cyclic tetrapyrroles have been considered for the construction of self-assembled systems via coordination chemistry. A closer mimic of natural light-harvesting complexes involves the use of metallated chlorins as synthetic models for naturally occurring bacteriochlorophylls;<sup>9</sup> this will not be discussed here.<sup>10</sup>

Besides coordination chemistry to build up porphyrin arrays, other groups have used hydrogen bonding interactions. Via a mix of coordination chemistry and hydrogen bonding a nonameric porphyrin assembly was built. Energy transfer from eight zinc porphyrins to a central free-base porphyrin was observed with 82% efficiency.<sup>11</sup> In 1996 DeGrado and coworkers reported the preparation of a photosynthetic reaction center maquette.<sup>12</sup> Self-assembly of two homodi- $\alpha$ -helical peptides in a four helix bundle structure brings two appended coproporphyrin I units together in a cofacial arrangement (Figure 1a). The system is supposed to mimic the reaction center protein from the

bacterium *Rhodospseudomonas viridis* containing the well-known chlorophyll special pair. Very preliminary results were reported about the photophysical behavior of the system. More recently, the group of Nolte has also been inspired by the same photosynthetic reaction center.<sup>13</sup> In a very elegant communication they reported the effect of an aromatic guest, complexed between donor and acceptor moieties. The relevance of this work is that they attempted to mimic the function of the aromatic ring of a tryptophan residue that is in close proximity to both the bacteriochlorophyll primary acceptor and the quinone to which, in the natural system, photoinduced electron transfer takes place. A diphenylglycoluril building block was used to spatially arrange a zinc porphyrin and a quinone moiety (Figure 1b). At the same time the molecule was shown to be a receptor (molecular clip) for a dihydroxybenzene derivative which is then localized between the porphyrin and the quinone. Enhanced electron transfer between these two parts of the molecule due to the presence of the aromatic guest molecule was observed.

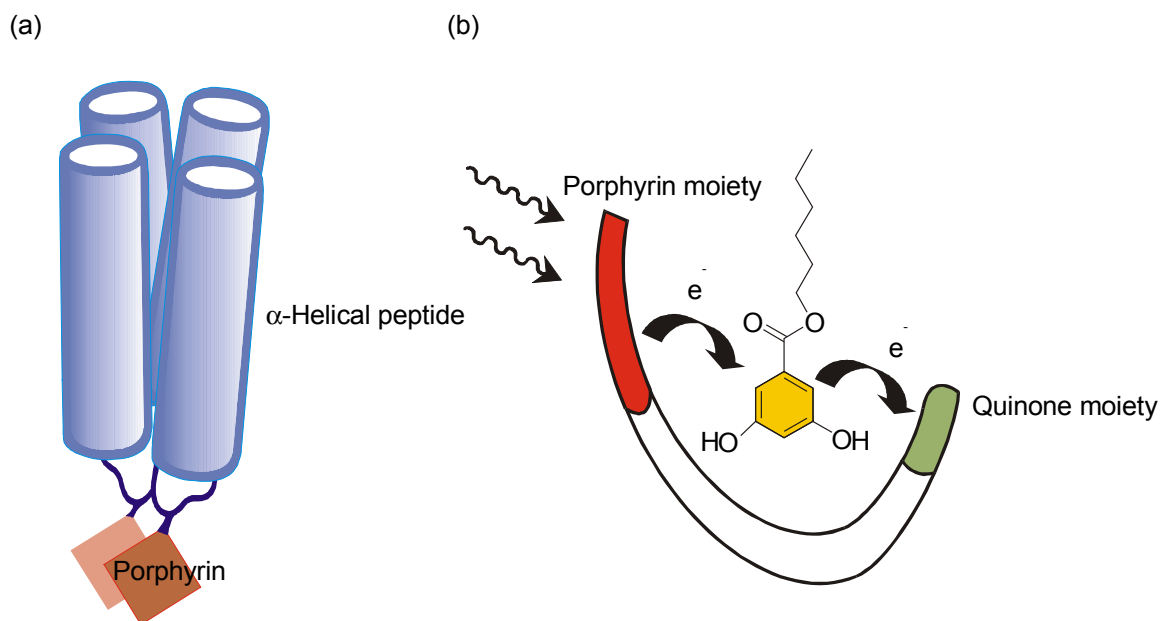


**Figure 1.** a) Self-assembly of two homodi- $\alpha$ -helical peptides in a four helix bundle structure brings two coproporphyrin I in cofacial arrangement. b) Nolte's molecular clip system. 3,5-dihydroxybenzoates are recognized and mediate the photoinduced electron transfer between the porphyrin and the quinone moieties.

Quadruple hydrogen bond motifs involving diacetamidopyridyl groups in the *meso* position of a porphyrin are effective for the formation of arrays.<sup>14</sup> The geometry of the

arrays is ultimately determined by the substitution pattern on the porphyrin, thus allowing the formation of linear tapes as well as cyclic tetramers. Sessler and coworkers reported the formation of a porphyrin-sapphyrin self-assembled complex.<sup>15</sup> Sapphyrins, pentapyrrolic “expanded porphyrin” macrocycles, are known to be excellent receptors for a variety of anions. This property has been exploited for the formation of an assembly with a porphyrin bearing a carboxylic acid group. The system was studied by <sup>1</sup>H NMR in order to prove the formation of the complex. UV and NMR experiments as well as X-ray crystallographic evidence on model compounds showed that the two chromophores are likely to be oriented perpendicular to each other. Nonetheless the system was shown to undergo fast excitation transfer with high efficiency (the sapphyrin being the low lying energy partner in the ensemble).

Another interesting aspect of photosynthetic systems that has attracted the attention of the scientific community is the chain of events occurring after a photon has been absorbed by the light-harvesting system, causing a photoinduced electron transfer. The charge separation caused by the photon absorption needs to be stabilized efficiently and quickly to allow conversion of the electromagnetic energy into chemical energy. In particular it is interesting to focus attention on the so-called donor side in the chain of events happening at Photosystem II. The photooxidized form of chlorophyll (formed upon electron transfer) is regenerated with electrons coming from the catalyzed oxidation of water to oxygen involving a redox active amino acid (named tyrosine<sub>Z</sub>) and a manganese cluster formed by four high-valent Mn ions. A very recent excellent review<sup>16</sup> summarizes the efforts of Åkermark and Styring in this field which is also of paramount importance for practical applications such as the conversion of solar energy into fuels (hydrogen). Their work focuses on the use of ruthenium-manganese complexes. The basic idea was to use Ru<sup>II</sup> tris-bipyridine as a substitute for chlorophyll and to show that in dinuclear Mn<sup>II</sup> – Ru<sup>II</sup> systems it is possible to have electron transfer from the Mn<sup>II</sup> moiety to the photogenerated Ru<sup>III</sup> species.

A more sophisticated mimic<sup>17</sup> involves the use of a phenolic moiety (covalently attached to one of the Ru<sup>II</sup> bipyridine ligands) that acts like the Tyr<sub>Z</sub> residue (Figure 2a). In particular, upon flash photolysis in acetonitrile or aqueous solution containing methylviologen (MV<sup>2+</sup>) as an electron acceptor, electron transfer from the phenolic

substituent to the photogenerated  $\text{Ru}^{\text{III}}$  occurs. The process is very fast ( $k_{\text{ET}} > 10^7 \text{ s}^{-1}$ ) in the system containing two dipicolylamine arms that are hydrogen bonded to the phenolic hydroxyl group. The importance of the hydrogen bonding network was clearly demonstrated by comparison with systems that lack this structural element. It is known that in the natural reaction center  $\text{Tyr}_Z$  is hydrogen bonded to  $\text{His}_{190}$ . EPR experiments performed in water during flash photolysis showed the formation of a neutral phenoxyl radical in close resemblance to what is known to happen in nature to the  $\text{Tyr}_Z$  residue.

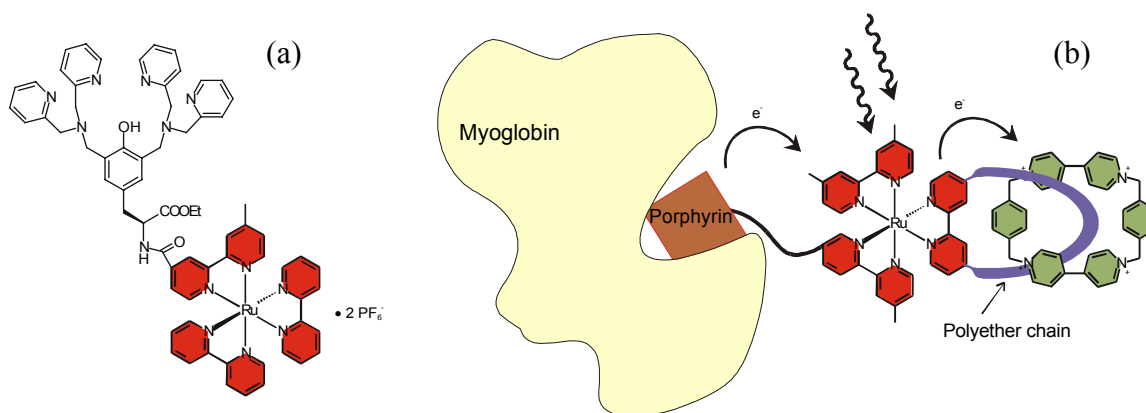


**Figure 2.** a) The  $\text{Ru}^{\text{II}}$  tris-bipyridine complex with an appended Tyr residue (chemically modified to introduce hydrogen bonding to the phenol group), mimicking the activity of the  $\text{Tyr}_Z$  residue in the so-called donor side of Photosystem II. b) The semisynthetic approach for the mimic of the photosynthetic reaction center.

In a related system Shinkai and coworkers showed the potential of a semisynthetic approach for the mimic of the photosynthetic reaction center (Figure 2b).<sup>18</sup> In semisynthetic approaches, natural building blocks are manipulated and/or connected in a non-natural way to give an artificial system. This idea has been exploited to prepare myoglobin based triads containing a metal protoporphyrin (this time used as donor) located in the myoglobin pocket, a  $\text{Ru}^{\text{II}}$  tris(bipyridyl) moiety as the sensitizer, and a mechanically linked (in the form of a catenane) cyclobis(paraquat-*p*-phenylene) unit ( $\text{BXV}^{4+}$ , as the acceptor). The present case demonstrates the degree of complexity that can be achieved by the use of several different self-assembly processes. They are involved in the reconstitution of the apoprotein with the porphyrin appended triads, in the formation of the central  $\text{Ru}^{\text{II}}$  complex starting from three different ligands and in the



synthesis of the catenane type ligand. Detailed investigations of the system showed the expected vectorial, stepwise electron transfer giving rise to a long-lived charge separated state, a chain of events that is known to operate in the natural photosynthetic reaction center.

Another system based  $\text{Ru}^{\text{II}}\text{tris}(\text{bpy})_3$  photosensitizer and  $\text{BXV}^{4+}$  acceptor should be mentioned here.<sup>19</sup> The well-known  $\pi$ -donor-acceptor complexes between *N,N'*-dialkylbipyridinium salts and electron rich aromatic compounds such as dialkoxybenzenes were used as the key feature for the noncovalent spatial organization of the  $\text{MXV}^{4+}$  acceptor around the  $\text{Ru}^{\text{II}}$  center. Modified bpy ligands bearing one to two dialkoxybenzene moieties were used to prepare dyads and polyads in a pseudorotaxane fashion. Photophysical analysis of the system revealed that the electron transfer process occurred in two distinct populations of the photosensitizer, viz. in the supramolecular assembly and in the free photosensitizer.

One important consideration when attempting to gain valuable information about the photosynthetic reaction center is that the size of a proposed model system should be comparable to that of the natural system. For the investigation of large model systems, dendrimers (hyperbranched, synthetic macromolecules with well-defined three-dimensional structures) are ideal prototypes. Their inherent characteristics and structural simplicity allow them to act as a bridge between the world of small molecular mimics and of large and complex natural systems.<sup>20</sup>

The first of such systems is based on PAMAM (polyamidoamine) dendrimers with 20-residue  $\alpha$ -helical peptides covalently linked to the peripheral amino groups.<sup>21</sup> Different dendrimer generations (up to generation 4, G4) were synthesized and studied. The molecular weight for the G4 dendrimer having 64 peptides linked to the PAMAM scaffold is around 160 kD, remarkably high for a synthetic system. The peptides contain one His residue in position 10 along the sequence. The authors showed that  $\text{Fe}^{\text{III}}$ - or  $\text{Zn}^{\text{II}}$ -mesoporphyrin IX are complexed by the dendrimer, with each porphyrin coordinated between two  $\alpha$ -helical peptidic strands giving rise to a multiporphyrin array (the systems are indicated as Fe-MP and Zn-MP respectively, Figure 3). Fluorescence studies in solution showed photoinduced electron transfer from the porphyrin to methylviologen ( $\text{MV}^{2+}$ ). More interestingly the system was shown to function effectively as an artificial

photosynthetic system. A solution containing triethanolamine as an electron donor, Zn-MP as photosensitizer and  $MV^{2+}$  as electron acceptor was used to demonstrate the production and accumulation of  $MV^+$  radicals upon photoirradiation. This result confirmed that the three dimensional array of porphyrins, prepared by self-assembly with the use of suitable peptide dendrimers, is an effective photosensitizer in the above mentioned artificial photosynthetic system.

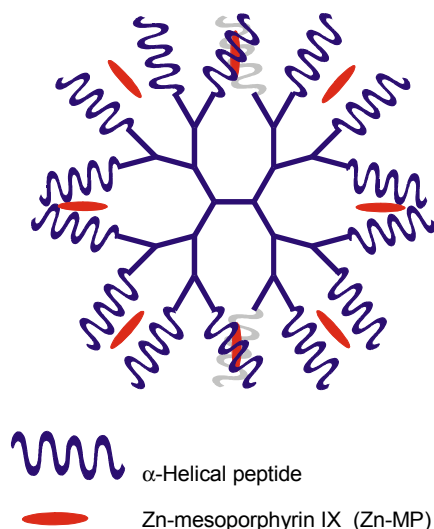


**Figure 3.** Light harvesting dendrimers.

### 2.2.2 *Aspecific models for electron transfer processes*

The focus of the following examples is not directly on the mimicry of the photosynthetic reaction center as discussed previously, but is somewhat more general in trying to understand some of the basic features of the electron transfer process itself. Metallodendrimers have been reported as suitable candidates to mimic natural light-harvesting systems and have been extensively studied and recently reviewed by Balzani and coworkers.<sup>22</sup> The strategy to build large polynuclear metal complexes is called by the authors “complexes as metals/ complexes as ligands”. The function of the systems is due to the intrinsic and specific properties of the building blocks (ability to undergo visible light absorption, luminescence, and reversible multi-electron processes).

Fréchet and coworkers used a different type of chromophore as an antenna.<sup>23</sup> Polybenzylether dendrons bearing a carboxylic acid functionality at the focal point (up to generation 4) are light-harvesting units that can be self-assembled around lanthanide

cations. The stoichiometry of the complexes is three dendritic wedges per cation. Studies on the system showed both an antenna effect that allows the energy transfer from the dendritic ligands to the central ion, and a shell effect leading to a decreased self-quenching of lanthanide fluorescence. Despite the very interesting properties of dendritic systems, their synthesis can be very demanding even if self-assembly is involved. Interestingly, more easily accessible linear light-harvesting polymers can be prepared following indications obtained from a dendritic model system.<sup>24</sup> Copolymerization of a  $\text{Ru}^{\text{II}}(\text{bpy})_3$  functionalized monomer with a coumarin-2 functionalized monomer in a 1:3 ratio afforded a polymer that exhibited quantitative energy transfer from the coumarin-2 units to the  $\text{Ru}^{\text{II}}$  centers.

In naturally occurring electron transfer processes (both thermal and photoinduced), hydrogen bonds and ionic interactions within the protein matrix play a very important role. Some model systems have tried to quantify the importance of these interactions. Sessler and coworkers used hydrogen bonds to mediate photoinduced electron transfer in a dimethylaniline-anthracene ensemble.<sup>25</sup> The ensemble was prepared via Watson-Crick base pairing principles (Figure 4a). The donor and the acceptor moieties were attached alternatively to one or the other base that participates in the recognition motif. This approach provides two different diads that behave very differently upon photoexcitation. Despite the fact that the reason for such different behavior was not understood, the interesting conclusion is that not only is the nature of the interaction mediating the long range electron transfer important (in this case hydrogen bonds), but also the directionality.

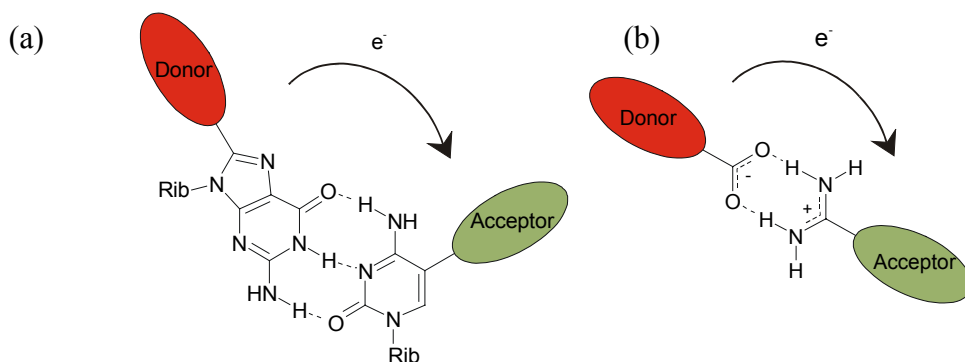


**Figure 4.** Asymmetric self-assembled donor-acceptor interfaces based on a) Watson-Crick base pairing principles, b) carboxylate-amidinium salt bridge.

Similar conclusions were reached for electron transfer processes mediated by salt bridges.<sup>26</sup> Amidinium-carboxylate interactions were used as an asymmetric salt bridge interface (Figure 4b) relevant for the understanding of naturally occurring proton-coupled electron transfer processes. The rate of photoinduced electron transfer through the donor-(amidinium-carboxylate)-acceptor salt bridge was 100 times slower than when the interface was inverted to donor-(carboxylate-amidinium)-acceptor.

### **2.2.3 Cytochrome and redox cofactor activity mimics**

The two most important energy-converting processes in biology are photosynthesis and respiration. They both involve redox reactions and therefore enzymes and proteins with redox active functionalities. Some model systems dealing with electron transfer processes based on peptides have been reported and discussed in a recent review.<sup>27</sup> Very promising results have been obtained in model systems for cytochrome *b*, the membrane spanning subunit of the mitochondrial cytochrome *bc<sub>1</sub>*, and of the photosynthetic cytochrome *bf* complexes.

In this respect, some relevant features of systems reported recently by Willner and Haehnel should be mentioned. They used the design principle of template-assembled synthetic proteins in conjunction with an antiparallel four-helix bundle motif, to prepare a cytochrome *b* model.<sup>28</sup> First self-assembly was used to incorporate two Fe<sup>III</sup>-protoporphyrin IX cofactors in the synthetic apoprotein. The electron transfer unit obtained was then covalently attached to a self-assembled monolayer on a gold surface bearing proper reactive groups. A third relevant self-assembly step involved the formation of affinity complexes between a cytochrome-dependent native protein such as nitrate reductase and the de novo synthesized electron-transporting protein attached to the monolayer (Figure 5).<sup>29</sup> With the aim of preparing a robust bioelectrocatalytic electrode, the complexed nitrate reductase layer was further cross-linked. It should be mentioned that other proteins could be fixed on the de novo protein modified monolayer, opening the way to novel interesting technological applications in such fields as bioelectronic devices.<sup>30</sup>

Redox processes are not limited to cytochromes and are also present in flavin-, quinone- and pyrroloquinolinequinone-dependent enzymes. The use of model systems for the

understanding of redox cofactor activity has been the subject of a recent review.<sup>31</sup> Self-assembly processes of interest were used in two systems based on flavin<sup>32</sup> and 6-azaflavin,<sup>33</sup> respectively. These two publications focus on the role of noncovalent interactions between the redox cofactor and the apoprotein (which is mimicked by a much simpler molecular receptor) in modifying the redox properties of the system.

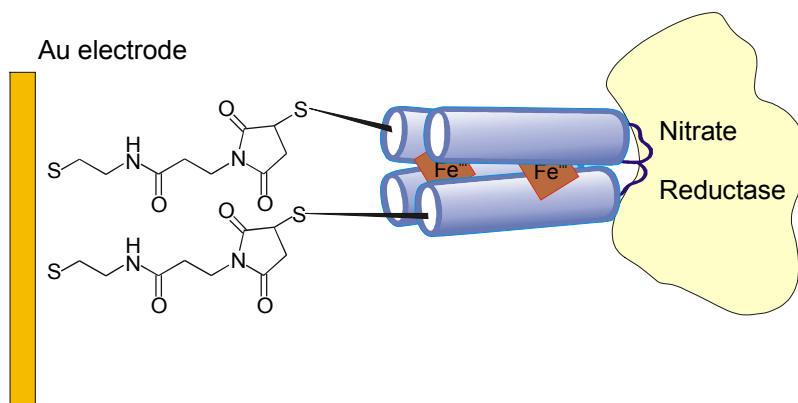


**Figure 5.** Molecular design of a bioelectrocatalytic electrode prepared via self-assembly followed by cross-linking of the nitrate reductase layer.

### 2.3 Catalysis and enzyme mimics

In biotransformations, catalysis and therefore enzymes are of fundamental importance. Model systems in this field are often called “artificial enzymes”. It is beyond the scope of this chapter to give a detailed explanation of this term and of all the implications that follow, but the interested reader is referred to an excellent review of Kirby that appeared in 1996.<sup>34</sup> The author provides a very critical analysis of enzyme model systems. One of the basic definitions for enzyme mimics is that these systems must involve an initial binding interaction between the substrate and the catalyst, thus giving rise to Michaelis-Menten kinetics. Focusing on self-assembly processes in enzyme model systems, a very broad classification based on the extent to which self-assembly is important could be made viz. self-assembly for the recognition of the substrate only or self-assembly for both the formation of the enzyme mimic and for the recognition of the substrate. The latter case is described more in detail because it exploits the complete potential of the noncovalent approach.

The group of Rebek reported the Diels-Alder reaction acceleration using self-assembled molecular capsules (Figure 6).<sup>35</sup> The system is formed upon dimerization of two molecules having a concave surface and featuring complementary patterns of hydrogen bonding sites. Complexation of the two reactants within the capsule and thus enhancement of their concentration was regarded as the reason for the increased reaction rate. One major problem common to many model systems involving reactions between two different substrates<sup>34</sup> is product inhibition and thus the lack of turnover.

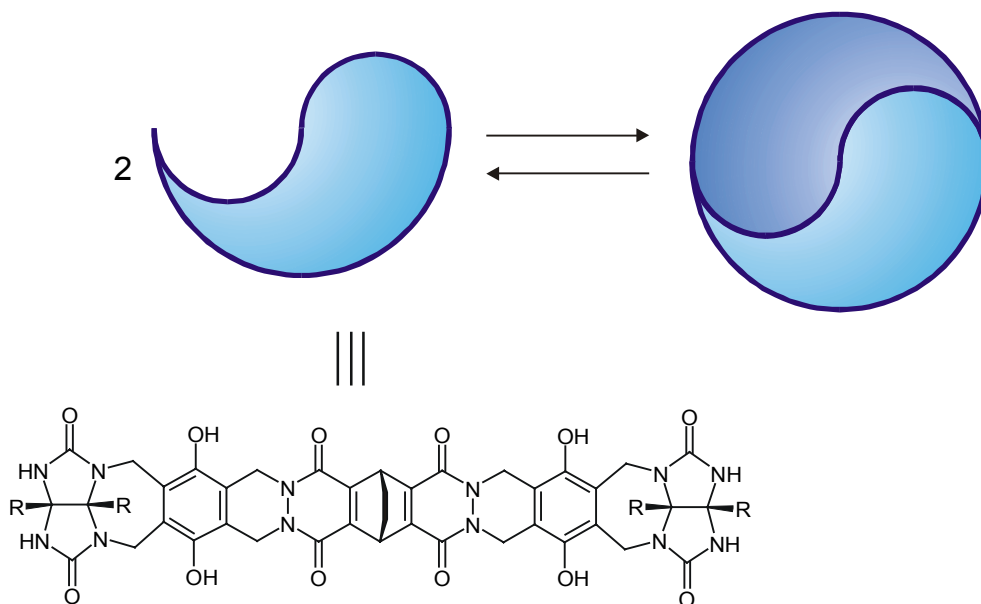


**Figure 6.** Self-assembled molecular capsules for the acceleration of Diels-Alder reactions.

A somewhat less characterized system has been reported involving the formation of peptide self-aggregates in aqueous solutions.<sup>36</sup> 16-Mer peptides containing alanine and lysine residues form very resistant macromolecular  $\beta$ -sheet structures involved in multilayer sheets or micelles. These aggregates bind nucleotides and organic phosphodiester and are effective in the hydrolysis of bis(4-nitrophenyl)phosphate. A  $10^3$ - $10^4$ -fold increase in the reaction rate was observed in the presence of the above mentioned peptide aggregates.

Hill and coworkers have addressed a very interesting aspect of natural systems viz. the ability of repairing damage.<sup>37</sup> A polyoxometalate catalyst self-assembles under the reaction conditions and this self-assembly process has been related to the catalytic

conversion of  $\alpha$ -terpinene to *p*-cymene. As a consequence, any destructive event on the catalyst can be repaired under the reaction conditions.

Mihara and coworkers designed  $\alpha$ -helical peptides able to bind a Fe-mesoporphyrin. With control of their three dimensional structure induced by the addition of trifluoroethanol, these systems have *N*-demethylase activity.<sup>38</sup> They further extended their study showing the relationship between the haem-binding properties of the designed peptides and the catalytic activity (peroxidase-like).<sup>39</sup> In particular, they were able to show that very tight haem-binding reduces the reactivity of the systems towards hydrogen peroxide in a way that resembles the natural strategy to transform a haemprotein (peroxidase-like) into an electron transfer protein (cytochrome-like) under physiological conditions.

The group of Nolte has reported a very interesting self-assembled catalyst as an enzyme mimic. This model features all the important components present in the natural cytochrome P450 system, viz. molecular oxygen as the oxidizing agent, a metalloporphyrin as the catalyst, an electron donor as the reducing agent, and a membrane system that holds all the components together.<sup>40</sup> Very detailed studies were performed to understand the effect of the nature of the bilayer and vesicular aggregates (and in particular of the charge carried by the different surfactants) on the system reactivity. A number of different substrates could be epoxidized with turnover numbers comparable to those observed for natural systems.

Finally, one catalytic system that involves self-assembly only in the recognition of the substrate should be mentioned. Ghadiri and coworkers prepared a *de novo* designed peptide ligase that catalyzes the condensation of short peptide fragments with rate acceleration as high as 4100-fold.<sup>41</sup> The catalytic activity was attributed to the efficient binding in close proximity of the two reactive peptidic fragments. Also in this case product inhibition was observed but the system represents the first example of a peptide catalyst with designed substrate binding sites able to significantly accelerate a bimolecular reaction.

Molecularly imprinted materials as enzyme mimics should also be mentioned. In these systems self-assembly is often used as the first step to create a suitable binding site, using a template molecule and functional monomers that are subsequently *covalently* fixed in a

second polymerization step. The template molecule is then washed away, leaving a material that is able to recognize desired substrates and catalyze their reaction. However, the field of molecularly imprinted materials is very broad and beyond the scope of this overview. Furthermore, molecular imprinting has been recently reviewed with regard to their applicability as enzyme models.<sup>42</sup>

## **2.4 Allosterism**

Allosterism is a form of chemical feedback found in many biological processes, i.e. cooperative dioxygen binding to hemoglobin and the hexamerization of arginine repressor. A system presenting a number of recognition sites may show allosterism if those binding sites are able to communicate upon substrate recognition. The biomimetic design of allosteric systems has been focused on the initial binding of a substrate and either the positive or negative effects (positive or negative allosterism, respectively) on subsequent binding events. The allosterism can be *heterotropic* or *homotropic*, depending on whether the second molecule is different or identical, respectively. The most prominent synthetic allosteric systems deal with *positive homotropic allosterism* and are well represented in the work of Shinkai and coworkers. They have chosen a tetrakis(4-pyridyl)porphyrin to build up a cerium(IV) bis(porphyrinate) double decker system (Figure 7).<sup>43</sup> This complex shows slow rotation of the two porphyrin planes with respect to one another at room temperature. The four pairs of 4-pyridyl groups are available as hydrogen bond acceptor sites for diols, hydroxycarboxylic acid, and dicarboxylic acid. The system displays a strong positive allosteric effect and is highly selective for BOC-aspartic acid and 1,2-cyclohexanedicarboxylic acid. The observed allosterism can be attributed to the successive suppression of the rotation of the porphyrin planes. Modification of this system with two pairs of boronic acid groups allows the cooperative recognition of two saccharide molecules in water.<sup>44</sup> The same structure can also bind oligosaccharides such as maltooligosaccharide and laminarioligosaccharide.



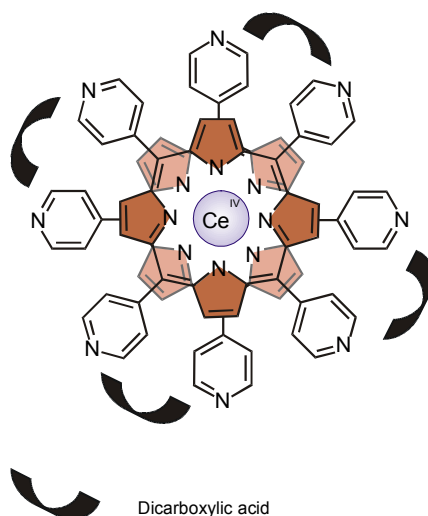


**Figure 7.** Cerium(IV) bis(porphyrinate) double-decker system showing positive allosterism upon recognition of BOC-aspartic acid and 1,2-cyclohexanedicarboxylic acid.

## 2.5 Membrane Transport

Biological membranes are crucial for biochemical transformations, intercellular contacts, organization, transport, energy transduction, and communication processes. Models of functional micelles and vesicles<sup>45</sup> and of molecular transport and organization in supported lipid membranes<sup>46</sup> have been recently reviewed. Hence, we focus on the phenomenon of chemical transport through membranes by artificial self-assembled channels. Very recently, Ghadiri and coworkers published an extensive review on nanotubular structures of molecular dimensions that perform diverse biological functions, with the emphasis on self-assembled systems.<sup>47</sup> Nevertheless, three additional examples not included in this review will be discussed.

A very interesting publication by Ghadiri and coworkers<sup>48</sup> describes a self-assembling transmembrane peptide nanotube channel, which mediated the highly efficient transport of glutamic acid. The nanotubes were formed by self-assembly via hydrogen bonds of cyclic decapeptides (7 Å van der Waals internal diameter) containing an even number of hydrophobic  $\alpha$ -amino acids with alternating *D* and *L* configuration. Amino acid transport was continuously monitored via an enzymatic assay that couples glutamine synthetase activity with the reactions catalyzed by pyruvate kinase and lactate dehydrogenase

(monitoring NADH oxidation at 340 nm). Conductance experiments were performed to assess the behavior of a single channel.

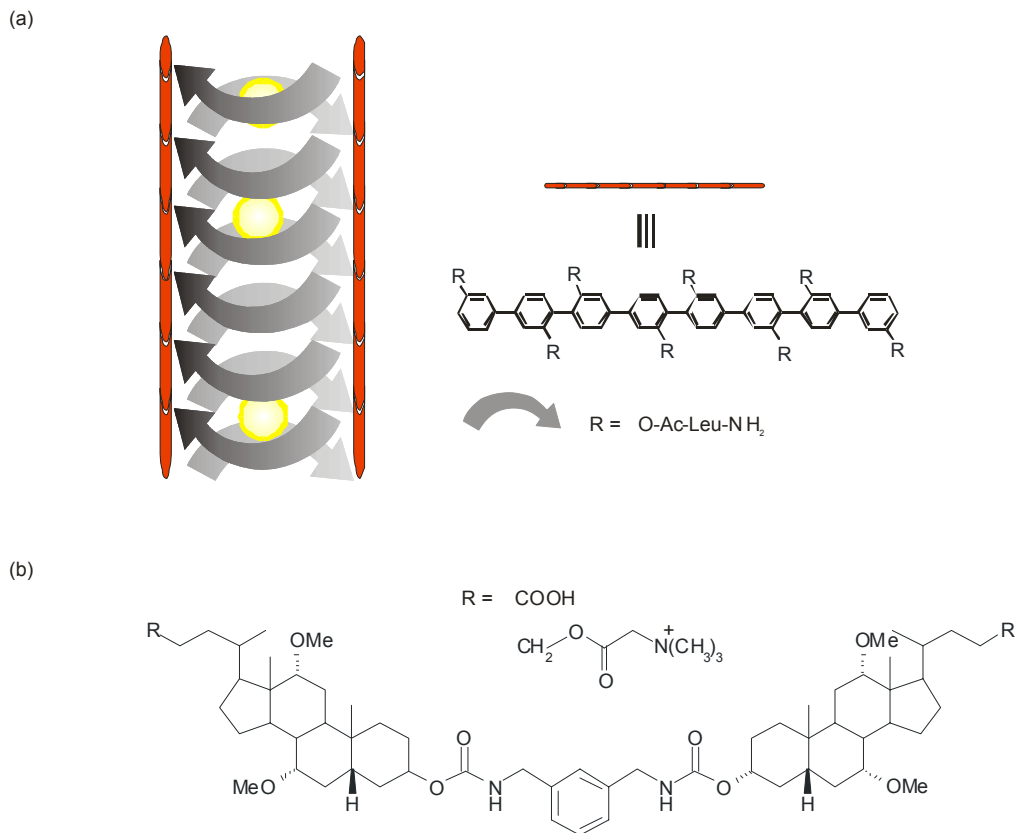


**Figure 8.** Biomimetic models of ion channel proteins. a) Octa-leucine based dimers and b) amphiphilic cholic acid derivatives with two different charged head groups (carboxylate or ammonium ions).

Dimeric rigid-rod  $\beta$ -barrels as biomimetic models of ion channel proteins were reported by Matile and coworkers.<sup>49</sup> The rigid rod octamers (octa-leucine) were prepared from octa-anisol. NMR and CD experiments provided evidence of the self-assembly by *intermolecular*  $\beta$ -sheet formation, and ESI-MS spectra strongly suggest the presence of ionophoric dimers (Figure 8a) (internal pores diameters  $>5$  Å). These structures are capable of mediating efficient ion transport across lipid bilayers.

Kokube and coworkers<sup>50</sup> prepared a new class of supramolecular transmembrane ion channels. These systems were constructed by linking two units of amphiphilic cholic acid methyl esters through bis-carbamate bonds. This moiety was then modified to yield two different structures, i.e. with a carboxylate group and an ammonium external head group, respectively (Figure 8b). Both compounds gave rise to the formation of stable ion

channels, characterized by relatively small conductances (5-20 pS) and long lasting (10 ms to 10 s) open states. The channels are able to discriminate  $K^+$  from  $Na^+$  and they exhibit high cation/anion selectivity, which is modulated by the structure of the ionic head group of the channels.

## 2.6 Artificial Molecular Machines

Natural molecular machines are extremely complicated systems rendering little chance of creating artificial molecular machines in the near future that model the natural counterparts. Nevertheless, in accordance with this far-reaching ambition, the number of discerning publications dealing with artificial molecular machines has steadily increased over the last few years. Recently, Stoddart, Balzani and coworkers have reviewed the most significant developments in the field of artificial molecular machines. The review focuses on supramolecular structures developed by *noncovalent synthesis* (pseudorotaxanes) and by *supramolecular assistance to covalent synthesis* (rotaxanes<sup>51</sup> and catenanes). Two natural molecular machines, i.e.  $F_1$ -ATPase (a rotary motor) and myosin (a linear motor) are also discussed. As the authors point out, the most interesting systems from the point of view of molecular machines are the [2]-pseudorotaxanes in which a guest molecule is threaded through the plane of a macrocycle. The reason for this is that the threading and rethreading are reminiscent of the action of a linear motor. Furthermore, the [2]-pseudorotaxanes are the only models that are self-assembled in the strictest sense (thermodynamic control).

There are many examples of artificial molecular machines, based on pseudorotaxanes, which undergo co-conformational change after chemical, electrochemical, and photochemical stimuli. Photons or electrons are certainly the best energy source to power molecular machines. It is well-established that  $N,N'$ -dialkylbipyridinium salts form  $\pi$ -donor-acceptor complexes with different electron rich aromatic compounds. Stoddart, Balzani and coworkers have extensively studied the supramolecular complexes (pseudorotaxanes) between dialkoxybenzenes and bipyridinium cyclophanes. They have shown that a Re-complex can be incorporated into the ring component of this type of pseudorotaxane as a photosensitizer (Figure 9).<sup>52</sup> This modification allows for the

fabrication of a sophisticated photochemically driven molecular machine of the pseudorotaxane type. The dethreading and rethreading motions are triggered by irradiation with visible light and oxygenation of the solution, respectively. The motions can be easily monitored by UV/Vis absorption and luminescence spectroscopy. Many dethreading/rethreading cycles can be performed with the same solution without any appreciable loss of signal. The reductant scavenger is the limiting factor for the (in principle) infinite cycle.

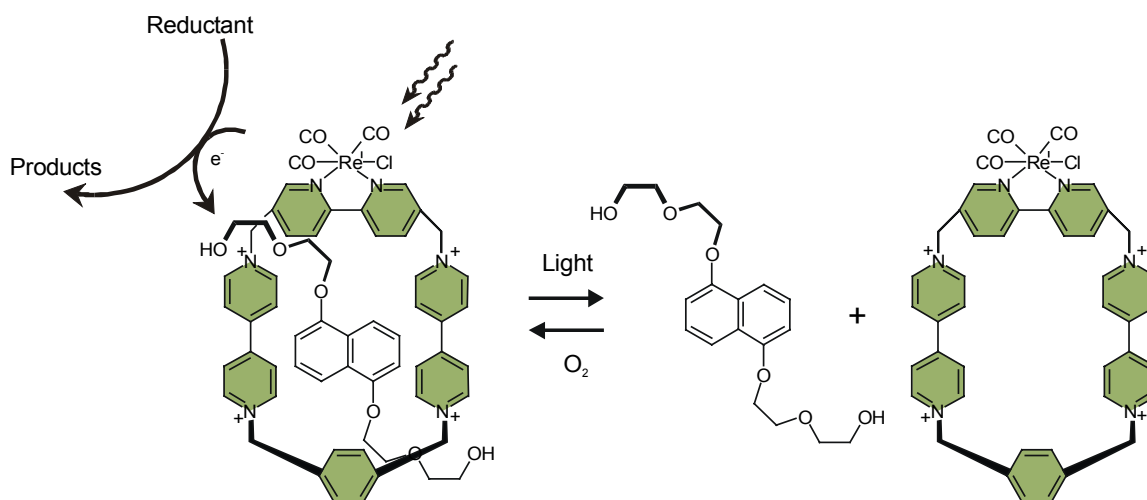


**Figure 9.** Mechanism of a linear molecular motor based on pseudorotaxane.

Harada and coworkers<sup>53</sup> have prepared poly-pseudorotaxanes based on ionic polymers and cyclodextrins.  $\beta$ -Cyclodextrins move along a polymer consisting of bipyridinium (viologen) moieties bridged by polymethylene chains (molecular shuttles). To avoid the escape of a cyclodextrin from the polymer chain, two molecular stoppers (rotaxane formation) were attached to the end of the polymer chain. This molecular machine has a shuttling behavior that is solvent and temperature sensitive and can be controlled by two interactions viz. hydrophobic interaction between a cyclodextrin ring and a station (polymethylene chain), and a repulsive interaction between the cyclodextrin ring and the 4,4'-bipyridinium linker.

In nature the chemical energy supplied by food is used to power the biological machines that sustain life. Similarly, chemical energy input can be used to control threading/dethreading processes in pseudorotaxanes. The system developed by Balzani

and coworkers<sup>54</sup> can be considered a molecular-level plug/socket device. The plug-in function is based on the threading of a ( $\pm$ )binaphthocrown ether by a (9-anthracenyl)benzylammonium ion. The association process can be reversed quantitatively (plug out) by addition of a suitable base such as tributylamine. In the plug-in state (pseudorotaxane), an energy-transfer process takes place. As a consequence of the reversibility of the acid/base reactions, the energy transfer process can be switched on and off at will.

## 2.7 Synthetic models for hemoglobin (Hb) and myoglobin (Mb)

Hemoglobin (Hb) and myoglobin (Mb) are the most known proteins involved in the transport and storage of O<sub>2</sub>, fulfilling an essential role for the existence of a large variety of living organisms on earth. The three dimensional structure of these compact globular proteins, which are characterized by the presence of  $\alpha$ -helical segments (labeled with capital letters), is shown in Figure 10.

Synthetic models of these proteins have been invaluable tools in unraveling the subtle complexities of reversible O<sub>2</sub> binding and CO inhibition. However, no attempts have been made so far to construct model systems in a noncovalent way. This is rather surprising since self-assembly and noncovalent interactions are widely present in natural systems.

### 2.7.1 Hemoglobin and myoglobin: cooperativity in O<sub>2</sub>-binding makes the difference

Evolution has led to the development of several proteins for O<sub>2</sub> transport and storage. In mammals, these functions are carried out by Hb (an O<sub>2</sub> carrier) and Mb (for O<sub>2</sub> storage in the muscles). Recently a third type of globin, neuroglobin,<sup>55</sup> has been discovered in human and mouse brain tissues, where it apparently has a function comparable to that of Mb in muscle cells. Other proteins able to bind dioxygen are hemerythrins<sup>56-58</sup> (storage) and hemocyanins<sup>56</sup> (transport) but their binding site is not a Fe<sup>II</sup> porphyrin (heme) and will not be considered since the research described in this thesis focuses on *synthetic models for heme containing O<sub>2</sub> carriers*.

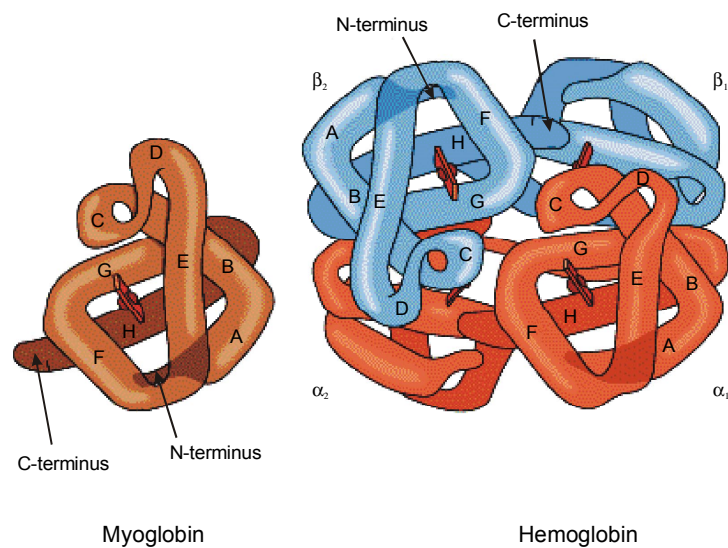


**Figure 10.** Schematic three dimensional structures of myoglobin and hemoglobin.

The O<sub>2</sub>-binding site of Hb and Mb is a Fe<sup>II</sup> protoporphyrin IX (the heme) located in a hydrophobic cavity formed by the folding of the protein (Figure11).<sup>56,59</sup>

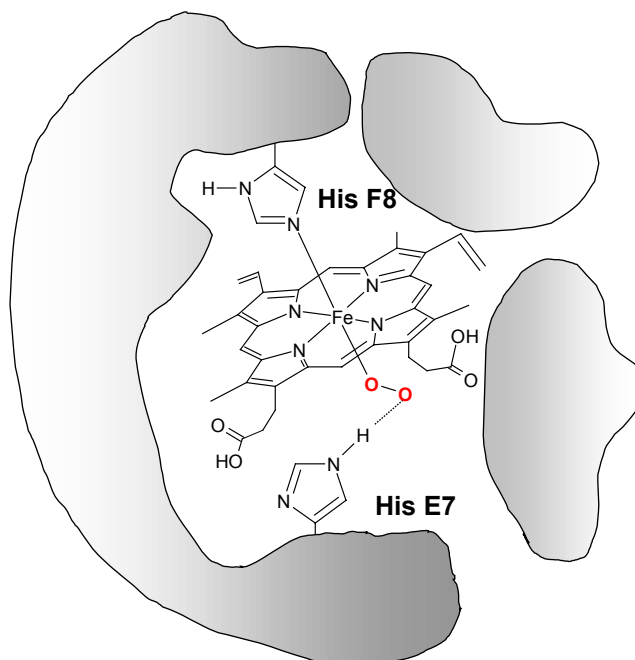


**Figure 11.** Schematic representation of the heme in O<sub>2</sub> binding hemeprotein. The Fe<sup>II</sup> atom of protoporphyrin IX is coordinated axially to the proximal histidine residue (His F8). The distal histidine (His E7) stabilizes the coordinated O<sub>2</sub> via hydrogen bonding.

The heme is held in its position by a multitude of noncovalent interactions, which include hydrophobic interactions and the coordination of the  $\text{Fe}^{\text{II}}$  atom to the imidazole ring of histidine F8 (proximal histidine).

Noncovalent interactions are also responsible for the differences between Mb and Hb. In fact Mb is a monomer (one peptidic chain of 153 amino acids and one heme cofactor) while Hb is a tetramer consisting of two  $\alpha$ -globins (peptidic chains folded in globular structures) and two  $\beta$ -globins, each very similar to Mb. The correct positioning of one chain with respect to the others in the tetrameric structure is due to the existence of noncovalent interactions such as salt-bridge formation and hydrophobic interactions. The direct consequence of these different structural features between the two proteins is the very well-known cooperativity in  $\text{O}_2$  binding displayed by Hb but not by Mb (see Figure 12).

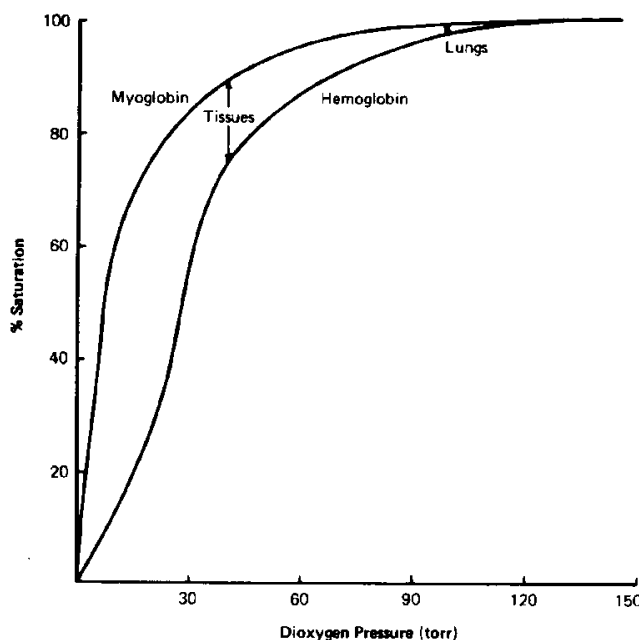


**Figure 12.** Dioxygen saturation curve for Mb and Hb at pH 7.4 and 25°C

To describe the observed cooperativity based on a two-state allosteric model displayed by Hb, Perutz introduced the symbols T and R.<sup>60,61</sup> Two structures for each subunit ( $\alpha$  or  $\beta$ ) are possible according to the model viz. a low  $\text{O}_2$  affinity structure (T or tense state) and a high  $\text{O}_2$  affinity structure (R or relaxed state). These two states differ in the folding of the

peptidic chain (tertiary structure) of each subunit and also in the relative orientation of the subunits in the tetramer (quaternary structure). The T and R states are present as an equilibrium mixture, with preference for T at low O<sub>2</sub> partial pressures. When the first O<sub>2</sub> molecule binds to a T state subunit, a certain amount of strain is induced in the local tertiary structure. This strain alters the interactions between the subunits, inducing a change in their tertiary structure, which facilitates the binding of an additional O<sub>2</sub> molecule (positive allosterism, see section 2.4).

### **2.7.2 *Synthetic models: stability and understanding of the O<sub>2</sub> adduct***

Most work in this field has been concentrated on porphyrin systems for the preparation of synthetic models for Hb and Mb active sites, because of the structural similarity between these compounds and the heme cofactor. The porphyrinic scaffold offers a large number of positions that can be chemically functionalized (Figure 13), and has led to the preparation of very elaborate structures by covalent modification of the porphyrin periphery. These modifications have allowed the protein environment in proximity to the heme to be reproduced. Excellent reviews describing extensively the progress in this eminent field of chemistry have been published.<sup>59,69-71</sup> These efforts have resulted in a large variety of porphyrins, which have been described as “capped”, “picket fence”, “pocket”, “strapped”, “cofacial” and “picnic basket”. The leading idea behind many of these synthetic systems is to understand the structure-activity relationship that could explain efficient and stable O<sub>2</sub> binding to natural heme proteins. Some examples are shown in Figure 14 and their affinities for O<sub>2</sub> are reported in Table 2.1. A more practical reason for these studies is the achievement of an increased stability towards O<sub>2</sub> (i.e. systems in which undesired decomposition reactions triggered by O<sub>2</sub> binding are minimized) in view of technological applications such as O<sub>2</sub> separation and storage.<sup>72</sup>



**Table 2.1.** Dioxygen binding constants for some  $\text{Co}^{\text{II}}$  and  $\text{Fe}^{\text{II}}$  porphyrins (see Figure 14) expressed as half oxygenation pressure  $P_{1/2}$ .<sup>a</sup>

Compound	$P_{1/2}(\text{O}_2)$ (Torr)	Conditions
Fe-Cu-4	31 Torr	0.2M 1-MeIm, benzene, 20 °C <sup>62</sup>
FeSP-15	15 Torr	0.2M 1-MeIm, benzene, 20 °C <sup>62</sup>
Fe(Cap)	$4.0 \times 10^3$ Torr	1,2-diMeIm, toluene, 25 °C <sup>64</sup>
Co(Cap)	$1.4 \times 10^5$ Torr	1-MeIm, toluene, 15 °C <sup>64</sup>
$\text{C}_2$ -capped $\text{C}_5$ -strapped	110 Torr	toluene, 0 °C <sup>68</sup>
Co TpivPP	140 Torr	1-MeIm, toluene, 25 °C <sup>67</sup>
Fe TpivPP	38 Torr	1,2-diMeIm, toluene, 25 °C <sup>66</sup>

<sup>a</sup>  $\text{O}_2$  partial pressure in the gas phase (in equilibrium with the porphyrin solution) under which 50% of the porphyrin binds  $\text{O}_2$ .

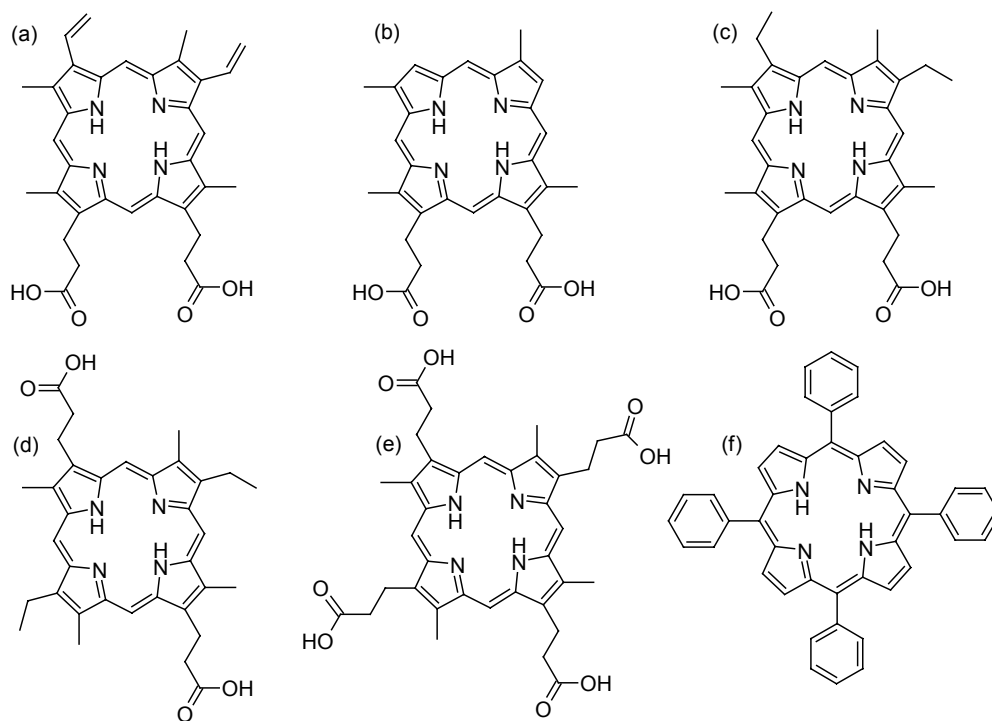
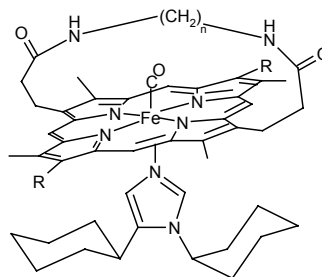
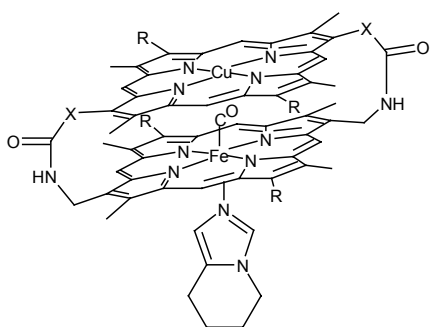
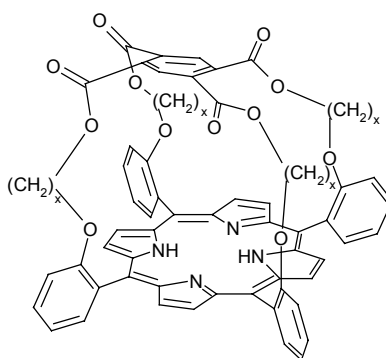


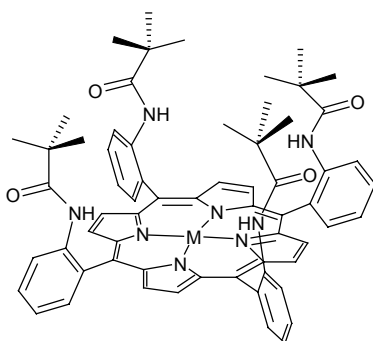
**Figure 13.** Porphyrin structures commonly encountered in literature that are associated with natural and synthetic heme protein systems. a) protoporphyrin IX; b) deuteroporphyrin IX; c) mesoporphyrin IX; d) mesoporphyrin; e) coproporphyrin; f) *meso*-tetraphenylporphyrin.



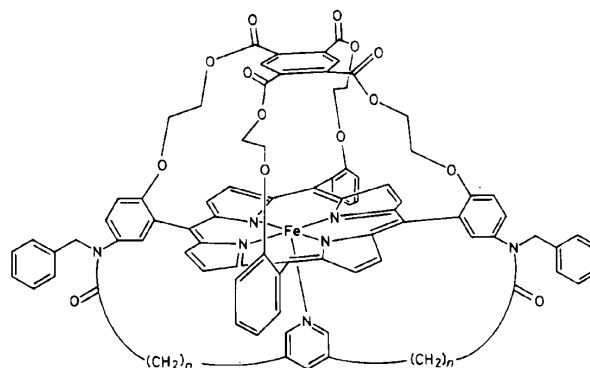
(a) Fe-Cu-4 and Fe-Cu-5 ( $X=CH_2$  or  $CH_2CH_2$ ) (b) FeSP-13, FeSP-14 and FeSP-15 ( $n=5, 6,$  and  $7$ ) (Chang<sup>62</sup>)



(c) CapH<sub>2</sub> ( $x=2$ ) and HmCapH<sub>2</sub> ( $x=3$ ) (Baldwin<sup>63</sup> and Basolo<sup>64</sup>)



(d) TpivotPP,  $M=Fe^{II}, Co^{II}$  (Collman<sup>65-67</sup>)



(e) C<sub>2</sub>-capped C<sub>n</sub>-strapped  $n=4$  or  $5$  (Baldwin<sup>68</sup>)

**Figure 14.** Superstructured porphyrin-based dioxygen carriers. a) "cofacial", b) "strapped", c) "capped", d) "picket fence", e) "capped-strapped".

Proteins Hb and Mb as well as model systems (collectively designated with the term O<sub>2</sub>-carriers) require that the iron atom be maintained in the ferrous (Fe<sup>II</sup>) state in order to

bind O<sub>2</sub>. This is not the thermodynamically stable state in the presence of O<sub>2</sub> but the proteins successfully retard the oxidation to the inactive Fe<sup>III</sup> state. Even then, the met-Hb (the oxidized Fe<sup>III</sup> form) content of our blood is usually around 3%.<sup>†</sup> Many factors contribute to the overall stability of an O<sub>2</sub>-carrier such as the solvent, the electron density on the Fe<sup>II</sup> ion (partly determined by the axial ligand *trans* to the O<sub>2</sub>) and the steric hindrance protecting the coordinated O<sub>2</sub>.<sup>59,70,73</sup> However, one important conclusion can be extracted from all the studies on O<sub>2</sub>-binding stability: the minimal requirement for a model system to be stable towards oxidation is to have a superstructure that protects the Fe-O<sub>2</sub> moiety from reacting with a second Fe-porphyrin. The picket fence porphyrin (FeT pivPP) reported by Collman represents one of the milestones in this field.<sup>65</sup> The compound has been reported to be remarkably stable due to the presence of the four pivalamido moieties which indeed effectively protect the Fe-O<sub>2</sub> moiety (see Figure 14).<sup>‡</sup>

Synthetic model systems should possess all (or at least most) of the important features of natural systems viz. i) a hydrophobic environment surrounding the metal-O<sub>2</sub> moiety, ii) a proper axial ligand to enhance the binding of O<sub>2</sub> to the metal, and iii) secondary interactions between the metal-O<sub>2</sub> moiety able to stabilize the complex.

The hydrophobic pocket, which in nature is achieved by burying the porphyrin within the protein matrix, has been generally accomplished in synthetic systems by the use of organic solvents and/or by the already mentioned superstructures around the porphyrin core (see Figure 14). The axial ligand requirement has been met by adding nitrogenous bases such as imidazole or pyridine derivatives or by covalent attachment of similar nitrogenous bases to the porphyrin structure. The third prerequisite is probably the most challenging to introduce into model systems because very subtle interactions such as steric hindrance and hydrogen bonding are involved. In fact, the contribution of these interactions in the natural systems is still a matter of debate among the scientific

---

<sup>†</sup> Therefore living organisms have repairing mechanisms: the enzyme NADH-cytochrome *b*<sub>5</sub> oxidoreductase reduces met-Mb or met-Hb to the respective Fe<sup>II</sup> deoxy species and thus prevents the accumulation of the inactive forms.<sup>73</sup>

<sup>‡</sup> When dissolved in an aprotic solvent such as toluene and in the presence of an axial base such as 1,2-dimethylimidazole, this O<sub>2</sub>-carrier remains stable for periods as long as several months.

community.<sup>69,74</sup> A reliable mimicry of these secondary interactions is especially important to understand which factors induce destabilization of the competing complex derived from binding of the endogenous toxic ligand carbon monoxide (CO) in natural systems.

The hypothesis that polarity effects cause discrimination between O<sub>2</sub> and CO and favoritism for O<sub>2</sub> can be traced back to the suggestion of Pauling in 1964.<sup>75</sup> Since then, many model systems have demonstrated the importance of these effects on O<sub>2</sub> binding (but not on CO) and are summarized in an excellent review that covers the literature until 1998.<sup>69,70</sup> The most important contribution to selective stabilization of coordinated O<sub>2</sub> has generally been attributed to hydrogen bonding interactions. For instance, it has been shown that a strong hydrogen bond between coordinated O<sub>2</sub> and tyrosine B10 (with the involvement of glutamine E7) in *Ascaris* Hb is responsible for its extraordinary O<sub>2</sub> avidity, four orders of magnitude higher than that of human Hb.<sup>76</sup> Recent contributions from the group of Naruta have shown the existence of hydrogen bonds between the Fe-O<sub>2</sub> moiety of a “single-coronet” porphyrin and hydroxyl groups attached to the binaphthyl bridges of the porphyrin (Figure 15).<sup>77</sup> Their work has also been extended to “twin-coronet”<sup>78</sup> porphyrins having thiolate axial ligands as models for cytochrome P450 (a heme-protein which is responsible for O<sub>2</sub> activation).<sup>79</sup> <sup>80</sup>In all cases, Raman spectroscopy was used to demonstrate that the coordinated O<sub>2</sub> is hydrogen bonded to inward pointing hydroxyl groups appended to the porphyrin superstructure.

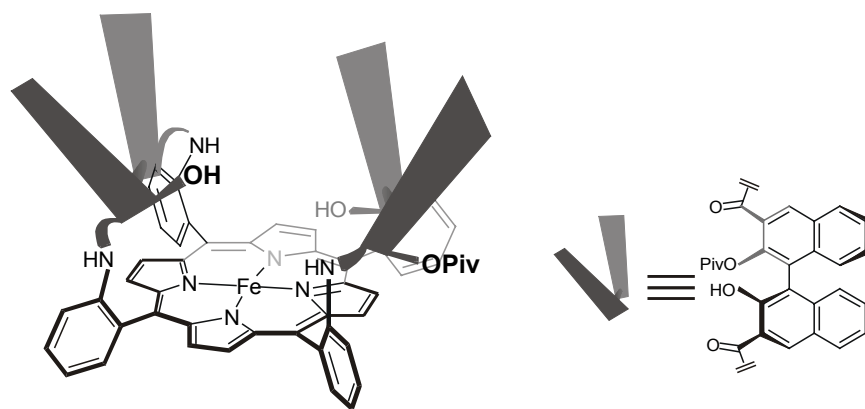


**Figure 15.** “Single-coronet” porphyrin (derived from combination of porphyrin and binaphthyl scaffolds). The inward pointing hydroxyl groups can hydrogen-bond to the O<sub>2</sub> coordinated to the Fe atom.

Very recently, progress in understanding the factors affecting Fe-O<sub>2</sub> stabilization in natural proteins has been made by using density functional theory (DFT) calculations in combination with SAM1 semi-empirical electronic structure methods.<sup>81-83</sup> These quantum chemistry calculations were used to estimate the interaction energies associated with H-bonds in the active site of *Ascaris* Hb, as well as in the  $\alpha$ - and  $\beta$ -subunits of human Hb in the R-state.<sup>81</sup> The results confirmed the existence of strong hydrogen bonds for all three Hbs and contradicted previous observations indicating the lack of such interaction for the  $\beta$ -subunit of human Hb. The authors pointed out that the global equilibrium for binding of a ligand to a heme-protein is a complex phenomena involving partition of the ligand between the solvent and the protein matrix, transport across the protein matrix and finally the binding process itself. Mutagenesis experiments on proteins may therefore provide misleading results since the residues involved in H-bonding are also involved in the kinetics of the process and a strong H-bond does not necessarily imply a high affinity constant for such complex systems.

### ***2.7.3 Synthetic systems having Co<sup>II</sup> in the active site: the stability issue***

The stability of simple Fe<sup>II</sup> porphyrins in oxygenated solutions is so low that for many years attempts to mimic Hb and Mb were unsuccessful. It was then discovered that Co<sup>II</sup> Schiff base complexes and Co<sup>II</sup> porphyrins can reversibly bind O<sub>2</sub> in 1:1 ratio under conditions that were found prohibitive for the stability of Fe<sup>II</sup> porphyrins. These Co<sup>II</sup> complexes-O<sub>2</sub> adducts are further related to the natural systems by the necessity of an axially coordinated donor ligand.<sup>59,84</sup> In fact, simple Co<sup>II</sup> porphyrins offer easy accessibility to pentacoordinated complexes upon addition of a nitrogenous base for axial ligation. In contrast, this remains a serious challenge when Fe<sup>II</sup> porphyrins are used, due to their strong tendency to form hexacoordinate complexes. Moreover, both oxygenated and deoxygenated Co<sup>II</sup> porphyrins are paramagnetic and can be studied by electron paramagnetic resonance (EPR) and electron nuclear double resonance (ENDOR) spectroscopies.<sup>84</sup>

The enhanced stability of Co<sup>II</sup> porphyrins allowed the preparation of coboglobins, the cobalt analogues of Hb and Mb, by reconstitution of the proteins with Co<sup>II</sup> protoporphyrin IX.<sup>85-89</sup> The study of coboglobins permitted the direct observation of the

effect of the protein environment by comparison of the spectroscopic properties and the O<sub>2</sub> binding of the coboglobins with those of Co<sup>II</sup> protoporphyrin IX dimethylester in solution.<sup>90</sup>

In addition to the use of simple porphyrins as synthetic models, the previously synthesized superstructured porphyrins were also prepared with Co<sup>II</sup> (instead of Fe<sup>II</sup>) as the O<sub>2</sub> binding unit. Three years after the first publication about FeTpivPP porphyrins,<sup>65</sup> the group of Collman reported the preparation of the analogue CoTpivPP and studied its O<sub>2</sub> binding equilibrium.<sup>67,91</sup> The group of Basolo then reported the preparation of Co<sup>II</sup> “capped” porphyrins<sup>64</sup> and found considerably smaller O<sub>2</sub> affinities in comparison to Collman’s TpivPP porphyrins (see Table 2.1). The reduced affinities were attributed to greater conformational strain accompanying the formation of the six-coordinate O<sub>2</sub> adducts. Interestingly, the so-called “homologous” capped porphyrins (HmCap, see Figure 13) containing longer spacers unexpectedly gave even lower affinities.<sup>64</sup>

These examples clearly illustrate one of the serious limitations of using synthetic models prepared by covalent modification of the porphyrin periphery. Such systems could in fact have a much higher rigidity than the noncovalent counterparts constituting the natural systems.

## **2.8 Concluding remarks**

With increasing emphasis on function rather than on structure, the importance of covalent synthesis is becoming surpassed by self-assembly processes. This development is also clearly observed in the synthetic biomimetic model systems discussed in the first part of this chapter (sections 2.2 – 2.6). A large variety of relatively simple building blocks, which possess a specific chemical function, are connected in a rational way via noncovalent interactions. The collective and cooperative action of such assemblies compares favorably in many cases with the much more complex natural systems.

It is surprising that so far there are no examples reported in the literature concerning the preparation and study of synthetic self-assembled model systems that mimic O<sub>2</sub> binding hemoproteins. Moreover, almost all the systems (based on porphyrins) studied so far are

limited by insolubility in aqueous media,<sup>92</sup> which would be the desirable solvent for a closer mimicry of the natural systems.

Based on the many successful examples using self-assembly strategies and porphyrin building blocks such as the reproduction of photosynthetic centers, cytochromes and redox cofactor activities, as well as oxidation catalysts (sections 2.2 and 2.3), it is very likely that a number of other biomimetic functions can be imitated by synthetic systems, including O<sub>2</sub> binding.

## 2.9 References and notes

1. *Biochemistry*, 4 ed.; Stryer, L.; W. H. Freeman and Company: New York, 1995.
2. Wojaczynski, J.; Latos-Grazynski, L. *Coord. Chem. Rev.* **2000**, *204*, 113-171.
3. Haycock, R. A.; Yartsev, A.; Michelsen, U.; Sundström, V.; Hunter, C. A. *Angew. Chem. Int. Ed.* **2000**, *39*, 3616-3619.
4. Haycock, R. A.; Hunter, C. A.; James, D. A.; Michelsen, U.; Sutton, L. R. *Org. Lett.* **2000**, *2*, 2435-2438.
5. Ambroise, A.; Li, J.; Yu, L.; Lindsey, J. S. *Org. Lett.* **2000**, *2*, 2563-2566.
6. Yamada, K.; Imahori, H.; Yoshizawa, E.; Gosztola, D.; Wasielewski, M. R.; Sakata, Y. *Chem. Lett.* **1999**, 235-236.
7. Li, X.; Ng, D. K. P. *Eur. J. Inorg. Chem.* **2000**, 1845-1848.
8. Guldi, Dirk M.; Luo, C.; Swartz, A.; Scheloske, M.; Hirsch, A. *Chem. Commun.* **2001**, 1066-1067.
9. Balaban, T. S.; Tamiaki, H.; Holzwarth, A. R.; Schaffner, K. *J. Phys. Chem. B* **1997**, *101*, 3424-3431.
10. Amakawa, M.; Tamiaki, H. *Bioorg. Med. Chem.* **1999**, *7*, 1141-1144. The article reports the preparation of stable self-aggregates in a solid film state using design

principles very similar to those present in naturally occurring systems (chlorosomes). However the work is more focused on structural aspects than on the function of the system.

11. Kuroda, Y.; Sugou, K.; Sasaki, K. *J. Am. Chem. Soc.* **2000**, *122*, 7833-7834.
12. Rabanal, F.; DeGrado, W. F.; Dutton, P. L. *J. Am. Chem. Soc.* **1996**, *118*, 473-474.
13. Reek, J. N. H.; Rowan, A. E.; de Gelder, R.; Beurskens, P. T.; Crossley, M. J.; de Feyter, S.; de Schryver, F.; Nolte, R. J. M. *Angew. Chem. Int. Ed.* **1997**, *36*, 361-363.
14. Drain, C. M.; Shi, X.; Milic, T.; Nifiatis, F. *Chem. Commun.* **2001**, 287-288.
15. Springs, S. L.; Gosztola, D.; Wasielewski, M. R.; Kral, V.; Andrievsky, A.; Sessler, J. L. *J. Am. Chem. Soc.* **1999**, *121*, 2281-2289.
16. Sun, L.; Hammarström, L.; Åkermark, B.; Styring, S. *Chem. Soc. Rev.* **2001**, *30*, 36-49. A detailed review with a large introductory section describing the most recent progress towards the understanding of the Photosystem II reaction center.
17. Sun, L.; Burkitt, M.; Tamm, M.; Raymond, M. K.; Abrahamsson, M.; LeGourriérec, D.; Frapart, Y.; Magnuson, A.; Kenéz, P. H.; Brandt, P.; Tran, A.; Hammarström, L.; Styring, S.; Åkermark, B. *J. Am. Chem. Soc.* **1999**, *121*, 6834-6842.
18. Hu, Y.-Z.; Tsukiji, S.; Shinkai, S.; Oishi, S.; Hamachi, I. *J. Am. Chem. Soc.* **2000**, *122*, 241-253.
19. David, E.; Born, R.; Kaganer, E.; Joselevich, E.; Durr, H.; Willner, I. *J. Am. Chem. Soc.* **1997**, *119*, 7778-7790.
20. Hecht, S.; Fréchet, J. M. J. *Angew. Chem. Int. Ed.* **2001**, *40*, 74-91. This recent review covers the application of dendrimers in biomimetic systems. Most of the reported examples are not based on self-assembly.



21. Sakamoto, M.; Ueno, A.; Mihara, H. *Chem. Eur. J.* **2001**, *7*, 2449-2458.
22. Balzani, V.; Campagna, S.; Denti, G.; Juris, A.; Serroni, S.; Venturi, M. *Acc. Chem. Res.* **1998**, *31*, 26-34.
23. Kawa, M.; Fréchet, J. M. J. *Chem. Mater.* **1998**, *10*, 286-296.
24. Schultze, X.; Serin, J.; Adronov, A.; Frechet, J. M. J. *Chem. Commun.* **2001**, 1160-1161.
25. Sessler, J. L.; Sathiosatham, M.; Brown, C. T.; Rhodes, T. A.; Wiederrecht, G. *J. Am. Chem. Soc.* **2001**, *123*, 3655-3660.
26. Kirby, J. P.; Roberts, J. A.; Nocera, D. G. *J. Am. Chem. Soc.* **1997**, *119*, 9230-9236.
27. Xing, G.; DeRose, V. J. *Curr. Opin. Chem. Biol.* **2001**, *5*, 196-200.
28. Rau, H. K.; Haehnel, W. *J. Am. Chem. Soc.* **1998**, *120*, 468-476.
29. Katz, E.; Heleg-Shabtai, V.; Willner, I.; Rau, H. K.; Haehnel, W. *Angew. Chem. Int. Ed.* **1998**, *37*, 3253-3256. Even if self-assembled monolayers have not been specifically considered in this review, it is worth mentioning this interesting communication. Several distinct self-assembly steps are used and integrated with covalent synthesis, resulting in novel electrodes for biosensor application.
30. Willner, I.; Hleg-Shabtai, V.; Katz, E.; Rau, H. K.; Haehnel, W. *J. Am. Chem. Soc.* **1999**, *121*, 6455-6468.
31. Rotello, V. M. *Curr. Opin. Chem. Biol.* **1999**, *3*, 747-751.
32. Breinlinger, E. C.; Keenan, C. J.; Rotello, V. M. *J. Am. Chem. Soc.* **1998**, *120*, 8606-8609.
33. Kajiki, T.; Moriya, H.; Hoshino, K.; Kondo, S.; Yano, Y. *Chem. Lett.* **1999**, 397-398.
34. Kirby, A. J. *Angew. Chem. Int. Ed.* **1996**, *35*, 707-724. This review provides very

clear definitions to introductory readers approaching the field of enzyme models and mimics.

35. Kang, J.; Rebek J. Jr *Nature* **1997**, *385*, 50-52.
36. Pérez-Payá, E.; Forood, B.; Houghten, R. A.; Blondelle, S. E. *J. Mol. Recognit.* **1996**, *9*, 488-493.
37. Hill, C. L.; Zeng, H.; Zhang, X. *J. Mol. Catal. A* **1996**, *113*, 185-190.
38. Sakamoto, S.; Sakurai, S.; Ueno, A.; Mihara, H. *Chem. Commun.* **1997**, 1221-1222.
39. Sakamoto, S.; Ueno, A.; Mihara, H. *J. Chem. Soc., Perkin 2* **1998**, 2395-2404.
40. Schenning, A. P. H. J.; Spelberg, J. H. L.; Hubert, D. H. W.; Feiters, M. C.; Nolte, R. J. M. *Chem. Eur. J.* **1998**, *4*, 871-880.
41. Kennan, A. J.; Haridas, V.; Severin, K.; Lee, D. H.; Ghadiri, M. R. *J. Am. Chem. Soc.* **2001**, *123*, 1797-1803.
42. Ramström, O.; Mosbach, K. *Curr. Opin. Chem. Biol.* **1999**, *3*, 759-764.
43. Takeuchi, M.; Imada, T.; Shinkai, S. *Angew. Chem. Int. Ed.* **1998**, *37*, 2096-2099.
44. Sugasaki, A.; Ikeda, M.; Takeuchi, M.; Shinkai, S. *Angew. Chem. Int. Ed.* **2000**, *39*, 3839-3842.
45. Scrimin, P.; Tecilla, P. *Curr. Opin. Chem. Biol.* **1999**, *3*, 730-735.
46. Boxer, S. G. *Curr. Opin. Chem. Biol.* **2000**, *4*, 704-709.
47. Bong, D. T.; Clark, T. D.; Granja, J. R.; Ghadiri, M. R. *Angew. Chem. Int. Ed.* **2001**, *40*, 988-1011.
48. Sanchez-Quesada, J.; Kim, H. S.; Ghadiri, M. R. *Angew. Chem. Int. Ed.* **2001**, *40*, 2503-2506.

49. Sakai, N.; Majumdar, N.; Matile, S. *J. Am. Chem. Soc.* **1999**, *121*, 4294-4295.
50. Kobuke, Y.; Nagatani, T. *J. Org. Chem.* **2001**, *66*, 5094-5101.
51. Collin, J.-P.; Dietrich-Buchecker, C.; Gavina, P.; Jimenez-Molero, M. C.; Sauvage, J.-P. *Acc. Chem. Res.* **2001**, *34*, 447-487. The account is focused on linear machines and motors based on rotaxanes. Especially interesting are Sauvage's examples of molecular muscles. The authors have designed a multicomponent system able to contract or stretch under direction of an external chemical signal.
52. Ashton, P. R.; Balzani, V.; Kocian, O.; Prodi, L.; Spencer, N.; Stoddart, J. F. *J. Am. Chem. Soc.* **1998**, *120*, 11190-11191.
53. Harada, A. *Acc. Chem. Res.* **2001**, *34*, 456-464.
54. Ishow, E.; Credi, A.; Balzani, S. F.; Mandolini, L. *Chem. Eur. J.* **1999**, *5*, 984-989.
55. Burmester, T.; Weich, B.; Reinhardt, S.; Hankein, T. *Nature* **2000**, *407*, 520-523.
56. Niederhoffer, E. C.; Timmons, J. H.; Martell, A. E. *Chem. Rev.* **1984**, *84*, 137-203.
57. Brunold, T. C.; Solomon, E. I. *J. Am. Chem. Soc.* **1999**, *121*, 8277-8287.
58. Brunold, T. C.; Solomon, E. I. *J. Am. Chem. Soc.* **1999**, *121*, 8288-8295.
59. Jones, R. D.; Summerville, D. A.; Basolo, F. *Chem. Rev.* **1979**, *79*, 139-179.
60. Perutz, M. F. *Nature* **1970**, *228*, 726-734.
61. Perutz, M. F.; Fermi, G.; Luisi, B.; Shaanan, B.; Liddington, R. C. *Acc. Chem. Res.* **1987**, *20*, 309-321.
62. Ward, B.; Wang, C.; Chang, C. K. *J. Am. Chem. Soc.* **1981**, *103*, 5236-5238.
63. Almog, J.; Baldwin, J. E.; Dyer, R. L.; Peters, M. *J. Am. Chem. Soc.* **1975**, *97*, 226-227.

64. Linard, J. E.; Ellis, P. E.; Budge, J. R.; Jones, R. D.; Basolo, F. *J. Am. Chem. Soc.* **1980**, *102*, 1896-1904.
65. Collman, J. P.; Gagne, R. R.; Reed, C. A.; Halbert, T. R.; Lang, G.; Robinson, W. *J. Am. Chem. Soc.* **1975**, *97*, 1427-1439.
66. Collman, J. P.; Brauman, J. I.; Doxsee, K. M.; Halbert, T. R.; Suslick, K. S. *Proc. Natl. Acad. Sci. USA* **1978**, *75*, 564-568.
67. Collman, J. P.; Brauman, J. I.; Doxsee, K. M.; Halbert, T. R.; Hayes, S. E.; Suslick, K. S. *J. Am. Chem. Soc.* **1978**, *100*, 2761-2766.
68. Baldwin, J. E.; Cameron, J. H.; Crossley, M. J.; Dagley, I. J.; Hall, S. R.; Klose, T. *J. Chem. Soc., Dalton Trans.* **1984**, 1739-1746.
69. Collman, J. P.; Fu, L. *Acc. Chem. Res.* **1999**, *32*, 455-463.
70. Momentau, M.; Reed, C. A. *Chem. Rev.* **1994**, *94*, 659-698.
71. Traylor, T. G. *Acc. Chem. Res.* **1981**, *14*, 102-109.
72. Figoli, A.; Sager, W. F. C.; Mulder, M. H. V. *J. Membrane Sci.* **2001**, *181*, 97-110.
73. Shikama, K. *Chem. Rev.* **1998**, *98*, 1357-1373.
74. Spiro, T. G.; Kozlowski, P. M. *Acc. Chem. Res.* **2001**, *34*, 137-144.
75. Pauling, L. *Nature* **1964**, *203*, 182-183.
76. Goldberg, D. E. *Chem. Rev.* **1999**, *99*, 3371-3378.
77. Kossanyi, A.; Tani, F.; Nakamura, N.; Naruta, Y. *Chem. Eur. J.* **2001**, *7*, 2862-2872.
78. Naruta, Y.; Tani, F.; Ishihara, N.; Maruyama, K. *J. Am. Chem. Soc.* **1991**, *113*, 6865-6872.

79. Matsu-ura, M.; Tani, F.; Nakayama, S.; Nakamura, N.; Naruta, Y. *Angew. Chem. Int. Ed.* **2000**, *39*, 1989-1991.
80. Tani, F.; Matsu-ura, M.; Nakayama, S.; Ichimura, M.; Nakamura, N.; Naruta, Y. *J. Am. Chem. Soc.* **2001**, *123*, 1133-1142.
81. Scherlis, D. A.; Estrin, D. A. *J. Am. Chem. Soc.* **2001**, *123*, 8436-8437.
82. Godbout, N.; Sanders, L. K.; Salzmann, R.; Havlin, R. H.; Wojdelski, M.; Oldfield, E. *J. Am. Chem. Soc.* **1999**, *121*, 3829-3844.
83. Vogel, K. M.; Kozlowski, P. M.; Zgierski, M. Z.; Spiro, T. G. *J. Am. Chem. Soc.* **1999**, *121*, 9915-9921.
84. Smith, T. D.; Pilbrow, J. R. *Coord. Chem. Rev.* **1981**, *39*, 295-283.
85. Ikeda-Saito, M.; Brunori, M.; Yonetani, T. *Biochim. Biophys. Acta* **1978**, *533*, 173-180.
86. Dickinson, L. C.; Chien, J. C. W. *Proc. Natl. Acad. Sci. USA* **1980**, *77*, 1235-1239.
87. Chien, J. C. W.; Dickinson, L. C. *Proc. Natl. Acad. Sci. USA* **1972**, *69*, 2783-2787.
88. Hori, H.; Ikeda-Saito, M.; Yonetani, T. *Nature* **1980**, *288*, 501-502.
89. Hori, H.; Ikeda-Saito, M.; Yonetani, T. *J. Biol. Chem.* **1982**, *257*, 3636-3642.
90. Hoffman, B. M.; Petering, D. H. *Proc. Natl. Acad. Sci. USA* **1970**, *67*, 637.
91. Steiger, B.; Baskin, J. S.; Anson, F. C.; Zewail, A. H. *Angew. Chem. Int. Ed.* **2000**, *39*, 257-259.
92. Jimenez, H. R.; Momentau, M. *New J. Chem.* **1994**, *18*, 569-574.

# NONCOVALENT SYNTHESIS OF CALIX[4]ARENE-CAPPED PORPHYRINS IN POLAR SOLVENTS VIA IONIC INTERACTIONS\*

*The first step towards a self-assembled system for the mimicry of O<sub>2</sub> binding hemeprotein is the preparation of a superstructured porphyrin architecture via noncovalent synthesis. The work presented here focuses on the use of ionic interactions as the recognition motif between building blocks (tetracationic porphyrins and tetraanionic calix[4]arenes). The self-assembly process is studied in polar solvents and in water/organic solvent mixtures.*

### 3.1 Introduction

There are few classes of chemical compounds that have attracted more attention from chemists than metalloporphyrins. These compounds play an important role as prosthetic groups in several proteins like hemoglobin,<sup>1</sup> the cytochrome P-450 mono-oxygenase family<sup>2</sup> and peroxidases.<sup>3</sup> Whereas the central metal ion (coordinated to the four pyrrolic nitrogens) is the functional unit in molecular recognition and catalysis, the selectivity in these processes as well as the stability of the systems are largely due to noncovalent interactions with the surrounding protein structure. Such interactions are possible because of the shielded position of the porphyrin within the pocket of the folded protein backbone.

---

\* Part of this chapter has been published: Fiammengo, R.; Timmerman, P.; de Jong, F.; Reinhoudt, D. N. *Chem. Commun.* **2000**, 2313-2314. Fiammengo, R.; Timmerman, P.; Huskens, J.; Versluis, K.; Heck, A. J. R.; Reinhoudt, D. N. *Tetrahedron* **2002**, 58(4), 757-764.

Synthetic chemists have extensively tried to mimic natural porphyrin systems via covalent modification of the porphyrin periphery, resulting in a multitude of porphyrin structures such as capped, strapped, picnic basket, twin coronet and others (see section 2.7.2).<sup>4-6</sup> A noncovalent approach to the modification of the porphyrin periphery has been attempted via coordination chemistry<sup>7</sup> or via hydrogen-bond interactions,<sup>8</sup> generally resulting in multiporphyrin systems. However, little attention has been paid to the use of ionic interactions.<sup>9-11</sup> Among the systems consisting of a single porphyrin unit there are examples of porphyrin-cyclodextrin complexes,<sup>12-14</sup> porphyrins in phospholipid vesicles,<sup>15</sup> and porphyrins interacting with other chromophoric units<sup>16</sup> or systems used for sensing purposes.<sup>17</sup>

This chapter deals with the use of multiple ionic interactions for the self-assembly of cationic zinc(II) *meso*-tetrakis(*N*-alkylpyridinium-3-yl) porphyrins **1a-d** and anionic 25,26,27,28-tetrakis(2-ethoxyethoxy)-calix[4]arene tetrasulfonate **2** (Figure 1).

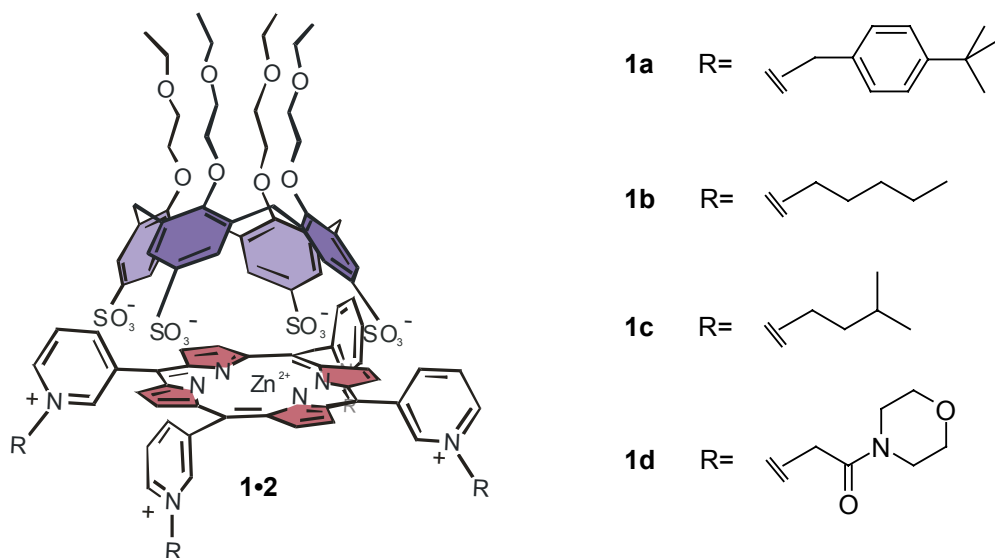


**Figure 1.** Molecular structures of assemblies **1•2** obtained from cationic porphyrins **1a-d** ( $\text{PF}_6^-$  as counterions) and anionic calix[4]arene **2** ( $\text{Na}^+$  as counterions).

The experiments were conducted in polar solvents such as MeOH, DMSO and DMPU<sup>†</sup> and in solvent mixtures containing as much as  $x_{\text{water}} = 45\%$  (molar fraction of water) in the case of the more polar porphyrin derivative **1d**. Moreover, the formation of ternary complexes with nitrogenous bases that coordinate to the zinc atom of the ionic complexes is described.

## 3.2 Results and discussion

### 3.2.1 Synthesis

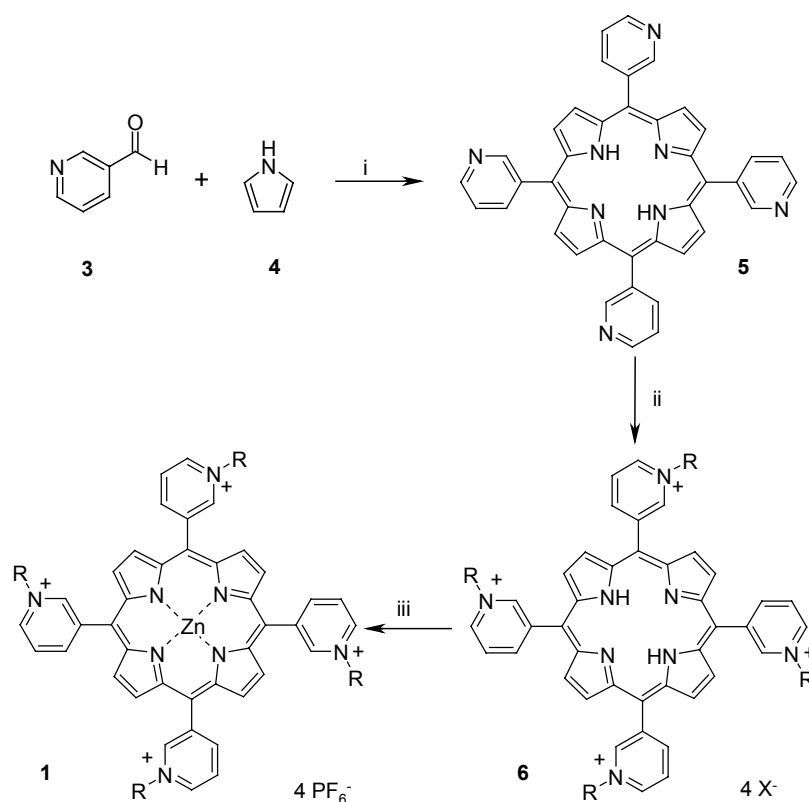


**Figure 2.** Synthetic route to zinc(II) *meso*-tetrakis(*N*-alkylpyridinium-3-yl) porphyrins **1a-d**. i) propionic acid / acetic acid (98:2), reflux, 1h; ii) alkyl-X (X=Br, Cl), DMF or CH<sub>3</sub>CN/NaI (see experimental section for details); iii) ZnAc<sub>2</sub>, MeOH, r.t., then NH<sub>4</sub>PF<sub>6</sub> (aq.).

<sup>†</sup> Abbreviations: MeOH=methanol; DMSO=dimethylsulfoxide; DMPU<sup>†</sup>=1,3-dimethyl-3,4,5,6-tetrahydropyrimidin-2(1*H*)-one; DMF=dimethylformamide.



Zinc (II) *meso*-tetrakis(*N*-alkylpyridinium-3-yl) porphyrins **1a-d** were prepared by condensation of pyridine-3-carboxyaldehyde **3** with pyrrole **4** in a refluxing propionic acid/acetic acid mixture (98:2) followed by alkylation with an excess of the appropriate alkyl bromide (chloride in case of compound **1d**) and subsequent zinc insertion (Figure 2).<sup>18</sup> The overall yields range from 14 to 18%, thus allowing the preparation of the target porphyrins in gram quantities. Tetrasulfonato calix[4]arene **2** was obtained in 84% yield by sulfonation of the parent 25,26,27,28-tetrakis(2-ethoxyethoxy)calix[4]arene<sup>19</sup> with concentrated sulfuric acid using only half of the amount of acid reported in literature<sup>20</sup> (for details, see experimental section).

### 3.2.2 Self-assembly Studies

*UV Vis Spectroscopy.* The formation of molecular assemblies **1•2** was first studied by UV-Vis spectroscopy, a suitable technique for porphyrin-based systems. In general, titration of a solution of porphyrin **1** ( $2\text{--}4 \times 10^{-6}$  M) with calix[4]arene **2** ( $1\text{--}2 \times 10^{-4}$  M) in MeOH gives a bathochromic shift of the porphyrin's Soret band (3-5 nm) and a 20-25% decrease in the molar absorptivity ( $\epsilon$ ) at  $\lambda_{\text{max}}$  (Figure 3).

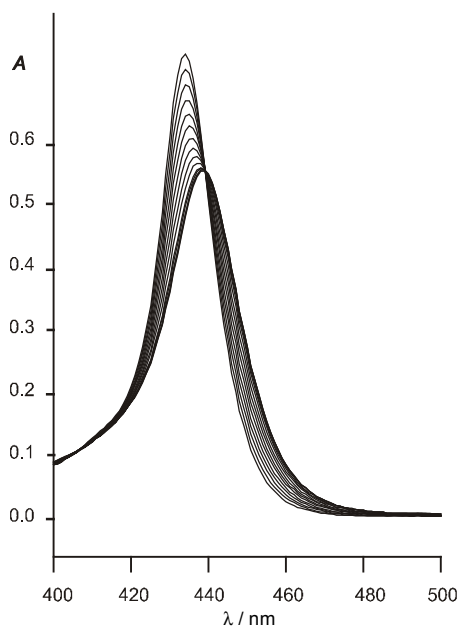


**Figure 3.** UV-Vis titration of Zn(II)porphyrinate **1a** ( $2.7 \times 10^{-6}$  M in MeOH) with calix[4]arene **2**.

Fitting of the spectral data to a 1:1 binding model afforded association constants  $K_{1\cdot2}$  in the range of  $10^7 \text{ M}^{-1}$  (see Table 1). From these data it is possible to see that alteration of the alkyl chains at the pyridyl nitrogens has almost no effect on the strength of the ion-pair complex. This result confirms our hypothesis that assembly of the 1:1 complexes in MeOH is primarily driven by the cooperative formation of four salt bridges between molecular components **1** and **2**. In order to exclude the possibility that the observed spectral changes are the result of nonspecific aggregation of porphyrins **1**, the UV spectrum of porphyrin **1a** was measured at various concentrations (between  $3 \times 10^{-7}$  and  $4 \times 10^{-5} \text{ M}$  in MeOH). Aggregation of the porphyrin was not observed over this concentration range.

**Table 1.** Association constants ( $K_{1\cdot2}$ ) for the formation of assemblies **1**•**2**

Assembly	Solvent	Log $K_{1\cdot2}$
<b>1a</b> • <b>2</b>	CH <sub>3</sub> OH	$7.11 \pm 0.04$
<b>1b</b> • <b>2</b>	CH <sub>3</sub> OH	$7.04 \pm 0.20$
<b>1c</b> • <b>2</b>	CH <sub>3</sub> OH	$7.15 \pm 0.09$
<b>1d</b> • <b>2</b>	CH <sub>3</sub> OH	$6.86 \pm 0.06$
<b>1d</b> • <b>2</b>	H <sub>2</sub> O/CH <sub>3</sub> OH ( $x_{\text{water}}=0.45$ )	$5.43 \pm 0.08^{\text{a}}$
<b>1a</b> • <b>2</b>	DMSO	$6.21 \pm 0.03$
		$5.22 \pm 0.06^{\text{b}}$
		$4.56 \pm 0.03^{\text{c}}$
<b>1a</b> • <b>2</b>	DMPU	$6.16 \pm 0.01$
<b>1a</b> • <b>2</b>	H <sub>2</sub> O/DMPU ( $x_{\text{water}}=0.26$ )	$6.04 \pm 0.02$

T=25 °C, [porphyrin] =  $2\text{--}3 \times 10^{-6} \text{ M}$  (UV-vis),  $1 \times 10^{-4} \text{ M}$  (ITC). Given errors are standard deviations of three measurements. <sup>a</sup> ITC measurement,  $1 \times 10^{-2} \text{ M}$  Bu<sub>4</sub>NClO<sub>4</sub>; <sup>b</sup>  $1 \times 10^{-2} \text{ M}$  Bu<sub>4</sub>NClO<sub>4</sub>; <sup>c</sup>  $1 \times 10^{-2} \text{ M}$  NaClO<sub>4</sub>

Metal-free porphyrin **1a** was used to study the effect of the metal on the assembly formation. The log  $K_{1\cdot2}$  value obtained in this case was  $8.19 \pm 0.19 \text{ M}^{-1}$  and clearly shows that the presence of the metal ion is not a prerequisite for complex formation. The even higher  $K_{1\cdot2}$  value is probably the consequence of the higher flexibility of the metal-free porphyrin, allowing a better interaction with calix[4]arene **2**. Therefore this result

suggests that the metal center might still be available for ligand coordination and guest recognition purposes (*vide infra*).

*<sup>1</sup>H NMR Spectroscopy.* <sup>1</sup>H NMR spectroscopy measurements in CD<sub>3</sub>CN/D<sub>2</sub>O mixtures (81:19) were performed to gain structural information about complexes **1•2**. The spectra of porphyrins **1** alone were studied first. It is well known that porphyrins like **1** can exist in four different atropisomeric forms ( $\alpha\alpha\alpha\alpha$ ,  $\alpha\alpha\alpha\beta$ ,  $\alpha\beta\alpha\beta$ , and  $\alpha\alpha\beta\beta$ ) due to the non-symmetric substitution at the *meso* aromatic rings (Figure 4).<sup>21</sup>

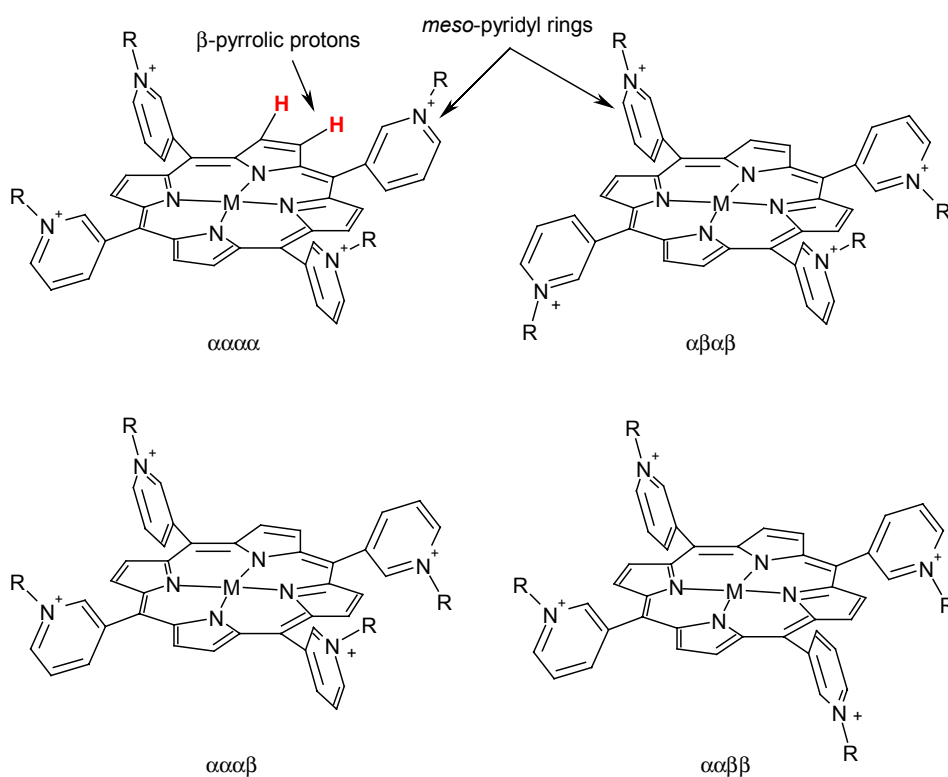


**Figure 4.** Atropisomeric forms for porphyrins **1**.

When the *N*-alkyl moiety is in position 3 relative to the connection of the *meso* pyridyl ring to the porphyrin macrocycle, atropisomerization can occur on a time-scale comparable to the NMR chemical shift time-scale. However, the coalescence temperature can vary depending on the conditions under which the measurement is performed (presence of salts, solvent, etc.)<sup>18</sup> but the equilibrium remains still fast enough to prevent the physical separation of the various isomers. For porphyrin **1a** two signals were

observed for the 8  $\beta$ -pyrrolic protons (COSY experiments show that the two signals belong to adjacent protons) and one signal for three of the four different pyridyl protons  $H_b$ - $H_d$  (Figure 5) which would indicate the presence of only one isomer with fourfold symmetry. However, proton  $H_a$  exhibits a pattern more complicated than expected for just *meta* couplings with protons  $H_b$  and  $H_d$ . Moreover, VT NMR experiments showed coalescence behavior for this signal, thus ruling out the possibility of only one isomer being present.

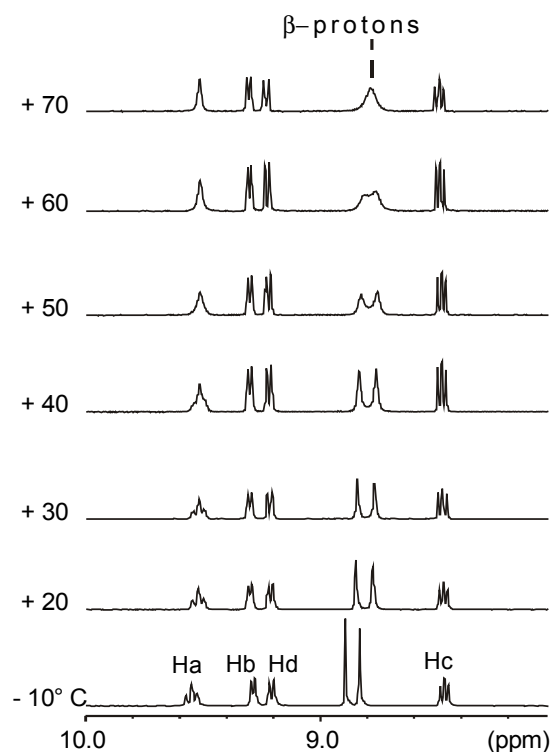


**Figure 5.** VT <sup>1</sup>H NMR experiments of porphyrin **1a** (1.6 mM samples in CD<sub>3</sub>CN/D<sub>2</sub>O 81:19 mixtures). Proton assignment as in Figure 6.

Based on this result we conclude that porphyrin **1a** exists as a mixture of isomers presenting accidental isochronicity for most of the NMR proton signals.<sup>21</sup> The isomers are slowly interconverting on the NMR time scale at 25 °C in CD<sub>3</sub>CN/D<sub>2</sub>O (81:19) and coalescence is observed around 60 °C for the  $\beta$ -protons. Very similar <sup>1</sup>H NMR spectra were observed for porphyrins **1b-1d** with the  $\beta$ -protons also appearing as singlets or as a cluster of signals.

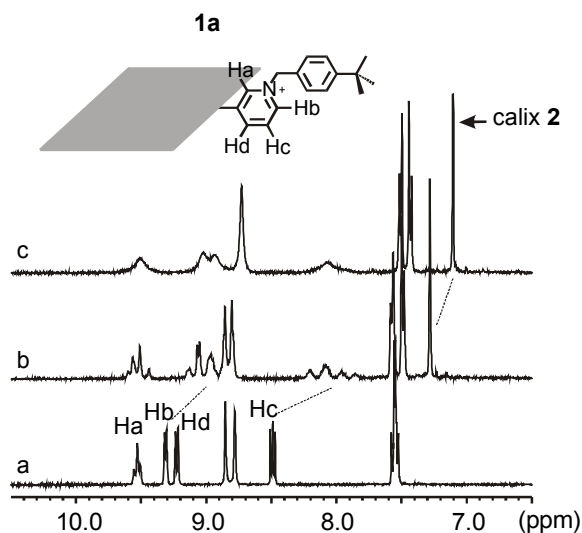


**Figure 6.**  $^1\text{H}$  NMR of (a) porphyrin **1a** (1.8 mM in  $\text{CD}_3\text{CN}/\text{D}_2\text{O}$  81:19) at 298 K, (b) 1:1 mixture of **1a** and **2** at 298 K, (c) 1:1 mixture of **1a** and **2** at 343 K.

Upon addition of 1 equiv of calix[4]arene **2** at room temperature, the porphyrin proton signals change in all cases to a complicate set of signals (see Figure 6 for **1a**) indicating the formation of assemblies **1•2**. This result agrees well with the presence of several isomers that are slowly interconverting on the NMR time scale (also observed for porphyrins **1**). The coalescence temperature measured for assembly **1a•2** is around 10 °C higher than for **1a** alone.<sup>‡</sup> In this assembly the porphyrin protons  $\text{H}_b$ ,  $\text{H}_c$ ,  $\text{H}_d$  present the most upfield shifted signals ( $\Delta\delta \sim 0.2\text{--}0.5$  ppm), which suggests that they are in the closest proximity to the calix[4]arene moiety.

Molecular simulation studies (CHARMm 24.0) support this interpretation.<sup>§</sup> Figure 7 clearly shows that the distance between the oppositely charged groups is minimal when calix[4]arene **2** approaches the porphyrin plane from the side opposite to where the alkyl groups are situated. The estimated O-N distances ( $\text{SO}_3 - \text{N-alkylpyridine}$ ) are 2.74 Å and

<sup>‡</sup> Ion-pair induced complexation has been reported to affect the kinetics of atropoisomerization.<sup>18</sup>

<sup>§</sup> For simplicity only the  $\alpha\alpha\alpha$ -porphyrin isomer is considered. In fact, porphyrin **1** is present as an equilibrating mixture of atropoisomers  $\alpha\alpha\alpha$ ,  $\alpha\alpha\alpha\beta$ ,  $\alpha\alpha\beta\beta$ , and  $\alpha\beta\alpha\beta$  in an expected statistical ratio of 1:4:2:1.<sup>21</sup> Nevertheless, the same considerations mentioned for the  $\alpha\alpha\alpha$  isomer would also be applicable to the  $\alpha\alpha\alpha\beta$  isomer (generally the most abundant), because both present two different porphyrin faces.

3.11 Å when the alkyl groups are pointing away or towards the calix[4]arene, respectively.

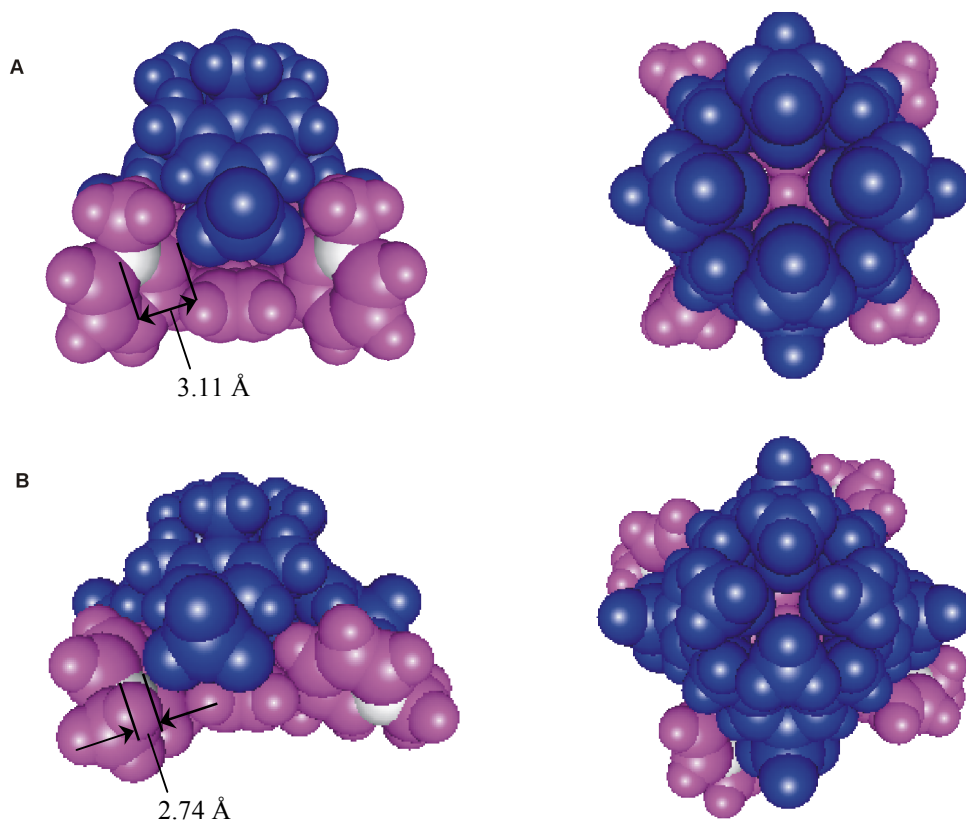


**Figure 7.** Molecular simulation (CHARMm 24.0) of assembly **1•2** with indication of the O-N distances (SO<sub>3</sub> - N-alkylpyridine). (A) *N*-alkyl groups pointing towards **2**, (B) *N*-alkyl groups pointing away from **2**. For simplicity, the *N*-alkyl groups shown are methyls. Compound **1** is in gray (the pyridyl *N* atoms are in white) and compound **2** is in dark gray.

Small upfield shifts (0.03-0.08 ppm) were also observed upon assembly formation for the aromatic and the methylene bridge protons of calix[4]arene **2**, but their multiplicity (according to the C<sub>4v</sub> symmetry of **2**) was unchanged. This indicates that exchange of the components within the assembly is fast on the NMR chemical shift time scale (the lowest temperature we could access was -10 °C).<sup>†</sup> Unfortunately, 2D ROESY experiments in CD<sub>3</sub>CN/D<sub>2</sub>O mixtures failed to show any crosspeak between the two building blocks. The

<sup>†</sup> Below -10 °C the D<sub>2</sub>O/CD<sub>3</sub>CN solvent mixture separates into two different phases.

reason for this is not entirely clear, but a similar observation was reported in the case of a molecular capsule based on charged cyclodextrins in water.<sup>22</sup>

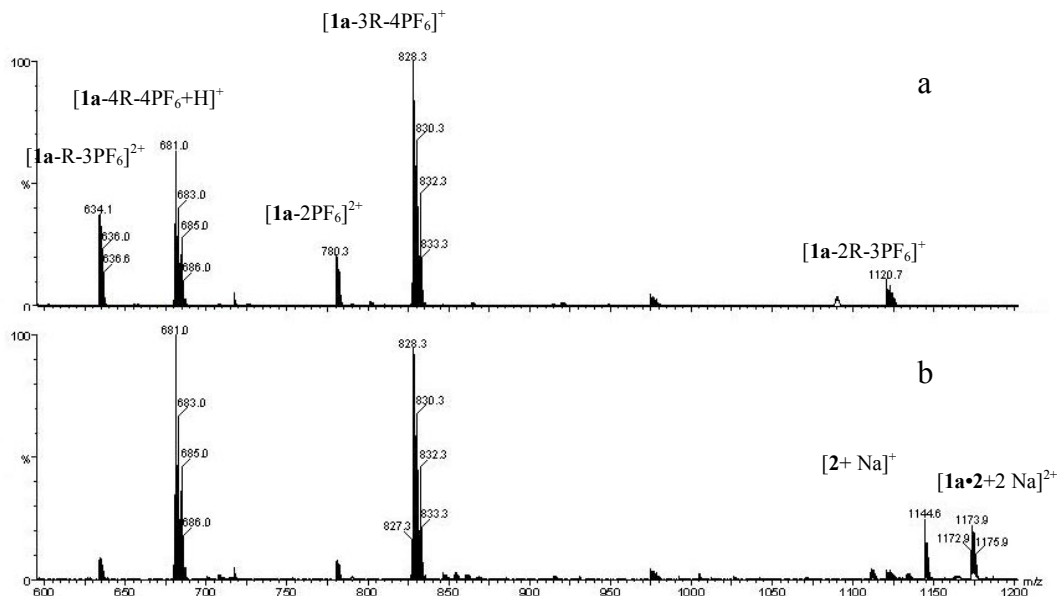


**Figure 8.** ESI-TOF mass spectra of (a) porphyrin **1a**, (b) assembly **1a•2**.

*ESI-TOF Mass Spectrometry.* Formation of assembly **1a•2** was also investigated by nano-ESI-TOF mass spectrometry.<sup>23</sup> Using the appropriate experimental conditions, ESI-MS allows the detection of intact noncovalent complexes.<sup>24</sup> Analysis of an equimolar mixture of **1a** and **2** dissolved in acetonitrile and further diluted with MeOH to a 50  $\mu$ M concentration showed a signal at  $m/z$  1173 for the doubly charged species  $[\mathbf{1a}\cdot\mathbf{2}+2\text{Na}]^{2+}$  (Figure 8). The spectrum also shows two large peaks at  $m/z$  681 and 828, corresponding to porphyrin **1a** that has lost four or three alkyl groups (R) respectively ( $[\mathbf{1a-4R-4PF}_6+\text{H}]^+$  and  $[\mathbf{1a-3R-4PF}_6]^+$ ), under the mass spectrometric conditions and a third peak at  $m/z$  1144 corresponding to free calix[4]arene  $[\mathbf{2}+\text{Na}]^+$ . Other small peaks are also present at  $m/z$  634 and 780 for the monodealkylated species  $[\mathbf{1a-R-3PF}_6]^{2+}$  and for the intact porphyrin  $[\mathbf{1a-2PF}_6]^{2+}$ . ESI-TOF-MS analysis of a sample of porphyrin **1a** alone also showed the same dealkylation pattern.

*Enthalpic and Entropic Contribution to the Binding Process.* For a better understanding of the assembly process, the thermodynamic parameters associated with the formation of **1•2** were determined either using variable temperature UV/vis titration experiments or isothermal titration microcalorimetry (ITC) measurements (Table 2).

**Table 2.** Thermodynamic parameters for the formation of **1•2**

Assembly	Solvent	$\Delta H$ (kJ mol <sup>-1</sup> )	$\Delta S$ (J mol <sup>-1</sup> K <sup>-1</sup> )
<b>1a•2</b>	MeOH	$-8.0 \pm 6.7^a$	$+129 \pm 24^a$
<b>1d•2</b>	MeOH/H <sub>2</sub> O ( $x_{water} = 0.45$ )	$+13.2 \pm 0.4^b$	$+148 \pm 3^b$

[porphyrin] =  $2-3 \times 10^{-6}$  M (UV-vis),  $9.5 \times 10^{-5}$  M (ITC). <sup>a</sup> VT UV,  $K_{1•2}$  measured at 7 different temperatures (errors are standard deviations obtained from the linear regression); <sup>b</sup> ITC, 25 °C,  $1 \times 10^{-2}$  M Bu<sub>4</sub>NClO<sub>4</sub> (errors are standard deviations of three measurements).

In pure MeOH, the formation of assembly **1a•2** did not show any appreciable heat effect in an attempted ITC measurement, thus preventing the use of this powerful technique in this specific case. The thermodynamic parameters were thus indirectly determined by van't Hoff analysis of VT UV-studies (see Figure 9). The low enthalpy measured in this way (especially if the error of the determination is considered) is in agreement with the ITC observation. The process is therefore almost entirely entropy driven.

The formation of assembly **1d•2** could instead be conveniently studied in a MeOH/H<sub>2</sub>O mixture ( $x_{water} = 45\%$ ) with Bu<sub>4</sub>NClO<sub>4</sub> ( $1 \times 10^{-2}$  M) as the support electrolyte via ITC measurements (see Figure 10) due to the more polar nature of porphyrin **1d**. The assembly formation is still strongly entropically driven ( $\Delta S = 148 \pm 3$  J K<sup>-1</sup> mol<sup>-1</sup>). The positive enthalpy change observed in this case ( $\Delta H = 13.2 \pm 0.4$  kJ mol<sup>-1</sup>) likely arises from a positive enthalpy of desolvation, which overrides the expected negative enthalpy for complex formation.  $K_{1•2}$  for the assembly **1d•2** in this solvent mixture is 1.43 logarithmic units (corresponding to 27 times) smaller than that measured in pure MeOH (see Table 1), reflecting the weakening of electrostatic interactions in a solvent mixture with a higher dielectric constant and containing 100 equivalents of Bu<sub>4</sub>NClO<sub>4</sub>.



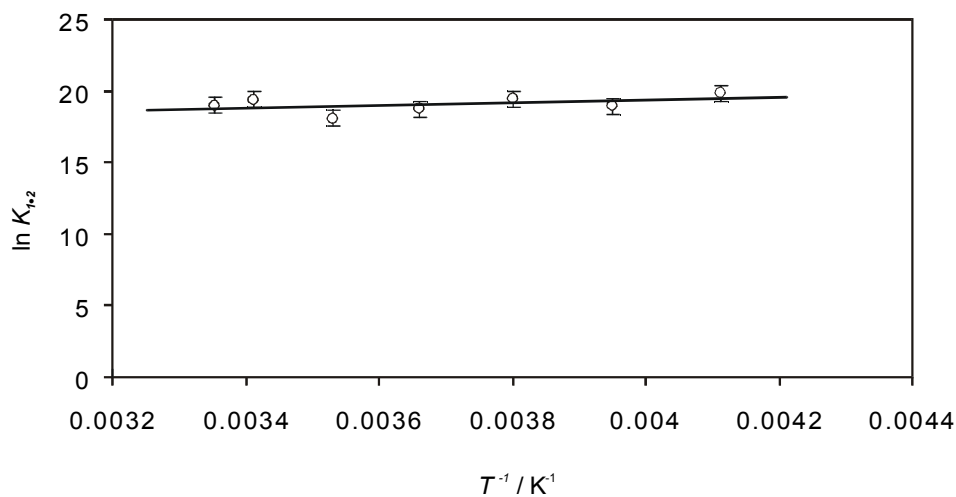


**Figure 9.** Van't Hoff plot from VT UV-studies for the formation of assembly **1a•2** in MeOH (temperature interval 243.1–298.2 K). Note that the concentration measure unit in these experiments is molality (m); therefore  $K_{1,2}$  is expressed in  $m^{-1}$ .

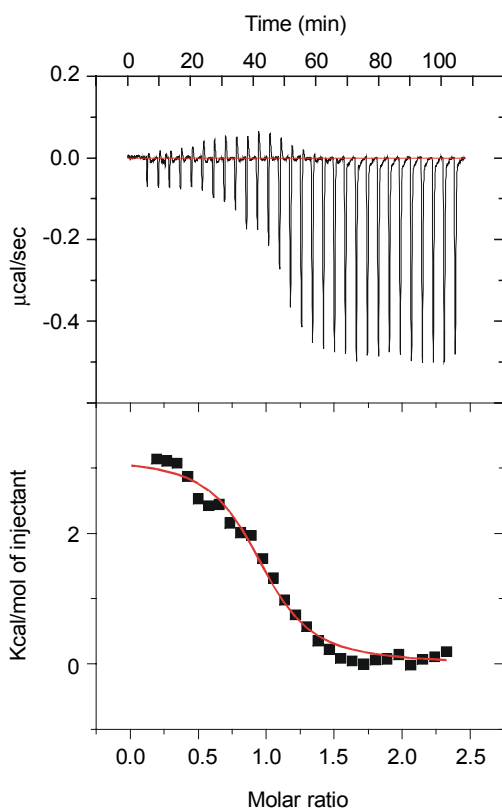


**Figure 10.** ITC titration of porphyrin **1d** ( $9.5 \times 10^{-5}$  M in MeOH/H<sub>2</sub>O,  $x_{\text{water}} = 45\%$ ,  $[\text{Bu}_4\text{NClO}_4] = 1 \times 10^{-2}$  M) with calix[4]arene **2** at 25 °C. The plot shows the heat evolved per injection of titrant as a function of [1d]/[2] ratio.

*Solvent and Salt Effects.* The stability of complexes **1•2** was investigated in different polar solvents and in the presence of added salts. The complexes remain stable in a range of polar solvents with a degree of complexation  $\geq 95\%$  at millimolar concentration (see Table 1). For system **1a•2**, the association constant in polar aprotic solvents, like DMSO and DMPU ( $\text{Log } K_{1,2} \sim 6.2$ ) is around one logarithmic unit (10 times) smaller than in MeOH ( $\text{Log } K_{1,2} = 7.11$ ). A similar value ( $\text{Log } K_{1,2} = 6.04$ ) was also obtained when water was added to DMPU ( $x_{\text{water}} = 0.26$ ). These results indicate that MeOH is the superior solvent for the assembly formation and suggest a stabilizing effect possibly due to the inclusion of one (or two hydrogen-bonded<sup>25</sup>) solvent molecule(s) within the assembly cavity. This idea is also supported by molecular simulation studies that confirm that one MeOH molecule can be accommodated without any distortion of the cavity (Figure 11).<sup>#</sup>

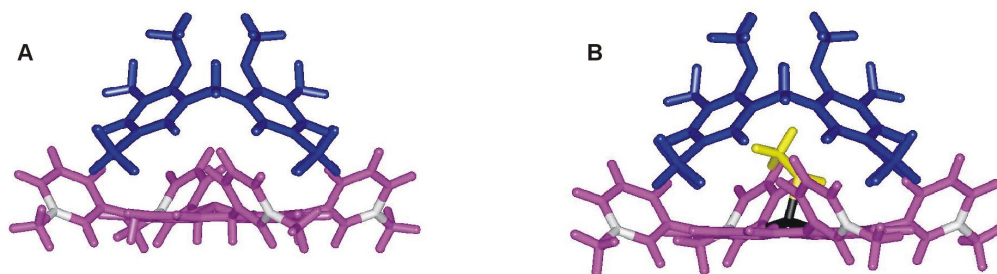


**Figure 11.** Molecular simulation (CHARMm 24.0) of assembly **1•2**: (A) empty cavity, (B) cavity filled with MeOH. For simplicity, the *N*-alkyl groups shown are methyls.

When stability measurements were performed in DMSO in the presence of  $10^{-2}$  M  $\text{Bu}_4\text{NClO}_4$  (4500 times the concentration of the building blocks),  $K_{1,2}$  was observed to decrease only 10 times ( $\text{Log } K_{1,2} = 5.22$ ) in comparison to pure DMSO ( $\text{Log } K_{1,2} = 6.21$ ). However, in the presence of  $10^{-2}$  M  $\text{NaClO}_4$  an association constant 45 times lower was obtained ( $\text{Log } K_{1,2} = 4.56$ ). A more detailed study of  $K_{1,2}$  as a function of the  $\text{NaClO}_4$  concentration showed that the effect is probably due to a specific interaction of the  $\text{Na}^+$  cation with calix[4]arene **2**. A logarithmic plot of  $K_{1,2}$  vs  $[\text{NaClO}_4]$  shows a bimodal

<sup>#</sup> Also for these molecular simulation studies, only the  $\alpha\alpha\alpha\alpha$  isomer has been considered. Under this condition, the simulation shows that bulkier solvents like DMSO and DMPU might be less efficient in

linear dependence of  $K_{1,2}$  with a slope of  $1.91 \pm 0.11$  for  $[\text{NaClO}_4] > 2 \times 10^{-3} \text{ M}$  (Figure 12), suggesting weak binding of two  $\text{Na}^+$  ions ( $\beta = 2.2 \times 10^{-5} \text{ M}^{-2}$ ) most likely to the lower rim of the calix[4]arene moiety.

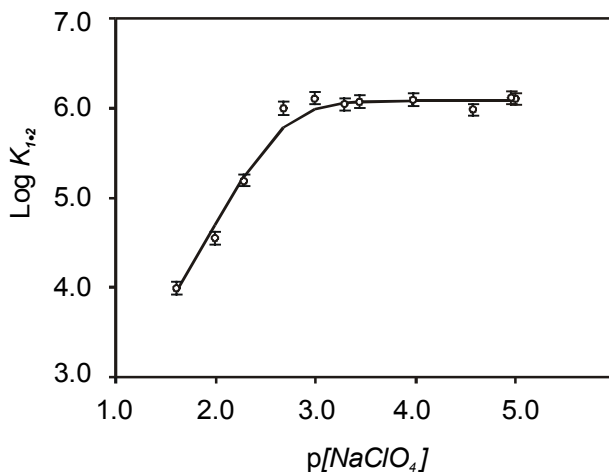


**Figure 12.** Effect of the presence of  $\text{NaClO}_4$  on the formation of assembly  $\mathbf{1a}\cdot\mathbf{2}$ .

The complexation appears to be cooperative as indicated by the sharp curvature at the breaking point. In terms of molecular structure of calix[4]arene  $\mathbf{2}$ , the observed cooperativity is most probably attributable to the preorganization of the ethoxy-ethoxy chains after the first  $\text{Na}^+$  ion has been complexed to the lower rim oxygens.

### 3.2.3 Ligand Binding Studies

We have also studied the coordination of axial ligands  $\mathbf{L}$  to the zinc center of assembly  $\mathbf{1a}\cdot\mathbf{2}$  to give ternary complexes  $\mathbf{1a}\cdot\mathbf{2}\cdot\mathbf{L}$ . Zinc porphyrins are known to bind only one axial ligand molecule and therefore represent the simplest model system to study axial coordination to metalloporphyrins.

UV-vis titration experiments using 1-methylimidazole (1-MeIm) or pyridine as axial ligands ( $\mathbf{L}$ ), clearly showed the formation of the expected ternary complexes  $\mathbf{1a}\cdot\mathbf{2}\cdot\mathbf{L}$ .

---

filling the cavity because they cause a distortion of the  $\mathbf{1}\cdot\mathbf{2}$  complex.

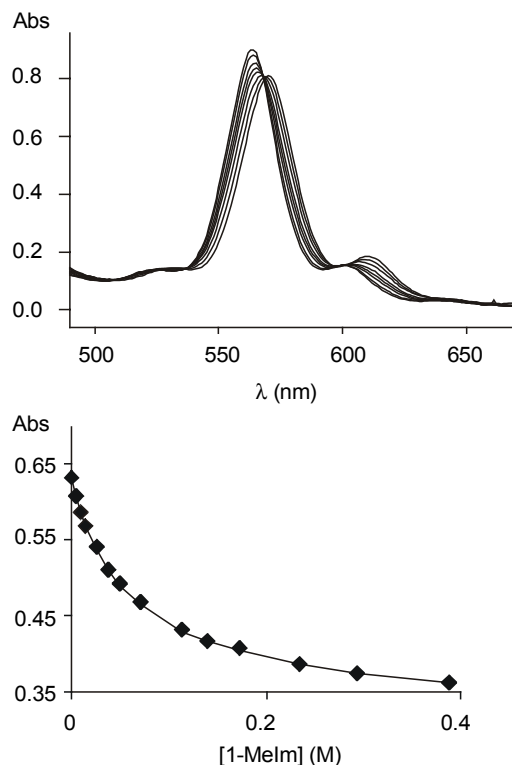


**Figure 13.** Spectral evolution of a 1:1 mixture of porphyrin **1a** and calix[4]arene **2** in MeOH ( $4 \times 10^{-5}$  M, assembly **1a•2** >95% in solution) titrated with 1-MeIm. The lower part shows the fitting of the titration curve at 555 nm.

The observed spectral changes in the Q bands region (see Figure 13) were fitted to a 1:1:1 equilibrium model in order to obtain values for the equilibrium constant  $K_{1a•2•L}$  (eqs. 1-3).



The binding constant for the axial ligand **L** to porphyrin **1a** ( $K_{1a•L}$ , eq. 2) was determined in a separate experiment and  $K_{1•2}$  is the formation constant for assembly **1a•2** (see Table 1) under the same experimental conditions. The ratio  $K_{1a•2•L}/K_{1•2}$  represents the ligand affinity displayed by assembly **1a•2**.

The results reported in Table 3 clearly show that in general  $K_{1a\cdot 2\cdot L}/K_{1\cdot 2} \leq K_{1a\cdot L}$ , which indicates that no cavity effect is observed.<sup>s</sup> Two potential reasons could be responsible for this observation: i) the cavity is too small to accommodate the ligand, and ii) the cavity is occupied by solvent molecules and there is not a very strong enthalpic effect for the ligand to drive the encapsulation process.

**Table 3.** Complexation of ligands by porphyrin **1a** and assembly **1a•2**

	1-MeIm		Pyridine	
	$K_{1a\cdot 2\cdot L} / K_{1\cdot 2} (M^{-1})$	$K_{1a\cdot L} (M^{-1})$	$K_{1a\cdot 2\cdot L} / K_{1\cdot 2} (M^{-1})$	$K_{1a\cdot L} (M^{-1})$
DMSO	$53 \pm 1$	$53 \pm 1$	n.d.	n.d.
MeOH	$17.0 \pm 0.5$	$62 \pm 1$	$2.0 \pm 0.2$	$5.9 \pm 0.1$

T = 25 °C, [porphyrin] = [calix] =  $3\text{--}4 \times 10^{-5}$  M (UV-vis). Given errors are standard deviations of three measurements.

The first option seems improbable considering that the absence of directionality in ion-pair interactions and their weak dependence on distance (proportional to  $r^{-1}$ ),<sup>26</sup> should result in rather flexible assemblies able to encapsulate either solvent molecules or the desired guest. The second option is therefore the most likely explanation: MeOH is in fact the solvent in which the largest drop in binding strength for a given ligand **L** is observed ( $K_{1\cdot 2\cdot L} / K_{1\cdot 2} \leq 1/3 K_{1\cdot L}$ ). This result is in agreement with the fact that MeOH was found to be the best solvent for the assembly formation, possibly due to a reasonably strong template effect (vide supra).

<sup>s</sup> It has generally been observed for covalently capped Zn-porphyrins that complexation of guests of appropriate dimension within the host cavity leads to enhanced binding affinity. However, the magnitude of the effect is determined by the rigidity of the host.<sup>29</sup>

### 3.3 Summary and Outlook

This chapter reports the high thermodynamic stability of noncovalent calix[4]arene-capped porphyrins in polar solvents and in organic solvent/water mixtures with as much as  $x_{water} = 45\%$ . These systems remain remarkably stable even upon addition of an excess of electrolytes such as  $Bu_4NClO_4$  or  $NaClO_4$ .

The results described in this chapter constitute the basis for the development of a fully water soluble system, i.e. a closer model for natural porphyrins under physiological conditions (Chapters 4 and 5). Moreover, as described in Chapter 4, the recognition properties of similar ion-pair driven assemblies in aqueous media are different from what was observed here, favoring encapsulation (according to the larger influence of hydrophobic interactions). The highly dynamic nature of these assemblies together with their peculiar ligand recognition properties could be useful in catalytic applications.

### 3.4 Experimental

#### 3.4.1 General information and instrumentation

All reagents used were purchased from Aldrich or Acros Organics and used without further purification. All the reactions were performed under nitrogen atmosphere. Compound **1b** was prepared according to literature.<sup>18</sup>

Infrared spectra were recorded on a FT-IR Perkin Elmer Spectrum BX spectrometer and only characteristic absorptions are reported.  $^1H$  NMR and  $^{13}C$  NMR spectra were performed on a Varian Unity INOVA (300 MHz) or a Varian Unity 400 WB NMR spectrometer.  $^1H$  NMR chemical shift values (300 MHz) are expressed in ppm relative to residual  $CHD_2OD$  ( $\delta$  3.30),  $CHD_2CN$  ( $\delta$  1.93), or  $CHCl_3$  ( $\delta$  7.26).  $^{13}C$  NMR chemical shift values (100 MHz) are expressed in ppm relative to residual  $CD_3OD$  ( $\delta$  49.0) or  $CD_3CN$  ( $\delta$  1.3). UV-vis measurements were performed on a Varian Cary 3E UV-vis spectrophotometer equipped with a Helma QX optical fiber probe (path length = 1.000 cm), using solvents of spectroscopic grade. Calorimetric measurements were carried out using a Microcal VP-ITC microcalorimeter with a cell volume of 1.4115 ml. Elemental analyses were carried out on a 1106 Carlo-Erba Strumentazione element analyzer.

Electrospray ionization mass spectra were recorded on a Micromass LCT time-of-flight mass spectrometer. Samples were introduced using a nanospray source. Molecular simulation studies were carried out as described elsewhere.<sup>27</sup>

### 3.4.2 Binding studies

*UV-Vis:* Association constants for assemblies **1•2** were evaluated by measuring the absorbance changes upon addition of increasing amount of a calix[4]arene **2** solution to a porphyrin **1** solution ( $2 - 3 \times 10^{-6}$  M). Each titration consisted of 15 to 20 additions. The calix[4]arene solution was at a concentration high enough so that the degree of complexation during the titration was between about 20 and 80%, and the overall dilution was less than 3%. The experimental spectral changes for assembly formation were fitted to a 1:1 binding model using a non-linear least squares fitting procedure<sup>28</sup> that considered the information coming from 6 different wavelengths (model written with program Scientist<sup>®</sup>, MicroMath<sup>®</sup>). The binding constants for axial ligands were determined according to a 1:1:1 binding model using a non-linear least squares fitting procedure considering the absorbance changes at one wavelength (the fitting procedure was generally repeated for two different wavelengths and the results averaged, model written with program Microsoft<sup>®</sup> Excel).

### 3.4.3 Synthesis

*General procedure for the preparation of [5,10,15,20-tetrakis(N-alkylpyridinium-3-yl)porphyrinato]zinc(II) (1a, 1c).*

A solution of 5,10,15,20-tetra(3-pyridyl)porphyrin **5** (100 mg, 0.161 mmol) and the appropriate alkylbromide (100-200 equivalents, *p-t*-butylbenzylbromide for **1a** and 1-bromo-3-methylbutane for **1c**) in DMF (30-50 ml) was stirred for 8-17 h at 80 °C. The reaction was monitored by TLC (silica gel 60F<sub>254</sub>, CH<sub>3</sub>CN/(3 mg/ml NH<sub>4</sub>PF<sub>6</sub> in H<sub>2</sub>O) 7:3). The DMF was evaporated under vacuum, the solid residue was triturated with diethyl ether and subsequently dried under vacuum. The crude products were used without further purification in the following metalation reaction.

Metallation with Zn was carried out by stirring the alkylated porphyrin in MeOH saturated with ZnAc<sub>2</sub> at room temperature for 1h, after which a solution of NH<sub>4</sub>PF<sub>6</sub> in

water was added to precipitate the metallated porphyrin. The solid product (metallated porphyrin **1** PF<sub>6</sub> salt) was filtered off and washed extensively with water and ether.

**5,10,15,20-tetrakis(*N-p-t*-butylbenzylpyridinium-3-yl)porphyrin (free base **1a**)**

Purification of an analytical sample of free-base **1a** was performed by dissolving the crude product in MeOH and precipitating by addition of a solution of NH<sub>4</sub>PF<sub>6</sub> in water. The precipitate was filtered off and washed extensively with water and ether. The chloride salt of **1a** was obtained by passing the PF<sub>6</sub> salt through an ion-exchange column (DOWEX 1-X8, 50-100 mesh, Cl-form) using CH<sub>3</sub>CN/H<sub>2</sub>O 1:1 v/v as the eluent. The eluted solution was concentrated under vacuum and lyophilized to afford the product as a brown solid. Yield: 85%.

<sup>1</sup>H NMR (CD<sub>3</sub>OD) δ 10.10 (m, 4H), 9.58 (d, J=6.0 Hz, 4H), 9.44 (d, J=7.9 Hz, 4H), 9.07 (br s, 8H), 8.61 (m, 4H), 7.65 (m, 16H), 6.18 (s, 8H), 1.34 (s, 36H); <sup>13</sup>C NMR δ 154.86, 150.40, 148.32, 145.79, 143.24, 131.71, 130.32, 128.47, 127.88, 114.41, 66.19, 35.73, 31.64; IR (KBr) 3414, 3068, 2962, 2868, 1628, 1499, 1465, 1196, 979, 794; UV-vis (MeOH) 422, 512, 544, 586, 643; Anal. Calcd for C<sub>84</sub>H<sub>86</sub>N<sub>8</sub>Cl<sub>4</sub>×9 H<sub>2</sub>O: C 66.75, H 6.93 N 7.41, Found: C 66.85, H 6.57, N 7.30.

Hexafluorophosphate salt:

<sup>1</sup>H NMR (CD<sub>3</sub>CN) δ 9.56 (m, 4H), 9.26 (m, 8H), 9.00 (s, 4H), 8.94(s, 4H), 8.52 (t, J=7.0 Hz, 4H), 7.58 (m, 16H), 6.02 (s, 8H), 1.30 (s, 36H), -3.15 (s, 2H).

**[5,10,15,20-tetrakis(*N-p-t*-butylbenzylpyridinium-3-yl)porphyrinato]zinc(II) (**1a**)**

Yield: 80% (alkylation + metallation)

<sup>1</sup>H NMR (CD<sub>3</sub>OD) δ 9.93 (m, 4H), 9.48 (m, 4H), 9.35 (d, J=7.7 Hz, 4H), 8.99 (s, 4H), 8.93 (s, 4H), 8.54 (t, J=7.0 Hz, 4H), 7.64 (m, 16H), 6.13 (s, 8H), 1.33 (s, 36H); UV-vis (MeOH) 433, 521, 560, 596; Anal. Calcd for C<sub>84</sub>H<sub>84</sub>N<sub>8</sub>P<sub>4</sub>F<sub>24</sub>Zn: C 54.51, H 4.57 N 6.05, Found: C 54.15, H 4.49, N 5.91.

**[5,10,15,20-tetrakis(*N*-(3-methylbutyl)pyridinium-3-yl)porphyrinato]zinc(II) (**1c**)**

Yield: 91 % (alkylation + metallation)



$^1\text{H}$  NMR ( $\text{CD}_3\text{CN}$ )  $\delta$  9.53 (m, 4H), 9.20 (m, 8H), 9.00 (m, 8H), 8.47 (t,  $J=7.0$  Hz, 4H), 4.85 (t,  $J=7.8$  Hz, 8H), 2.15 (m, 8H), 1.87 (sept,  $J=6.5$  Hz, 4H), 1.05 (d,  $J=6.5$  Hz, 24H);  $^{13}\text{C}$  NMR  $\delta$  151.36, 149.52, 147.09, 145.11, 143.96, 133.99, 128.02, 114.26, 62.02, 40.96, 26.80, 22.58; IR (KBr) 3107, 2960, 2875, 1629, 1498, 1200, 1159, 843, 558; UV-vis (MeOH) 431, 520, 559, 597, 633; Anal. Calcd for  $\text{C}_{60}\text{H}_{68}\text{N}_8\text{F}_{24}\text{P}_4\text{Zn}$ : C 46.60, H 4.43 N 7.25, Found: C 46.41, H 4.29, N 7.33.

**[5,10,15,20-tetrakis(*N*-(4-acetylmorpholyl)pyridinium-3-yl)porphyrinato]zinc(II)**

**(1d)**

5,10,15,20-tetra(3-pyridyl)porphyrin **5** (200 mg, 0.323 mmol) and chloroacetyl morpholine (240 mg, 1.45 mmol) were dissolved in acetonitrile (30 ml). NaI (218 mg, 1.45 mmol) was added and the mixture was refluxed for 21 h. The solvent was then removed under vacuum and the residue triturated with ether and redissolved in MeOH. The product was precipitated by addition of  $\text{NH}_4\text{PF}_6$  in water, filtered off and washed with water and ether to afford crude alkylated porphyrin in 91% yield (0.28 mmol, 502 mg). Metallation with  $\text{ZnAc}_2$  as previously described, afforded **1d** as a purple solid in 85% yield.

$^1\text{H}$  NMR ( $\text{CD}_3\text{CN}$ )  $\delta$  9.26 (m, 4H), 9.17 (d,  $J=8.0$  Hz, 4H), 8.91 (s, 12H), 8.36 (t,  $J=7.0$  Hz, 4H), 5.63 (s, 8H), 3.63-3.36 (m, 32H);  $^{13}\text{C}$  NMR  $\delta$  164.02, 151.33, 150.43, 149.24, 146.21, 143.00, 133.97, 127.47, 114.17, 67.201, 66.96, 62.96, 46.17, 43.87; IR (KBr) 3101, 2932, 2866, 1661, 1450, 1246, 1112, 842, 558; UV-vis (MeOH) 432, 520, 559, 596, 636; Anal. Calcd for  $\text{C}_{64}\text{H}_{64}\text{N}_{12}\text{O}_8\text{F}_{24}\text{P}_4\text{Zn}$ : C 43.32, H 3.64 N 9.47, Found: C 43.31, H 3.42, N 9.42.

**5,11,17,23-Tetrasulfonato-25,26,27,28-tetrakis(2-ethoxyethoxy)calix[4]arene,**

**tetrasodiumsalt (2).** The compound was prepared by a slightly modified literature procedure.<sup>20</sup>

25,26,27,28-tetrakis(2-ethoxyethoxy)calix[4]arene<sup>19</sup> (2.00 g, 2.80 mmol) was dissolved in  $\text{H}_2\text{SO}_4$  (96%, 5 ml) and stirred at room temperature for 2 h. The reaction mixture was then quenched by pouring it carefully into water and neutralized by addition of a NaOH solution. The water was then removed under reduced pressure and the solid residue was

extracted overnight with MeOH using a Soxhlet extractor. The crude product was then purified by reversed phase chromatography (Merck Lobar column, LiChroprep RP8, 40-63  $\mu\text{m}$ ) eluting initially with pure water until no more inorganic sulfates were detected (i.e. no precipitation observed upon addition of  $\text{BaCl}_2$  to the eluate). Pure **2** was obtained by elution in a step-gradient to 70% EtOH/H<sub>2</sub>O (v/v). The eluted fractions were concentrated under vacuum and lyophilized affording **2** as a white solid in 84% yield (2.36 mmol, 2.65 g). The analytical data for the compound were identical to the reported ones.<sup>20</sup>

### 3.5 References

1. *Biochemistry*, 4th ed.; Stryer, L.; W.H. Freeman & Co: New York, 1995.
2. *Cytochrome P-450: Structure, Mechanism and Biochemistry*, 2nd ed.; Ortiz de Montellano, P. R., ed.; Plenum Press: New York, 1995.
3. *Peroxidases in Chemistry and Biology*; Everse, J.; Everse, K. E.; Grisham, M. P., ed.; CRC Press: Boca Raton, FL, 1991; Vol. I and II.
4. Feiters, M. C. *Comprehensive Supramolecular Chemistry*; Atwood, J. L.; Davies, J. E. D.; MacNicol, D. D.; Vögtle, F.; Reinhoudt, D. N.; Lehn, J.-M., eds; Elsevier Science Ltd. Pergamon: Elmsford, 1996; Vol. 10, pp 267-360.
5. Momenteau, M.; Reed, C. A. *Chem. Rev.* **1994**, *94*, 659-698.
6. Jones, R. D.; Summerville, D. A.; Basolo, F. *Chem. Rev.* **1979**, *79*, 139-179.
7. Wojaczynski, J.; Latos-Grazynski, L. *Coord. Chem. Rev.* **2000**, *204*, 113-171.
8. Drain, C. M.; Russel, K. C.; Lehn, J.-M. *Chem. Commun.* **1996**, 337-338.
9. Ruhlmann, L.; Nakamura, A.; Vos, J. G.; Fuhrhop, J.-H. *Inorg. Chem.* **1998**, *37*, 6052.
10. Yamamoto, K.; Nakazawa, S.; Matsufuji, A.; Taguchi, T. *J. Chem. Soc., Dalton*

- Trans.* **2001**, 251-258.
11. Sirish, M.; Schneider, H.-J. *Chem. Commun.* **2000**, 23-24.
  12. Zhao, S.; Luong, J. H. T. *J. Chem. Soc., Chem. Commun.* **1995**, 663-664.
  13. Ribò, J. M.; Farrera, J.-A.; Valero, M. L.; Virgili, A. *Tetrahedron* **1995**, *51*, 3705-3712.
  14. Manka, J. S.; Lawrence, D. S. *J. Am. Chem. Soc.* **1990**, *112*, 2440-2442.
  15. Lahiri, J.; Fate, G. D.; Ungashe, S. B.; Groves, J. T. *J. Am. Chem. Soc.* **1996**, *118*, 2347-2358.
  16. Tecilla, P.; Dixon, R. P.; Slobodkin, G.; Alavi, D. S.; Waldeck, D. H.; Hamilton, A. D. *J. Am. Chem. Soc.* **1990**, *112*, 9408-9410.
  17. Takeuchi, M.; Kijima, H.; Hamachi, I.; Shinkai, S. *Bull. Chem. Soc. Jpn.* **1997**, *70*, 699-705.
  18. Mizutani, T.; Horiguchi, T.; Koyama, H.; Uratani, I.; Ogoshi, H. *Bull. Chem. Soc. Jpn.* **1998**, *71*, 413-418.
  19. Arduini, A.; Casnati, A.; Fabbi, M.; Minari, P.; Pochini, A.; Sicuri, A. R.; Ungaro, R. *Supramolecular Chemistry* **1993**, *1*, 235-246.
  20. Casnati, A.; Ting, Y.; Berti, D.; Fabbi, M.; Pochini, A.; Ungaro, R.; Sciotto, D.; Lombardo, G. G. *Tetrahedron* **1993**, *49*, 9815-9822.
  21. Crossley, M. J.; Field, L. D.; Forster, A. J.; Harding, M. M.; Sternhell, S. *J. Am. Chem. Soc.* **1987**, *109*, 341-348.
  22. Hamelin, B.; Jullien, L.; Derouet, C.; Hervé du Penhoat, C.; Berthault, P. *J. Am. Chem. Soc.* **1998**, *120*, 8438-8447.
  23. Brody, M. S.; Schalley, C. A.; Rudkevich, D. M.; Rebek, Jr. *J. Angew. Chem., Int. Ed.* **1999**, *38*, 1640-1644.

24. Staroske, T.; O'Brien, D. P.; Jørgensen, T. J. D.; Roepstorff, P.; William, D. H.; Heck, A. J. R. *Chem. Eur. J.* **2000**, *6*, 504-509.
25. Bonar-Law, R. P.; Sanders, J. K. M. *J. Am. Chem. Soc.* **1995**, *117*, 259-271.
26. Hossain, M. A.; Schneider, H.-J. *Chem. Eur. J.* **1999**, *5*, 1284-1290.
27. Timmerman, P.; Weidmann, J.-L.; Jolliffe, K. A.; Prins, L. J.; Reinhoudt, D. N.; Shinkai, S.; Frish, L.; Cohen, Y. *J. Chem. Soc., Perkin Trans. 2* **2000**, 2077-2089.
28. Leggett, D. J.; Kelly, S. L.; Shiue, L. R.; Wu, Y. T.; Chang, D.; Kadish, K. M. *Talanta* **1983**, *30*, 579-586.
29. Rudkevich, D. M.; Verboom, W.; Reinhoudt, D. N. *J. Org. Chem.* **1995**, *60*, 6585-6587.



### STRUCTURAL WATER SOLUBLE MODELS OF THE HEME-PROTEIN ACTIVE SITE VIA SELF-ASSEMBLY\*

*The noncovalent strategy outlined in Chapter 3 for the preparation of cage-like complexes with anionic calix[4]arenes and cationic porphyrins has been applied to the preparation of water soluble structural mimics of heme-protein active sites. Novel porphyrin-peptide conjugates have been used as building blocks. The complexes encapsulate small nitrogenous bases such as 4-methylpyridine and 1-methylimidazole but bind the bulkier caffeine on the solvent exposed porphyrin face.*

#### 4.1 Introduction

Synthetic models of heme-protein active sites have been investigated extensively to understand the basic structural features associated with the functioning of different biological systems.<sup>1-3</sup> From the structural point of view, the active site of a heme-protein is essentially a hydrophobic cavity of appropriate dimensions enclosed between the protein matrix and the metal porphyrin. This cavity is accessible to exogenous ligands like O<sub>2</sub> and CO in the case of hemoglobin and myoglobin,<sup>4</sup> or to a substrate molecule in case of cytochrome P450 (see Figure 11 Chapter 2 for a schematic representation of the active site in O<sub>2</sub> binding heme-protein).<sup>5</sup>

Two different approaches to the mimicry of heme-protein active sites are described in the literature i.e. covalent<sup>1,2</sup> and noncovalent<sup>6,7</sup> synthesis. Using the first approach, a great

---

\* Part of this chapter has been submitted for publication: Fiammengo, R.; Wojciechowski, K.; Crego-Calama, M.; Timmerman, P.; Reinhoudt, D. N.

number of synthetic model systems have been prepared in which the hydrophobic cavity (resembling the natural active site) is formed combining covalently porphyrins with organic substituents. Remarkable examples of this strategy are the “picket fence”,<sup>8,9</sup> “pocket”,<sup>10</sup> and “capped”<sup>11,12</sup> porphyrins. However, most of these systems suffer from the limitation of being water not soluble,<sup>13,14</sup> which is an important requisite when mimicry of a natural system is attempted. Covalent porphyrin-peptide conjugates have also been widely used to model the heme group and its closest proteic environment in water.<sup>3</sup>

In addition to the synthetic simplicity, the main advantage of the noncovalent approach is that it allows more accurate reproduction of the interactions between the porphyrin core and the proteic matrix in natural proteins.<sup>15</sup> Water soluble peptide-porphyrin combinations based on metal coordination have been obtained,<sup>3,16</sup> but major challenges such as control over the folding properties of the chosen peptides remain.

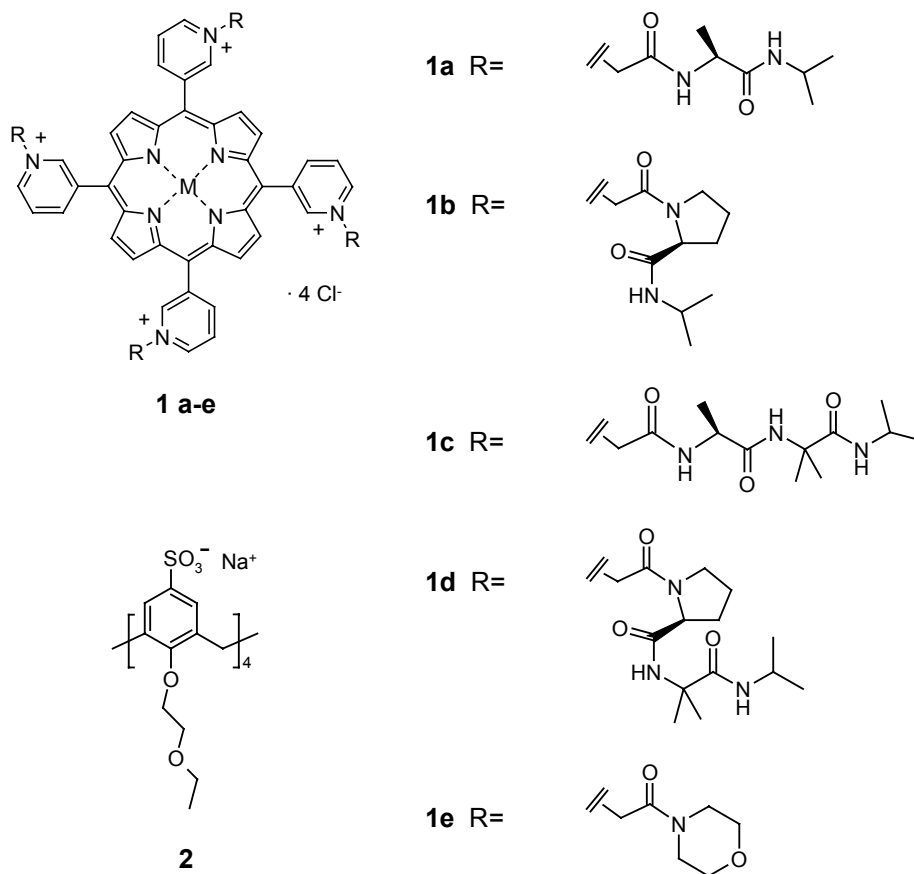
According to the major focus of this thesis viz. the development of self-assembly systems that possess biomimetic functions,<sup>17</sup> the work reported in this chapter concerns water soluble self-assembled models of heme-protein active sites. These are the first examples of simple structural analogues of the heme-proteins active site obtained via self-assembly of cage-like complexes by ionic interaction.<sup>18-20</sup>

In Chapter 3 the formation of strong 1:1 complexes between tetracationic Zn-porphyrinates and tetraanionic tetrasulfonato calix[4]arene **2** (see Chart 1) in polar organic solvents such as methanol, DMSO and DMPU, or in organic solvent/water mixtures has been described.<sup>21</sup> Unfortunately, the solubility of the assemblies in pure water was too low. Here, an improved design of the porphyrin building blocks, which allows the self-assembly process to occur in pure water, is presented. The short peptides attached to the pyridyl nitrogens of porphyrins **1** ( $M = \text{Zn}^{2+}$ ,  $\text{Co}^{2+}$  see Chart 1) are responsible for the relatively large water solubility of assemblies **1•2** (concentrations up to 2-5 mM).<sup>22</sup> These ensembles exhibited association constants  $K_{1,2}$  in aqueous carbonate buffer solution as high as  $10^5 \text{ M}^{-1}$  (for structure of the assembly see Figure 2).

Furthermore, in previous noncovalent synthetic models for heme-protein reported by other groups,<sup>6,23</sup> no attention was given to the binding properties of the metal porphyrin moiety. In Chapter 3 it was shown that self-assembled cage-like porphyrin-calix[4]arene complexes form ternary complexes upon addition of nitrogenous ligands.<sup>21</sup> Nevertheless,

binding of the added ligands to the Zn-porphyrin moiety in polar solvents consistently occurred on the solvent exposed porphyrin face, probably due to unfavorable competition with the solvent for the assembly cavity. In contrast, the data reported here show that, *using water as the solvent* for assemblies **1•2**, coordination of nitrogenous bases to the Zn-center affords ternary complexes with diverse topology. The structure of the complexes is directed by the sterical requirements of the base used. Small bases such as 4-methyl pyridine are complexed preferentially inside the hydrophobic cavity of assemblies **1c•2** and **1e•2**, while larger molecules such as caffeine are bound outside the cavity (**1c•2**) on the solvent-exposed porphyrin face. Moreover, Co<sup>II</sup> porphyrins (Co-**1b**) can also be self-assembled with calix[4]arene **2**, thus opening the way towards *functional* model of heme-protein active-sites (for instance O<sub>2</sub> binding mimics).

Chart 1





## 4.2 Results and discussion

### 4.2.1 Synthesis

Alkylation of the 5,10,15,20-tetra(3-pyridyl)porphyrin pyridyl nitrogens with polar side chains derived from amino acid, dipeptide amides, or morpholine affords water soluble porphyrins **1a-e**.<sup>24</sup> Calix[4]arene tetrasulfonate **2** was prepared according to the procedure described in Chapter 3.

Assemblies **1•2** are easily prepared by mixing aqueous solutions of the molecular building blocks **1a-e** and **2**. Remarkably, no precipitation is observed upon addition of up to 3 equivalents of calix[4]arene **2** to porphyrin solutions of concentrations up to 2-5 mM,<sup>25</sup> conditions ensuring >95% assembly formation (based on  $K_{I,2}$ , vide infra).

### 4.2.2 Assembly formation

*ITC studies.* Self-assembly of Zn porphyrins **1a-e** with calix[4]arene tetrasulfonate **2** was studied in aqueous solutions using isothermal titration microcalorimetry (ITC). The association constants (see Tables 1 and 2) are quite insensitive to the nature of the *N*-substituents. Under similar conditions, the largest difference in binding strength is less than a factor of two for the series of porphyrins **1a-e**.

**Table 1.** Association constants ( $K_{I,2}$ ) for cationic porphyrins **1a-e** (0.090-0.105 M) and anionic calix[4]arene **2** (sodium carbonate buffer, pH = 9.6,  $I = 0.010$  M).

	Log $K_{I,2}$	$\Delta H^\circ$ (kJ mol <sup>-1</sup> )	$\Delta S^\circ$ (J mol <sup>-1</sup> K <sup>-1</sup> )
<b>1a•2</b>	4.90 ± 0.02	-23.9 ± 0.3	-14 ± 1
<b>1b•2</b>	4.82 ± 0.02	-32.5 ± 0.3	-17 ± 1
<b>1c•2</b>	4.68 ± 0.02	-25.8 ± 0.4	-3 ± 2
<b>1d•2</b>	4.90 ± 0.02	-28.9 ± 0.3	+3 ± 1
<b>1e•2</b>	4.69 ± 0.01 <sup>a</sup>	-25.5 ± 0.3	+5 ± 1
	5.62 ± 0.05 <sup>b</sup>	-20.8 ± 0.3	+38 ± 2
	5.43 ± 0.08 <sup>c</sup>	+13.2 ± 0.4	+148 ± 3

<sup>a</sup> Carbonate buffer pH = 9.7,  $I = 0.020$  M; <sup>b</sup> no added salts; <sup>c</sup> MeOH/water ( $x_{\text{water}} = 0.45$ ),  $1 \times 10^{-2}$  M Bu<sub>4</sub>NClO<sub>4</sub>.<sup>21</sup>

Self-assembly of complexes **1a-d•2** in carbonate buffered solutions ( $I = 0.010$  M) is characterized by negative enthalpy and small (close to zero) entropic contributions (Table 1). However, at a higher buffer concentration ( $I = 0.045$  M, Table 2) the formation of **1a-d•2** is accompanied by larger negative enthalpy and entropy changes. The changes tend to compensate each other and the net result is a moderate decrease of the association constants (2-5 times,  $\Delta\text{Log}K_{1,2} \sim 0.4-0.7$ ).

**Table 2.** Association constants ( $K_{1,2}$ ) for cationic porphyrins **1a-e** (0.090 - 0.105 M) and anionic calix[4]arene **2** (sodium carbonate buffer, pH = 10,  $I = 0.045$  M).

	Log $K_{1,2}$	$\Delta H^\circ$ (kJ mol <sup>-1</sup> )	$\Delta S^\circ$ (J mol <sup>-1</sup> K <sup>-1</sup> )
<b>1a•2</b>	4.26 ± 0.04	-33 ± 3	-29 ± 12
<b>1b•2</b>	4.40 ± 0.02	-36 ± 1	-38 ± 5
<b>1c•2</b>	4.11 ± 0.03	-43 ± 2	-64 ± 8
<b>1d•2</b>	4.23 ± 0.02	-40 ± 1	-54 ± 5
Co- <b>1b•2</b>	3.80 ± 0.04	-42 ± 4	-71 ± 15

Measurements on the less soluble assembly **1e•2** also confirm the correlation between changes in buffer concentration and changes in thermodynamic parameters. In the absence of buffer, formation of **1e•2** is even less enthalpically favored ( $\Delta H^\circ = -20.8$  kJ mol<sup>-1</sup>) but much more entropically favored ( $\Delta S^\circ = +38$  J mol<sup>-1</sup> K<sup>-1</sup>). The overall effect is an association strength approximately one order of magnitude higher (Log  $K_{1,2} = 5.62$  vs 4.69 in the presence of carbonate buffer,  $I = 0.020$  M). These observations suggest that assembly formation in aqueous solution is primarily driven by multiple ionic interactions between the two building blocks.

Qualitatively, complex formation is expected to present a negative enthalpy (coulombic energy) and negative entropy (bimolecular reaction). However, desolvation of the ionic groups upon assembly formation is accompanied by a positive entropic contribution (release of ordered solvent molecule to the bulk) and a positive (endothermic) enthalpic contribution. In polar solvents and aqueous solutions the contribution of desolvation is as relevant (and sometimes even more important) as the contribution associated with

complexation.<sup>26-28</sup> Therefore, the balance between these two contributions is the reason for the rather large differences observed in the measured thermodynamic parameters when the same assembly process takes place in different media. Here, the data suggest that at lower salt concentration (resulting in a more ordered solvent shell around the ionic groups) the importance of desolvation in driving the assembly process becomes greater. For instance, desolvation dominates the self-assembly of **1e•2** in MeOH/water ( $x_{\text{water}} = 0.45$ ) with 0.01 M of  $\text{Bu}_4\text{NClO}_4$ , resulting in a positive  $\Delta H^\circ = +13.2 \text{ kJ mol}^{-1}$  and positive  $\Delta S^\circ = +148 \text{ mol}^{-1} \text{ K}^{-1}$ .<sup>21</sup>

*UV-vis studies.* Formation of assembly **1e•2** was confirmed by UV-vis spectrophotometric titrations.<sup>29</sup> Addition of a solution of calix[4]arene **2** to **1e** in aqueous carbonate buffer ( $I = 7.2 \text{ mM}$ ) produced spectral variations in the porphyrin Soret band region (400-480 nm) similar to what was previously observed for the formation of assembly **1e•2** in methanol.<sup>21</sup> The spectral variations (bathochromic shift  $\Delta\lambda_{\text{max}} = 2\text{-}3 \text{ nm}$ ,  $\Delta\epsilon$  at  $\lambda_{\text{max}} = 10\text{-}15\%$ ) could be fitted to a 1:1 model.

**Table 3.** Association constants ( $K_{1e\cdot 2}$  in  $\text{M}^{-1}$ ) for the formation of assembly **1e•2** in water at 25 °C, from UV-vis titrations.

Medium	Log $K_{1\cdot 2}$
$\text{NaNO}_3$ , $I \sim 10 \text{ mM}$ , pH = 8.0	$5.28 \pm 0.03$
$\text{NaNO}_3$ , $I \sim 10 \text{ mM}$ , pH = 4.2 <sup>a</sup>	$5.24 \pm 0.02$
$\text{NaNO}_3$ , $I \sim 10 \text{ mM}$ , pH = 9.5 <sup>b</sup>	$5.24 \pm 0.02$
Phosphate buffer, $I = 8.0 \text{ mM}$ , pH = 7.0	$5.23 \pm 0.02$
Carbonate buffer, $I = 7.2 \text{ mM}$ , pH = 9.4	$5.38 \pm 0.01$
$\text{CH}_3\text{OH}$ <sup>21</sup>	$6.86 \pm 0.06$

<sup>a</sup> pH adjusted with 0.1 M HCl; <sup>b</sup> pH adjusted with 0.1 M NaOH.

Hydrophilic anions such as nitrates, phosphates or carbonates were chosen in these studies because preliminary experiments indicated that anions such as borates and perchlorates were causing aggregation. Formation of assembly **1e•2** was observed in basic, neutral, and acidic solutions. The presence of various electrolytes had no influence

on the association constant  $K_{1\cdot2}$  (Table 3). These data compare well with those obtained via ITC considering that the slightly different conditions ( $\text{Log } K_{1\cdot2} = 5.62$ , in the absence of added salts and 4.69 in carbonate buffer  $I = 0.020$  M, see Table 2).

*Conductometric studies.* Additional proof for the 1:1 stoichiometry for assembly **1e•2** was obtained from a conductometric titration. Changes in conductivity of the solution were observed during the titration of porphyrin **1e** with calix[4]arene **2** due to the formation of the ion-pair complex. Extrapolation of the linear sections of the plot afforded the end-titration point (the point where the two solid lines intersect), which was found to be 0.85 equivalents. This is in reasonable agreement with the proposed stoichiometry (Figure 1).

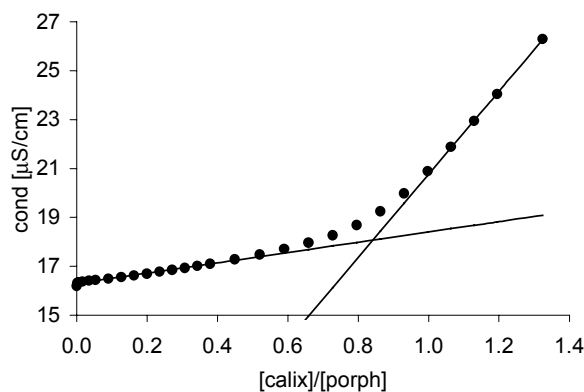


**Figure 1.** Conductometric titration of porphyrin **1e** ( $4.3 \times 10^{-5}$  M) with calix[4]arene **2** ( $8.3 \times 10^{-4}$  M),  $\text{H}_2\text{O}$ ,  $T = 25$  °C.

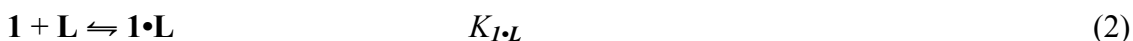
*$^1\text{H}$  NMR studies.* Structural information about assembly **1e•2** was obtained from  $^1\text{H}$ -NMR experiments. The addition of 1 equiv of calix[4]arene **2** to porphyrin **1e** in  $\text{D}_2\text{O}/\text{CD}_3\text{OD}$  (9:1) produced large upfield shifts of the calix[4]arene protons due to the anisotropic shielding from the porphyrin ring. The methylene bridges ( $\text{H}_b$ , Figure 2) and the  $\text{CH}_2$  directly connected to the lower rim oxygens ( $\text{H}_c$ ) are the most upfield shifted ( $\Delta\delta = 0.7$ - $0.85$  ppm), due to their closer position to the porphyrin center.<sup>30</sup> Moreover, all the signals are significantly broadened, indicating an exchange equilibria rate approaching the chemical shift time scale.



### 4.2.3 Selective binding of nitrogenous ligands<sup>32</sup>

In the naturally occurring heme-protein the position occupied by the metal porphyrin within the peptidic matrix is such that the two different porphyrin faces can be distinguished. At the vicinal site, coordination of an amino acid residue to the metal center takes place, while the more open nature of the distal site allows binding of exogenous ligands (see Chapter 2 Figure 11). These structural characteristics have been reproduced in many covalent synthetic models.<sup>1</sup> However, similar efforts using the noncovalent approach have been less common.<sup>6,23</sup> Our self-assembled heme-protein mimics **1•2** present two differentiated porphyrin faces, one enclosing a small cavity in conjunction with calix[4]arene **2** and the other open to the solvent (but susceptible to the influence of the peptidic chains, *vide infra*).

UV-vis measurements were used to study the formation of ternary complexes between porphyrins **1**, calix[4]arene **2** and a ligand **L**. The experimental data were fitted to a 1:1:1 mathematical model encompassing the simultaneous occurrence of three equilibria in solution (equations 1-3).<sup>33</sup>



The coordination strength of the axial ligand **L** to porphyrin **1** ( $K_{\mathbf{1}\cdot\mathbf{L}}$  in eq. 2) was determined in separate experiments. The affinity displayed by the assembly **1•2** for a ligand **L** is given by the ratio  $K_{\mathbf{1}\cdot\mathbf{2}\cdot\mathbf{L}}/K_{\mathbf{1}\cdot\mathbf{2}} = K_{rec}$ . According to this model,  $K_{rec} = 0.5 \times K_{\mathbf{1}\cdot\mathbf{L}}$  if calix[4]arene **2** is completely blocking one porphyrin side without any other effect on the metal coordination ability (this conclusion should apply to large guests that cannot be encapsulated). On the other hand, for covalently capped Zn-porphyrins<sup>34</sup> it has been observed that complexation of guests of appropriate dimension within the host cavity leads to enhanced binding affinity and therefore  $K_{rec} \geq K_{\mathbf{1}\cdot\mathbf{L}}$  should be expected.<sup>35-38</sup> However, the magnitude of this effect is determined by the rigidity of the host, the possibility of additional specific interactions between the ligand and the porphyrin superstructure (e.g. H-bonds),<sup>39,40</sup> and by the solvent.<sup>41-44</sup>

A small, axially symmetrical base such as 4-methylpyridine (4-MePyr) binds to self-assembled receptors **1c•2** and **1e•2** with increased affinity ( $K_{rec} = 58 \text{ M}^{-1}$  and  $38 \text{ M}^{-1}$ , respectively) when compared to **1c** and **1e** ( $K_{I\cdot L} = 35 \text{ M}^{-1}$  and  $7 \text{ M}^{-1}$ , respectively), suggesting ligand encapsulation ( $K_{rec} > K_{I\cdot L}$ ).

**Table 4.** Binding constant for nitrogenous bases to assemblies **1c•2** and **1e•2** and to porphyrin **1c**, **1e** (carbonate buffer,  $I = 0.008 \text{ M}$ ,  $\text{pH} = 9.6$ ,  $T = 25 \text{ }^\circ\text{C}$ )

Assembly	Guest	$K_{rec} (\text{M}^{-1})$	Porphyrin	$K_{I\cdot L} (\text{M}^{-1})$
<b>1c•2<sup>a</sup></b>	4-MePyr	$(5.8 \pm 0.5) \times 10^1$	<b>1c</b>	$(3.5 \pm 0.1) \times 10^1$
<b>1e•2<sup>a</sup></b>		$(3.8 \pm 0.3) \times 10^1$	<b>1e</b>	$(0.7 \pm 0.1) \times 10^1$
<b>1c•2<sup>b</sup></b>	caffeine	$(0.80 \pm 0.1) \times 10^3$	<b>1c</b>	$(3.26 \pm 0.05) \times 10^3$
<b>1e•2<sup>a</sup></b>	1-MeIm	$(2.0 \pm 0.3) \times 10^2$	<b>1e</b>	$(4.5 \pm 0.2) \times 10^1$

<sup>a</sup> Prepared in situ from **1c** (or **1e**) and 1.2 - 1.5 equiv **2**; <sup>b</sup> prepared in situ from **1c** and 11 equiv **2** (see experimental part for details).

However, the rather large difference in  $K_{I\cdot L}$  for 4-MePyr displayed by **1c** vs. the very similar **1e** suggests that not only metal coordination influences the binding, but that additional factors are also playing a role. This difference in affinity is consistent with increased binding of small ligands (such as 1-methylimidazole, 1-MeIm) to porphyrin **1c**, caused by the folding of the long *N*-substituted chains towards the porphyrin core.<sup>24</sup> Therefore, to ascertain the real increase in affinity obtained upon encapsulation of 4-MePyr by assembly **1c•2**,  $K_{rec}$  should instead be compared to  $K_{I\cdot L}$  for **1e** in order to eliminate the bias caused by this phenomenon. The result is enhanced binding by a factor of eight attributable to encapsulation. Similar UV-vis experiments with **1e•2** showed encapsulation of a different guest, 1-MeIm, with  $K_{rec}$  four times higher than  $K_{I\cdot L}$ .

<sup>1</sup>H NMR measurements support that complexation is taking place in the cavity (Figure 3). Addition of 1 equiv of 4-MePyr to a 1 mM solution of assembly **1c•2** (from equimolar amounts of porphyrin **1c** and calix[4]arene **2**) in D<sub>2</sub>O/CD<sub>3</sub>OD 9:1 results in upfield shifted 4-MePyr proton signals when compared to the spectrum of the guest alone (Figure 3b vs 3d). The signal for proton H<sub>b</sub>, *ortho* to the nitrogen atom, is the most upshifted ( $\Delta\delta \sim 0.4 \text{ ppm}$ ).<sup>45</sup> This shift, caused by the porphyrin ring current, is also observed in case

of complexation of 4-MePyr to porphyrin **1c** alone (Figure 3c). However, small but reproducible upfield shifts ( $\Delta\delta = 0.05\text{-}0.06$  ppm) are observed for protons  $H_i$  and  $H_j$  when binding of 4-MePyr to **1c•2** is compared to binding to **1c** (Figure 3b vs Figure 3c). This observation supports the formation of the inclusion complex, with the observed shifts caused by the shielding from the calix[4]arene moiety. Additionally, proton  $H_h$ , (closer to the porphyrin, but further away from the calix[4]arene) does not show any additional shift when binding to **1c•2** is compared to **1c**.

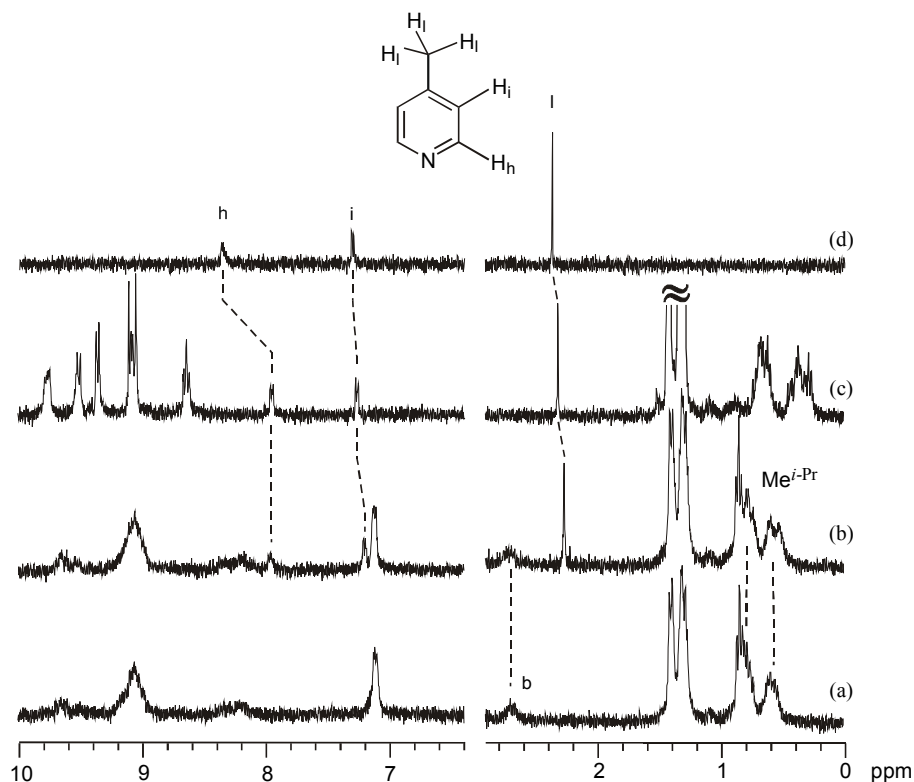


**Figure 3.**  $^1\text{H}$  NMR spectra of (a) assembly **1c•2**, (b) **1c•2** + 1 eq 4-MePyr, (c) porphyrin **1c** + 1 eq 4-MePyr, (d) 4-MePyr. 1 mM solutions in 9:1  $\text{D}_2\text{O}/\text{CD}_3\text{OD}$ . Only the structure of the ligand is shown for clarity.

Moreover, complexation experiments using the bulkier ligand caffeine show no encapsulation. From UV-vis titrations a  $K_{rec} = 800 \text{ M}^{-1}$  for the self-assembled receptor **1c•2** was calculated. This value is one fourth of  $K_{I-L}$  for **1c** ( $3260 \text{ M}^{-1}$ ). The decreased affinity confirms that caffeine is too big to fit in the cavity and binding is taking place only on the open face of the self-assembled receptor. This decrease also suggests larger



unfavorable interactions with the long peptidic chains, which are probably arranged predominantly on the open face of the porphyrin as a consequence of the ion-pair complex **1c•2** formation (vide supra).

Structural information about the complex is gained by  $^1\text{H}$  NMR experiments performed under the same conditions used for 4-MePyr (Figure 4). The binding mode of caffeine to porphyrins **1a-e** (and other similar ones) is substantially different from the binding mode of ligands like imidazole or pyridine derivatives.<sup>24</sup> The steric bulk of the ligand (due to methyl group  $\text{Me}_o$ ) and the tendency towards stacking are responsible for a non-perpendicular arrangement of caffeine with respect to the porphyrin plane. Nevertheless, the data suggest direct interaction with the Zn atom via the nitrogen N-9.

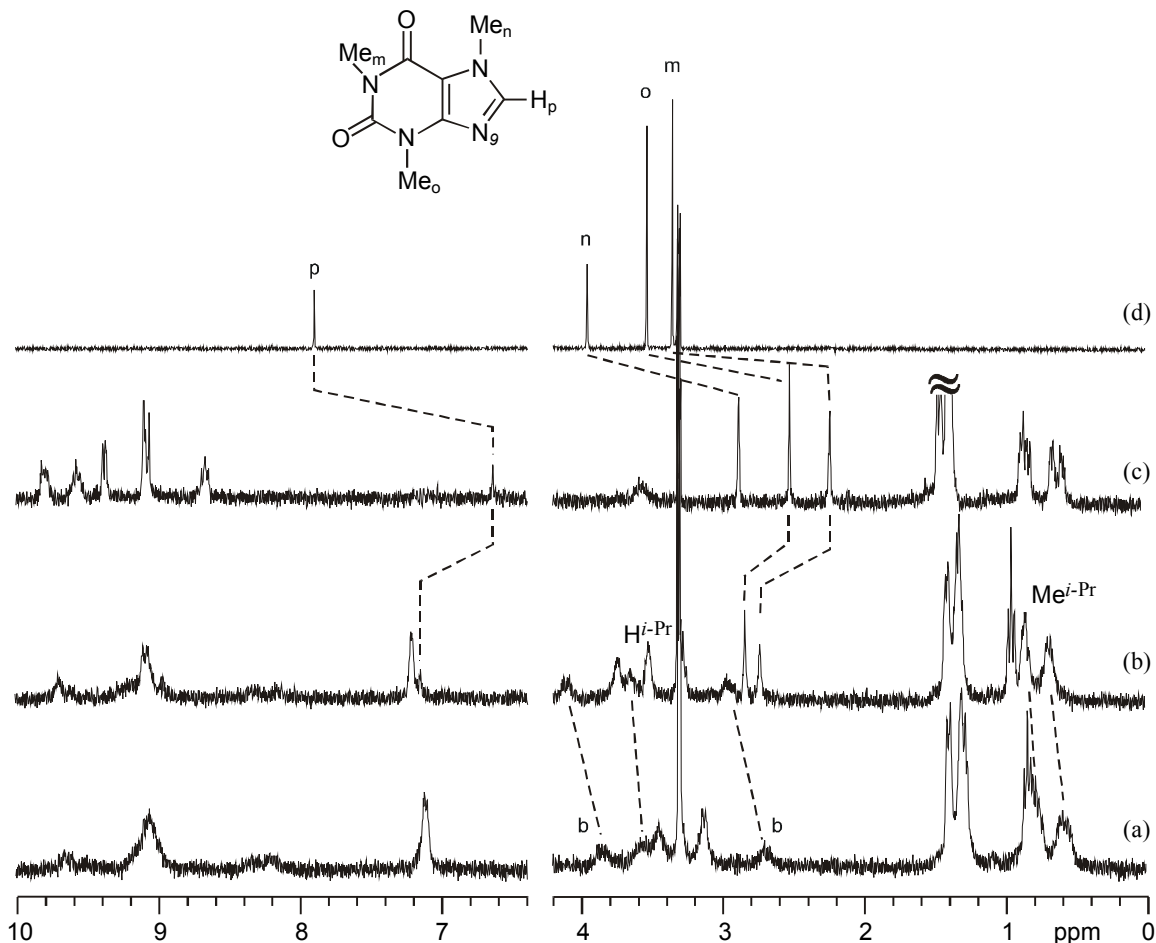


**Figure 4.**  $^1\text{H}$  NMR spectra of (a) assembly **1c•2**, (b) **1c•2**+1 equiv caffeine, (c) porphyrin **1c**+1 equiv caffeine, (d) caffeine. (1 mM solutions in 9:1  $\text{D}_2\text{O}/\text{CD}_3\text{OD}$ ). For assignment protons  $\text{Me}^{i\text{-Pr}}$  and  $\text{H}^{i\text{-Pr}}$  see Figure 2. Only the structure of the ligand is shown for clarity.

Protons  $H_p$  and  $Me_n$  closest to the porphyrin center are the most upfield shifted, consistent with this mode of interaction between caffeine and porphyrin **1c** (Figure 4c). When caffeine is bound to the self-assembled receptor **1c•2**, all its proton signals are remarkably less upfield shifted than when the ligand is bound to porphyrin **1c** alone (Table 5). This behavior is exactly opposite to what was observed for encapsulation of 4-MePyr (vide supra).

**Table 5.** Chemical shifts observed for the binding of caffeine to porphyrin receptor **1c** and to assembly **1c•2** (1 mM in 9:1 D<sub>2</sub>O/CD<sub>3</sub>OD).

	caffeine	<b>1c</b> + 1 equiv caffeine	<b>1c•2</b> + 1 equiv caffeine
	$\delta_f$ (ppm)	$\Delta\delta = \delta - \delta_f$ (ppm)	$\Delta\delta = \delta - \delta_f$ (ppm)
$H_p$	7.89	-1.36	-0.75
$Me_m$	3.34	-1.07	-
$Me_o$	3.53	-1.05	-0.70
$Me_n$	3.95	-1.14	-0.62

$\delta_f$  chemical shift for uncomplexed caffeine. For proton assignment see Figure 4.

In contrast to those from 4-MePyr, the signals relative to the methylene bridges of the calix[4]arene moiety ( $H_b$ ) and to the *i*-Pr groups of the peptidic chains in assembly **1c•2** are shifted downfield ( $\Delta\delta$ -0.1–0.2 ppm, and smaller  $\Delta\delta$  values are observed for the other calix[4]arene signals) upon caffeine binding, indicating a larger reorganization to accommodate the ligand at the open porphyrin face (Figure 4b).

### 4.3 Conclusions

The formation of self-assembled cage-like complexes **1a-c•2** in aqueous solution has been shown with a combination of experimental techniques. The study of the thermodynamic parameters associated with the process via ITC suggests that the association between cationic porphyrins **1** and anionic calix[4]arene **2** is primarily driven by ionic interaction. The assembly process does not involve the metal center and

formation of ternary complexes upon addition of suitable ligands has been achieved. The topology of these complexes depends on the molecular dimensions of the guest. The possibility of selectively addressing the desired porphyrin face by appropriate choice of the ligand may be used to obtain more complex architectures such as quaternary complexes with two different ligands. It is also shown that “inert” zinc porphyrins can be replaced by cobalt porphyrin, allowing the evolution from structural to functional models of heme-proteins (see Chapter 5).

## 4.4 Experimental part

### 4.4.1 General information and instrumentation

$^1\text{H}$  NMR spectra were performed on a Varian Unity INOVA (300 MHz). Chemical shift values are expressed in ppm ( $\delta$ ) relative to residual  $\text{CHD}_2\text{OD}$  ( $\delta$  3.30). UV-vis measurements were performed on a Varian Cary 3E UV-vis spectrophotometer equipped with a Helma QX optical fiber probe (path length=1.000 cm), using solvents of spectroscopic grade. Calorimetric measurements were carried out using a Microcal VP-ITC microcalorimeter with a cell volume of 1.4115 mL.

Synthesis of porphyrins **1**<sup>24</sup> and of calix[4]arene **2**,<sup>21</sup> buffer preparation, dilution experiments to confirm the absence of porphyrin aggregation and UV-vis studies of the assembly formation are described in Chapters 3 and 7. Cobalt porphyrin Co-**1b** has been prepared using the same free base precursor<sup>24</sup> used to prepare Zn-**1b**. Metallation with  $\text{CoAc}_2$  was carried out under the same experimental conditions used for the insertion of Zn.

### 4.4.2 Binding studies

*Capsule formation and UV-vis studies of guest recognition:* Assembly **1c•2** and **1e•2** were prepared in situ by addition of calix[4]arene **2** to the porphyrin in carbonate buffer solution ( $I = 0.008$  M,  $\text{pH} = 9.6$ ) in order to reach > 80% assembly formation in the final solution. The amount of calix[4]arene **2** needed was calculated from the assembly formation constants  $K_{1,2}$  measured under the same conditions used for the guest recognition experiments. Eleven equiv of **2** were used to prepare assembly **1c•2** for

titration with caffeine and 1.2-1.5 equiv were instead used to prepare assemblies **1c•2** and **1e•2** when titrated with 4-MePyr or 1-MeIm. The binding of guests to porphyrins **1c**, **1e** and to assemblies **1c•2** and **1e•2** was evaluated by UV-vis titration. Spectral variation as a function of ligand concentration was monitored in the Soret band region (400-480 nm) for caffeine or in the Q-band region (500-630 nm) for 4-MePyr and 1-MeIm. Porphyrin concentrations were  $2.6 \times 10^{-6}$  M and  $\times 10^{-5}$  M, respectively.

Each titration consisted of 13 to 20 data points. The experimental spectral changes were fitted to a 1:1 or to a 1:1:1 binding model (see text). A nonlinear least-squares fitting procedure considering simultaneously 6 different wavelenghts was used in the case of 1:1 complexation (model written with the program Scientist<sup>®</sup>, MicroMath<sup>®</sup>). A nonlinear least-squares fitting procedure, considering separately 4-5 different wavelenghts followed by an average of the results was used for 1:1:1 complexation (model written with the program Microsoft<sup>®</sup> Excel).

*Microcalorimetry (ITC):* Aliquots of a calix[4]arene **2** solution (1.05 mM) in carbonate buffer ( $I = 0.010$  M, pH = 9.6 or  $I = 0.045$  M, pH = 10.0) contained in a buret were added to the porphyrin **1** solution (in the same buffer) contained in the calorimetric cell (porphyrin concentration 0.090-0.105 mM). Data were fitted for metalated receptors and to a 1:2 (receptor/guest) model in the case of free base receptor **1d**. Fittings of the experimental data to a 1:1 binding model were obtained using Origin<sup>®</sup> implemented with the calorimetric set up provided by Microcal Inc.

#### 4.5 References and notes

1. For detailed review articles about covalent superstrucutered porphyrins as model systems for heme proteins see: Collman, J. P.; Fu, L. *Acc. Chem. Res.* **1999**, *32*, 455-463. Collman, J. P. *Inorg. Chem.* **1997**, *36*, 5145-5155. Collman, J. P.; Eberspacher, T.; Fu, L.; Herrmann, P. C. *J. Mol. Cat. A* **1997**, *117*, 9-20. Momentau, M.; Reed, C. A. *Chem. Rev.* **1994**, *94*, 659-698. Traylor, T. G. *Acc. Chem. Res.* **1981**, *14*, 102-109. Jones, R. D.; Summerville, D. A.; Basolo F. *Chem. Rev.* **1979**, *79*, 139-179. For other more recent examples of superstructured

- porphyrins: Tani, F.; Matsu-ura, M.; Nakayama, S.; Ichimura, M.; Nakamura, N.; Naruta, Y. *J. Am. Chem. Soc.* **2001**, *123*, 1133-1142. Kossanyi, A.; Tani, F.; Nakamura, N.; Naruta, Y. *Chem. Eur. J.* **2001**, *7*, 2862-2872. Gazeau, S.; Pècaut, J.; Marchon, J.-C. *Chem. Commun.* **2001**, 1644-1645. Nakagawa, H.; Nagano, T.; Higuchi, T. *Org. Lett.* **2001**, *3*, 1805-1807. Starnes, S. D.; Rudkevich, D. M.; Rebek, J., Jr. *J. Am. Chem. Soc.* **2001**, *123*, 4659-4669. Smeets, S.; Asokan, F.; Motmans, F.; Dehaen, W. *J. Org. Chem.* **2000**, *65*, 5882-5885. Schwenninger, R.; Ramondenc, Y.; Wurst, K.; Schlögl, J.; Kräutler, B. *Chem. Eur. J.* **2000**, *6*, 1214-1223.
2. Porphyrin-core dendrimers: Hecht, S.; vladimirov, N.; Fréchet, J. M. J. *J. Am. Chem. Soc.* **2001**, *123*, 18-25. Pollak, K. W.; Sandford, E. M.; Fréchet, J. M. J. *J. Mat. Chem.* **1998**, *8*, 519-527. Jiang, D.-L.; Aida, T. *J. Am. Chem. Soc.* **1998**, *120*, 10895-10901. Jiang, D.-L.; Aida, T. *J. Macromol. Sci., Pure Appl. Chem.* **1997**, *A34*, 2047-2055. Jin, R.-H.; Aida, T.; Inoue, S. *Chem. Commun.* **1993**, 1260-1262. Weyermann, P.; Gisselbrecht, J.-P.; Boudon, C.; Diederich, F.; Gross, M. *Angew. Chem., Int. Ed. Engl.* **1999**, *38*, 3215-3219. Collman, J. P.; Fu, L.; Zingg, A.; Diederich, F. *Chem. Commun.* **1997**, 193-194. Bhyrappa, P.; Vaijayanthimala, G.; Suslick, K. S. *J. Am. Chem. Soc.* **1999**, *121*, 262-263. Bhyrappa, P.; Young, J. K.; Moore, J. S.; Suslick, K. S. *J. Am. Chem. Soc.* **1996**, *118*, 5708-5711.
  3. For peptide-based heme-protein models see Lombardi, A.; Nastri, F.; Pavone, V. *Chem. Rev.* **2001**, *101*, 3165-3189 and references therein.
  4. Spiro, T. G.; Kozlowski, P. M. *Acc. Chem. Res.* **2001**, *34*, 137-144.
  5. For supramolecular cytochrome P450 mimics in which the reproduction of the substrate binding site is taken into consideration see Feiters, M. C.; Rowan, A. E.; Nolte, R. J. M. *Chem. Soc. Rev.* **2000**, *29*, 375-384 and references cited therein.
  6. For noncovalent modification of porphyrin in aqueous solution using complexation with cyclodextrins, see: Zhao, S.; Luong, J. H. T. *Chem. Commun.* **1995**, 663-664. Ribò, J. M.; Farrera, J.-A.; Valero, M. L.; Virgili, A. *Tetrahedron* **1995**, *51*, 3705-

3712. Dick, D. L.; Rao, T. V. S.; Sukumaran, D.; Lawrence, D. S. *J. Am. Chem. Soc.* **1992**, *114*, 2664-2669. Carofiglio, T.; Fornasier, R.; Lucchini, V.; Rosso, C.; Tonellato, U. *Tetrahedron Lett.* **1996**, *37*, 8019-8022. Venema, F.; Nelissen, H. F. M.; Berthault, P.; Birlirakis, N.; Rowan, A. E.; Feiters, M. C.; Nolte, R. J. M. *Chem. Eur. J.* **1998**, *4*, 2237-2250. Michels, J. J.; Fiammengo, R.; Timmerman, P.; Huskens, J.; Reinhoudt, D. N. *J. Incl. Phenom.* **2001**, *41*, 163-172.
7. Norsten, T. B.; Chichak, K.; Branda, N. R. *Tetrahedron* **2002**, *58*, 639-651.
8. Collman, J. P.; Gagne, R. R.; Reed, C. A.; Halbert, T. R.; Lang, G.; Robinson, W. T. *J. Am. Chem. Soc.* **1975**, *97*, 1427-1439.
9. Collman, J. P.; Brauman, J. I.; Doxsee, K. M.; Halbert, T. R.; Suslick, K. S. *Proc. Natl. Acad. Sci. USA* **1978**, *75*, 564-568.
10. Collman, J. P.; Brauman, J. I.; Collins, T. J.; Iverson, B. L.; Lang, G.; Pettman, R. B.; Sessler, J. L.; Walters, M. A. *J. Am. Chem. Soc.* **1983**, *105*, 3038-3052.
11. Ellis, P. E. Jr.; Linard, J. E.; Szymanski, T.; Jones, R. D.; Budge, J. R.; Basolo, F. *J. Am. Chem. Soc.* **1980**, *102*, 1889-1896.
12. Linard, J. E.; Ellis, P. E. Jr.; Budge, J. R.; Jones, R. D.; Basolo, F. *J. Am. Chem. Soc.* **1980**, *102*, 1896-1904.
13. Jimenez, H. R.; Momentau, M. *New J. Chem.* **1994**, *18*, 569-574.
14. Vinogradov, S. A.; Lo, L.-W.; Wilson, D. F. *Chem. Eur. J.* **1999**, *5*, 1338-1347.
15. For examples of noncovalent porphyrin-peptide systems (with a single porphyrin unit) considering explicitly the interactions between the porphyrin core and the peptidic environment see: Huffman, D. L.; Suslick, K. S. *Inorg. Chem.* **2000**, *39*, 5418-5419. Liu, D.; Williamson, D. A.; Kennedy, M. L.; Williams, T. D.; Morton, M. M.; Benson, D. R. Huffman, D. L.; Suslick, K. S. *J. Am. Chem. Soc.* **1999**, *121*, 11798-11812.

16. For other examples of noncovalent porphyrin-peptide systems (with a single porphyrin unit) see: Tomizaki, K.; Murata, T.; Kaneko, K.; Miike, A.; Nishino, N. *J. Chem. Soc., Perkin Trans. 2* **2000**, 1067-1074. Sakamoto, S.; Obataya, I.; Ueno, A.; Mihara, H. *Chem. Commun.* **1999**, 1111-1112. Sakamoto, S.; Ueno, A.; Mihara, H. *Chem. Commun.* **1998**, 1073-1074. Sakamoto, S.; Sakurai, S.; Ueno, A.; Mihara, H. *Chem. Commun.* **1997**, 1221-1222. Sharp, R. E.; Diers, J. R.; Bocian, D. F.; Dutton, P. L. *J. Am. Chem. Soc.* **1998**, *120*, 7103-7104. Liu, D.; Lee, K.-H.; Benson, D. R. *Chem. Commun.* **1999**, 1205-1206. Arnold, P. A.; Shelton, W. R.; Benson, D. R. *J. Am. Chem. Soc.* **1997**, *119*, 3181-3182. Karpishin, T. B.; Vannelli, T. A.; Glover, K. J. *J. Am. Chem. Soc.* **1997**, *119*, 9063-9064. Choma, C. T.; Lear, J. D.; Nelson, M. J.; Dutton, P. L.; Robertson, D. E.; DeGrado, W. F. *J. Am. Chem. Soc.* **1994**, *116*, 856-865.
17. Fiammengo, R.; Crego-Calama, M.; Reinhoudt, D. N. *Curr. Opin. Chem. Biol.* **2001**, *5*, 660-673.
18. Fiammengo, R.; Timmerman, P.; de Jong, F.; Reinhoudt, D. N. *Chem. Commun.* **2000**, 2313-2314.
19. For 5,10,15,20-tetrakis(4-*N*-methylpyridyl)porphyrin (*free-base*) – tetrasulfonato calix[4]arenes assemblies: Di Costanzo, L.; Geremia, S.; Randaccio, L.; Purrello, R.; Lauceri, R.; Sciotto, D.; Gulino, F. G.; Pavone, V. *Angew. Chem., Int. Ed. Engl.* **2001**, *40*, 4245-4247. Lang, K.; Kubát, P.; Lhoták, P.; Mosinger, J.; Wagnerová, D. *M. Photochem. Photobiol.* **2001**, *74*, 558-565.
20. For the first well defined cage-like complexes obtained via ionic interactions for guest encapsulation see: Corbellini, F.; Fiammengo, R.; Timmerman, P.; Crego-Calama, M.; Versluis, K.; Heck, A. J. R.; Luyten, I.; Reinhoudt, D. N. *J. Am. Chem. Soc.* **2002**, *124*, 6569-6575. For other assemblies obtained via ionic interactions with no inner space for guest encapsulation see: Grawe, T.; Schrader, T.; Zadnard, R.; Kraft, A. *J. Org. Chem.* **2002**, *67*, 3755-3763. Grawe, T.; Schrader, T.; Gurrath, M.; Kraft, A.; Osterod, F. *Org. Lett.* **2000**, *2*, 29-32. Grawe, T.; Schrader, T.; Gurrath, M.; Kraft, A.; Osterod, F. *J. Phys. Org. Chem.* **2000**, *13*, 670-673.

21. Fiammengo, R.; Timmerman, P.; Huskens, J.; Versluis, K.; Heck, A. J. R.; Reinhoudt, D. N. *Tetrahedron* **2002**, *58*, 757-764. See also Chapter 3.
22. The range of concentrations for these water soluble systems is comparable to the solubility of natural heme-proteins viz. 160 g/l for hemoglobin in human blood, which corresponds to ~2.5 mM.
23. Karpishin, T. B.; Vannelli, T. A.; Glover, K. J. *J. Am. Chem. Soc.* **1997**, *119*, 9063-9064.
24. Fiammengo, R.; Crego-Calama, M.; Timmerman, P.; Reinhoudt, D. N. *J. Am. Chem. Soc.* **2002** submitted. See also Chapter 7.
25. The solubility of assemblies **1 (d-e)•2** are  $\leq 1$  mM due to the higher hydrophobicity of the porphyrin moieties.
26. Schneider, H.-J.; Kramer, R.; Simova, S.; Schneider, U. *J. Am. Chem. Soc.* **1988**, *110*, 6442-6448.
27. Diederich F.; Dick, K.; Griebel, D. *J. Am. Chem. Soc.* **1986**, *108*, 2273-2286.
28. Gelb, R. I.; Lee, B. T.; Zompa, L. J. *J. Am. Chem. Soc.* **1985**, *107*, 909-916.
29. [porphyrin **1e**] =  $2-3 \times 10^{-6}$  M. [Calix[4]arene **2**] =  $8.3 \times 10^{-4}$  M. Very good linearity between absorbance and concentration was observed in a dilution experiments performed in the range  $8 \times 10^{-5} - 1 \times 10^{-7}$  M, confirming non aggregation of the porphyrin under these conditions.
30. The closer position of protons H<sub>b</sub> and H<sub>c</sub> to the porphyrin center can be better visualized in the molecular simulation structure (CHARMm 24.0) of assembly **1•2** (see Figure 7, Chapter 3).
31. In contrast, **1a-b** bearing single amino acid based (short) chains do not show these interactions.
32. Basic pH was chosen for the assembly process because it is the same media where



complexation of nitrogenous bases is also studied in order to neglect the protonation equilibria of the bases. Ionic strength  $I \sim 0.008$  M for the titrated porphyrin solution was chosen to equalize the ionic strength of the calix[4]arene solution ( $8 \times 10^{-4}$  M) used as titrant. In this way constant ionic strength was ensured throughout the titration while keeping at a minimum level the amount of added salts, which have been shown to decrease the constant for assembly formation  $K_{1,2}$ .

33. Binding of the neutral ligands to calix[4]arene **2** has been excluded according to previous studies on this compound, see: Arena, G.; Contino, A.; Gulino, F. G.; Magrì, A.; Sciotto, D.; Ungaro, R. *Tetrahedron Lett.* **2000**, *41*, 9327-9330. Arena, G.; Contino, A.; Gulino, F. G.; Magrì, A.; Sansone, F.; Sciotto, D.; Ungaro, R. *Tetrahedron Lett.* **1999**, *40*, 15967-1600.
34. For general reviews on supramolecular modified porphyrins used for ligand recognition: Weiss, J. *J. Incl. Phenom.* **2001**, *40*, 1-22. Robertson, A.; Shinkai, S. *Coord. Chem. Rev.* **2000**, *205*, 157-199.
35. Rudkevich, D. M.; Verboom, W.; Reinhoudt, D. N. *J. Org. Chem.* **1995**, *60*, 6585-6587.
36. Middel, O.; Verboom, W.; Reinhoudt, D. N. *J. Org. Chem.* **2001**, *66*, 3998-4005.
37. Imai, H.; Uemori, Y. *J. Chem. Soc., Perkin Trans. 2* **1994**, 1793-1797.
38. Elemans, J. A. A. W.; Claase, M. B.; Aarts, P. P. M.; Rowan, A. E.; Schenning, A. P. H. J.; Nolte, R. J. M. *J. Org. Chem.* **1999**, *64*, 7009-7016.
39. Bonar-Law, R. P.; Sanders, J. K. M. *J. Am. Chem. Soc.* **1995**, *117*, 259-271.
40. Bonar-Law, R. P.; Sanders, J. K. M. *J. Chem. Soc., Chem. Commun* **1991**, 574-577.
41. Imai, H.; Munakata, H.; Takahashi, A.; Nakagawa, S.; Ihara, Y.; Uemori, Y. *J. Chem. Soc., Perkin Trans. 2* **1999**, 2565-2568.
42. Benson, D. R.; Valentekovich, R.; Knobler, C. B.; Diederich, F. *Tetrahedron* **1991**,

47, 2401-2422.

43. Imai, H.; Nakagawa, S.; Kyuno, E. *J. Am. Chem. Soc.* **1992**, *114*, 6719-6723.
44. Collman, J. P.; Brauman, J. I.; Fitzgerald, J. P.; Hampton, P. D.; Naruta, Y.; Sparapany, J. W.; Ibers, J. A. *J. Am. Chem. Soc.* **1988**, *110*, 3477-3486.
45. The magnitude of the shift is consistent with that observed for the *ortho* proton of pyridine complexed by a Zn-porphyrin-cyclophane receptor ( $\Delta\delta \sim 0.45$  ppm for a 2.2 mM receptor solution in CD<sub>3</sub>OD, 1.3 equiv of pyridine), see ref. 42.

## **CRYSTALLIZATION ATTEMPTS OF WATER-SOLUBLE ASSEMBLIES 1•2\***

### **Methodology<sup>1-3</sup> and results**

Three main crystallization techniques are based on vapor diffusion: hanging drop, sitting drop, and sandwich drop. The hanging drop technique was used in the attempted crystallization of the assemblies **1•2**. In a typical experiment the hanging drop is prepared from 4  $\mu\text{l}$  of assembly **1•2** solution mixed with 2  $\mu\text{l}$  of reservoir solution containing the precipitating agent and occasionally other additives (see experimental section for further details). The drop is then further equilibrated with the reservoir solution. During this time diffusion of the volatiles (water and/or organic solvents) from the drop to the reservoir takes place due to the different vapor pressure of the two solutions. The main parameters influencing the evaporation kinetics and therefore the velocity of nucleation are: temperature, initial drop volume and dilution with respect to the reservoir, the nature of the additive and precipitating agents added and finally the concentration of the species to be crystallized.

Unfortunately, the formation of crystals was not observed in any case, but rather the assemblies tended to precipitate as amorphous solids (Figure 1) or to separate as viscous oils.

---

\* For this work Dr. Silvano Geremia (Centro di Eccellenza di Biocristallografia, Dipartimento di Scienze Chimiche, University of Trieste, Italy) is gratefully acknowledged.

## Experimental part

Assemblies **1•2** have been prepared mixing 2  $\mu\text{l}$  of a 7.0 mM solution of porphyrins **1a-d** with 2  $\mu\text{l}$  of a 7.0 mM solution of calix[4]arene tetrasulfonate **2** (see Chart 1 Chapter 4 for structures) and 2  $\mu\text{l}$  of the desired reservoir solution. These solutions were equilibrated with the reservoir containing different precipitating agents and/ or additives as listed below.

*Assembly 1a•2.* PEG 300: 5-40%; PEG 1000: 15-40%; PEG 1500: 10-48%; PEG: 2000 15-40%; Glycerol: 10%, 20%, 30%; Glycerol + 1.0 M LiCl: 10%, 20%, 30%; PEG 300 (32%) + LiCl (0.5, 1.0, 1.5 M); Ethylene glycol: 25%; Dioxane: 25%; PEG 300 (32%) + ethanol (10%, 15%, 20%).

For assemblies **1b-d•2** similar conditions were used. Larger drops (4  $\mu\text{l}$  reservoir, 2  $\mu\text{l}$  calix, 2  $\mu\text{l}$  porphyrin) and lower temperatures ( $T = 4\text{ }^{\circ}\text{C}$ ) have also been used.

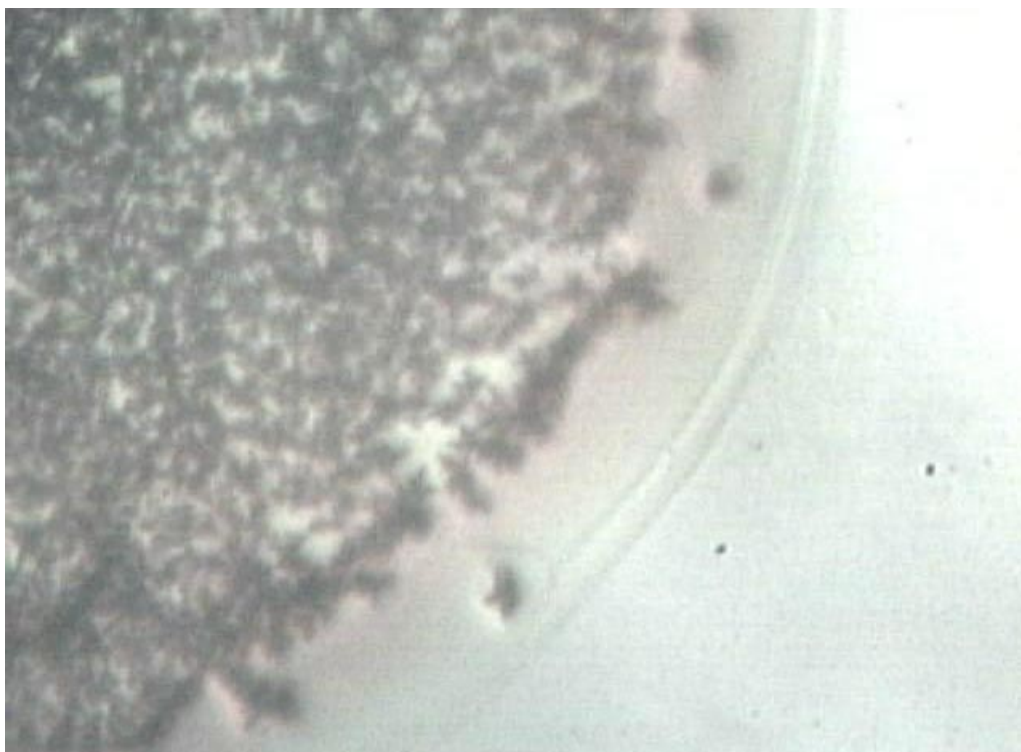


**Figure 1.** Image of the amorphous solid precipitated in the hanging drop of assembly **1c•2** obtained using PEG 1500 30%.

## References

1. Randaccio, L.; Geremia, S.; Stener, M.; Toffoli, D.; Zangrando, E. *Eur. J. Inorg. Chem.* **2002**, 93-103.
2. Randaccio, L.; Furlan, M.; Geremia, S.; Slouf, M.; Srnova, I.; Toffoli, D. *Inorg. Chem.* **2000**, 39, 3403-3413.
3. Randaccio, L.; Geremia, S.; Nardin, G.; Slouf, M.; Srnova, I. *Inorg. Chem.* **1999**, 38, 4087-4092.

### TOWARDS WATER SOLUBLE FUNCTIONAL MODELS OF O<sub>2</sub> BINDING HEME-PROTEINS VIA SELF-ASSEMBLY\*

*Water soluble noncovalent mimics for O<sub>2</sub> binding heme-proteins have been prepared using the ion-pair complexes of calix[4]arenes and porphyrins as described in Chapter 3 and 4. To obtain functional models, the inert Zn porphyrins have been replaced by Co<sup>II</sup> porphyrins, which are able to bind O<sub>2</sub>. These novel functional models have been studied in relation to their O<sub>2</sub> binding ability and their use in O<sub>2</sub>/N<sub>2</sub> membrane separation.*

#### 5.1 Introduction

Transport and storage of O<sub>2</sub> is of fundamental importance to most living organisms. In mammals, these two functions are carried out by heme-proteins such as hemoglobin and myoglobin.<sup>1</sup> Surprisingly, there are no examples reported so far of biomimetic O<sub>2</sub> binders and transporters obtained via noncovalent synthesis in water. This Chapter deals with self-assembly of tetracationic Co<sup>II</sup> porphyrins and tetraanionic calix[4]arenes to form water soluble O<sub>2</sub> binding heme-protein models. The strategy followed for the preparation of these systems has been described in detail in Chapters 3 and 4 in which *structural* models of heme-protein based on Zn-porphyrins are described. Nevertheless, to obtain *functional* models, the inert Zn<sup>2+</sup> ion has to be replaced by Fe<sup>2+</sup> or Co<sup>2+</sup> since these Fe and Co porphyrins are able to bind O<sub>2</sub>. *Functional* models are generally more attractive than

*structural* models because of their potential applications, e.g. as synthetic O<sub>2</sub> carriers. Actually, the idea of using synthetic O<sub>2</sub> carriers for the separation of O<sub>2</sub> and N<sub>2</sub> has long been pursued. In particular, supported liquid membranes employing synthetic O<sub>2</sub> carriers have been recognized for their potential use in biomedical applications. They could be used in small portable devices to produce O<sub>2</sub> enriched air for patients suffering from respiratory or lung diseases such as asthma and emphysema.<sup>2</sup> The self-assembled O<sub>2</sub> carriers presented in this Chapter might be especially interesting in this area because of their water solubility<sup>3</sup> and modest synthetic efforts. From the biomimetic point of view, water solubility is very important because biological processes take place in aqueous solutions. Only a few reports have dealt with binding of O<sub>2</sub> to simple water soluble Co<sup>II</sup> porphyrins,<sup>4,5</sup> and the use of covalent superstructured porphyrins in water has only been reported by Collman and coworkers.<sup>6-8</sup> In general, Co<sup>II</sup> porphyrins are chosen because of their higher stability towards autoxidation, which eventually lead to the inactivation of the carrier, compared to Fe<sup>II</sup> porphyrins.<sup>9</sup>

## 5.2 Results and discussion

### 5.2.1 Synthesis

Metallation of free base porphyrins **1** with cobalt II was performed at 40 °C using 10-20 equiv of Co(Ac)<sub>2</sub> in deoxygenated MeOH. Porphyrins **1a** and **1b** (Figure 1) were isolated as hexafluorophosphate salts by precipitation upon addition of NH<sub>4</sub>PF<sub>6</sub>.<sup>10,11</sup> The preparation of tetrasulfonato calix[4]arene **2** has been reported elsewhere.<sup>10</sup>

### 5.2.2 Assembly formation

The assembly formation between Co<sup>II</sup> porphyrins **1b** and calix[4]arene **2** has been studied via ITC. Assembly **1b•2** is formed with  $\text{Log}K_{1,2} = 3.80 \pm 0.04$  in aqueous carbonate buffered solution at pH 10 and  $I = 0.045 \text{ M}$  ( $K_{1,2}$  in M<sup>-1</sup>). This result clearly confirms that,

---

\* Prof. J. Reedijk and Mr. G. A. van Albada (University of Leiden, The Netherlands) are gratefully acknowledged for the support offered with EPR measurements. We thank Prof. M. Wessling (University of Twente, The Netherlands) for helpful discussions on membrane measurements.

with respect to assembly formation, Co-porphyrins **1** behave similarly to the Zn-porphyrins discussed in Chapters 4, for which Log  $K_{1,2}$  was in the range 4.1-4.4.

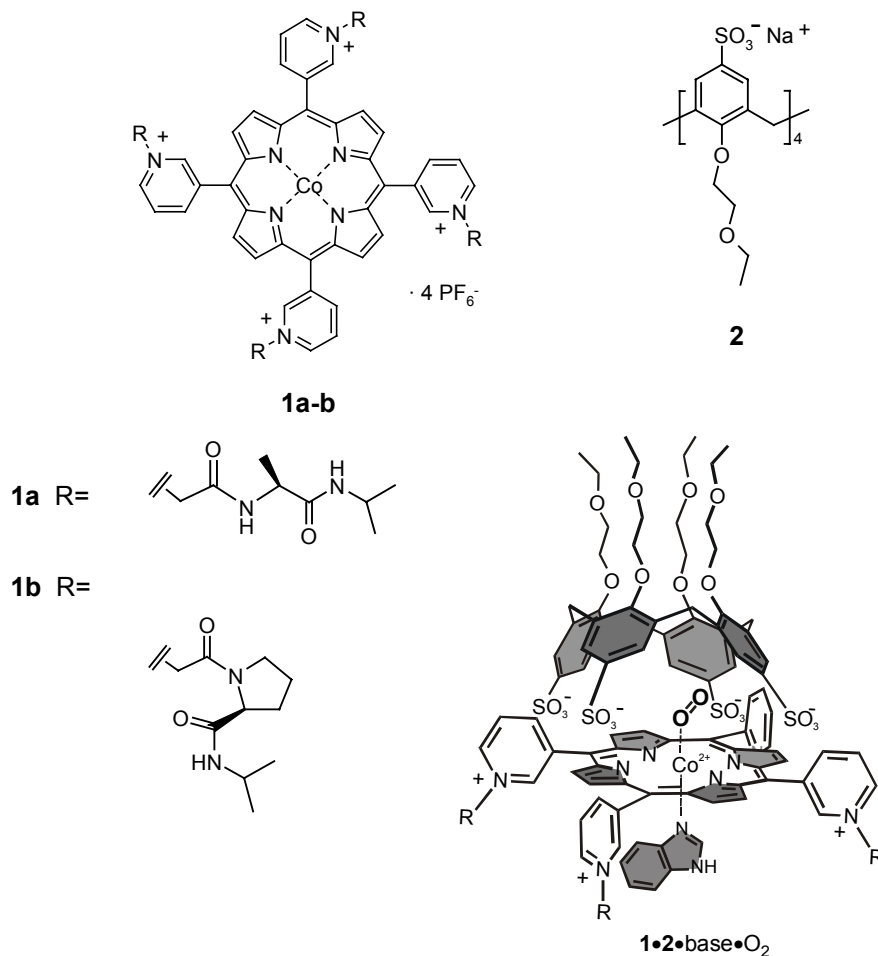


**Figure 1.** Molecular structures of the building blocks used to prepare assemblies **1•2** and hypothetical structure for base/O<sub>2</sub> adducts (**1•2•base•O<sub>2</sub>**), base=Benzimidazole.

### 5.2.3 O<sub>2</sub> binding

*UV-vis studies.* Attempts to study O<sub>2</sub> binding by assemblies **1•2** in the presence of excess base<sup>12</sup> such as 1-methylimidazole (1-MeIm) or benzimidazole (BIm) in MeOH or in MeOH/H<sub>2</sub>O mixtures at -10 °C were not successful. The UV-vis spectra were changing during the measuring time giving non-reproducible results. It is important to stress that UV-vis is probably not suitable to study complex solutions containing porphyrin, calix[4]arene, base, and O<sub>2</sub>. Many species are present in equilibrium and many possible chemical transformations, like  $\mu$ -peroxo dimer formation (vide infra) or other degradative



processes could take place.<sup>13</sup> Attempts to measure O<sub>2</sub> binding to porphyrin **1b** alone in the presence of BIm in MeOH (or in MeOH/H<sub>2</sub>O mixtures) were also not successful, probably due to the use of polar protic solvents. To confirm this hypothesis, O<sub>2</sub> binding was studied in acetonitrile. The UV-vis spectral changes (Figures 2 and 3) occurring upon equilibration of a solution containing **1b** and 1-Melm (0.15 M) with O<sub>2</sub>/N<sub>2</sub> gas mixtures of varying composition (expressed as O<sub>2</sub> partial pressure  $pO_2$ ) were followed. The measurements were performed at -30 °C to promote binding and to reduce the possibility of irreversible oxidation of the porphyrin.

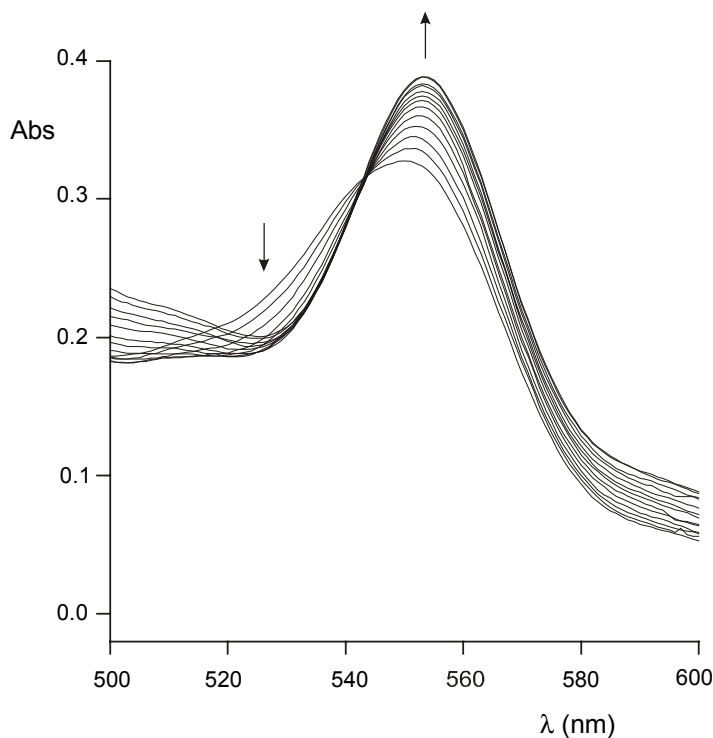


**Figure 2.** Spectral changes as a function of increasing  $pO_2$  in equilibrium with a solution of **1b** at -30 °C.  $[1b] = 2.1 \times 10^{-5}$  M, in CH<sub>3</sub>CN,  $[1\text{-Melm}] = 0.15$  M. Max.  $pO_2 = 76$  Torr.

The spectral variations at 553 (Figure 3) and 551 nm in response to the increase in  $pO_2$  were fitted to a 1:1 binding isotherm using a nonlinear least-squares fitting procedure affording a binding constant of  $K_{O_2} = 0.137$  Torr<sup>-1</sup> (half oxygenation pressure  $P_{1/2} = 1/K_{O_2} = 7.3$  Torr). Despite the fact that tetracationic alkylpyridinium porphyrins have been known for more than 30 years,<sup>14</sup> their O<sub>2</sub> binding ability of Co derivatives has not been reported in quantitative terms. However, the  $P_{1/2}$  value determined for **1b** can be compared to the values for the simple Co<sup>II</sup>-protoporphyrinIX-dimethylester, for which

values of  $P_{1/2}$  in non polar and polar solvents are available (axial base 1-MeIm, -23 °C,  $P_{1/2} = 417$  Torr in toluene and  $P_{1/2} = 12.6$  Torr in DMF).<sup>15</sup>

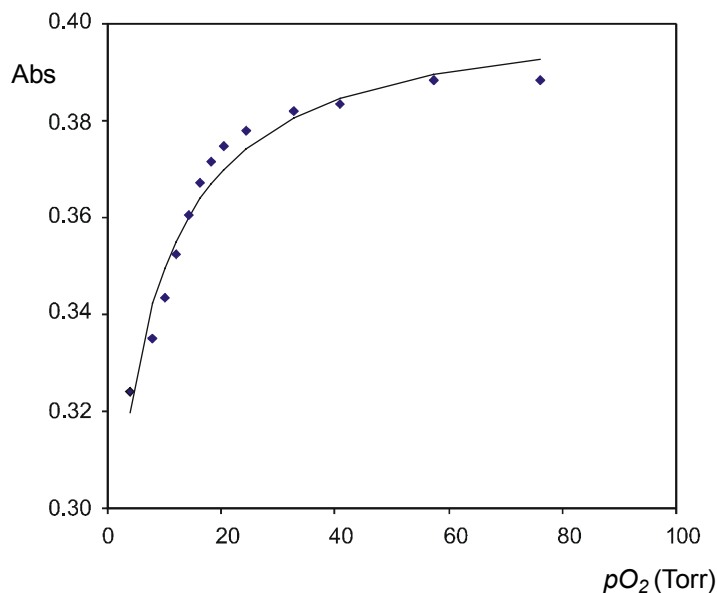


**Figure 3.** Absorbance changes at 553 nm as a function of the  $pO_2$  in equilibrium with a  $2.1 \times 10^{-5}$  M solution of **1b** in CH<sub>3</sub>CN, [1-MeIm] = 0.15 M. Solid line is the fitted curve according to a 1:1 binding isotherm.

*EPR studies.* Because of the complications encountered in the UV-vis measurements (vide supra), EPR (electron paramagnetic resonance) studies were performed to directly detect the formation of O<sub>2</sub> complexes (Figure 4).<sup>16</sup> Co<sup>II</sup> porphyrins and their 1:1 complex with O<sub>2</sub> are paramagnetic species and can be studied via EPR spectroscopy. The Co<sup>2+</sup> ion ( $3d^7$ ) is low spin in porphyrins with one unpaired electron residing in the  $d_{z^2}$ -orbital. O<sub>2</sub> binds to Co affording end-on complexes for which the electron density for the unpaired electron is largely delocalized on the terminal oxygen atom. For this reason these complexes have been described as superoxo-like complexes (Co<sup>III</sup>-O<sub>2</sub><sup>-</sup> formalism).

The EPR spectra for porphyrins **1a** and **1b** recorded in frozen 40:60 MeOH/H<sub>2</sub>O mixtures at 77K (Figures 5a and 6a) are very similar and characteristic of Co<sup>II</sup> porphyrins (axially symmetric molecules with  $S = 1/2$ ,  $I = 7/2$ ). These spectra were obtained in the presence of O<sub>2</sub> since the solutions were prepared in open air. However, there is no spectral evidence for O<sub>2</sub> binding under these conditions.<sup>17</sup>

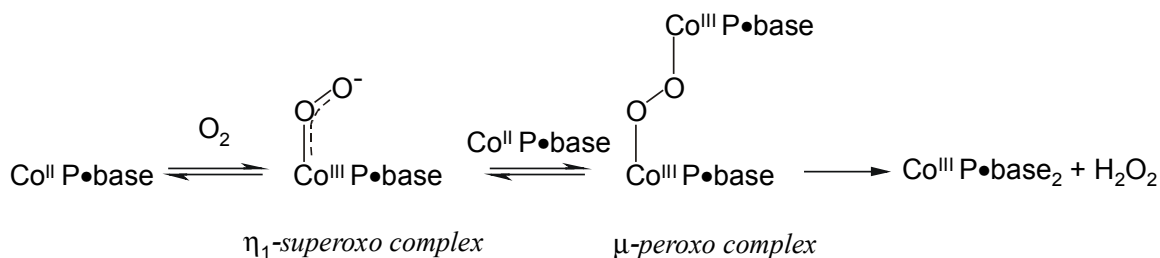


**Figure 4.** Equilibria and reactions for  $\text{Co}^{\text{II}}$  porphyrin systems upon oxygenation. Base indicates a coordinating molecule like a nitrogenous base or a solvent molecule (MeOH,  $\text{H}_2\text{O}$  in this study).

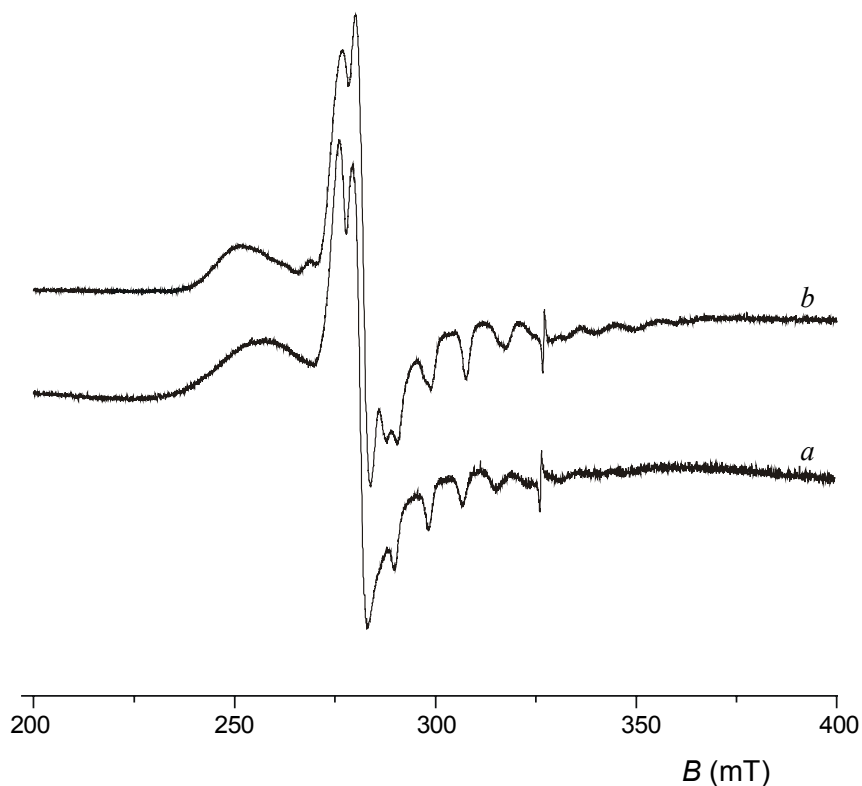


**Figure 5.** EPR spectra of a frozen solution of *a*) **1a** ( $1.26 \times 10^{-3}$  M) and *b*) **1a•2** (**1a**  $1.26 \times 10^{-3}$  M, 1.7 equiv **2**) in 40:60 MeOH/ $\text{H}_2\text{O}$  at 77 K.

The EPR spectra are mainly characterized by two components of the  $g$  tensor viz.  $g_{\perp}$  and  $g_{\parallel}$  (Table 1). Subsequently, solutions of **1a** and **1b** in 40:60 MeOH/ $\text{H}_2\text{O}$  were left in contact with air for periods up to 20 h at room temperature. After this time no decrease in signal intensity of the EPR spectra was observed, showing that no oxidation (formation of  $\text{Co}^{\text{III}}$  porphyrin species) or  $\mu$ -peroxo dimer formation (2:1  $\text{Co}^{\text{II}}$  porphyrin- $\text{O}_2$  complexes,

formally described as diamagnetic Co<sup>III</sup>-O-O-Co<sup>III</sup> species) takes place under these conditions (see Figure 4).

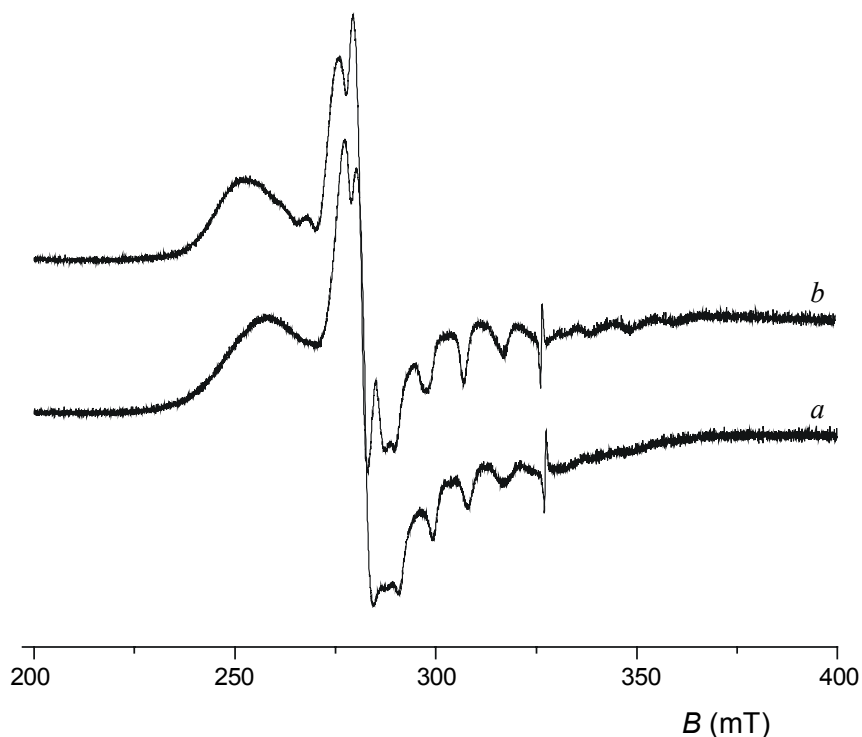


**Figure 6.** EPR spectra of a frozen solution of a) **1b** ( $1.28 \times 10^{-3}$  M) and b) **1b•2** (**1b**  $1.28 \times 10^{-3}$  M, 1.7 equiv **2**) in 40:60 MeOH/H<sub>2</sub>O at 77K.

**Table 1.** EPR parameters for **1a** and **1b** in 40:60 MeOH/H<sub>2</sub>O frozen solutions at 77 K.

	$g_{\perp}$	$g_{\parallel}$	$A_{\parallel}$ (G)
<b>1a</b>	2.324	2.044	84
<b>1b</b>	2.324	2.044	86
<b>3</b> (DMSO) <sup>18</sup>	2.317	2.042	80
<b>3</b> (DMF) <sup>18</sup>	2.335	2.061	83

When imidazole (Im) or BzI was added to **1a** (or **1b**) in 40:60 MeOH/H<sub>2</sub>O in the presence of air, the formation of O<sub>2</sub> adducts Co<sup>II</sup>P•base•O<sub>2</sub> was indicated by the appearance of a new signal at  $g \sim 2.01$  in the EPR spectra.<sup>19</sup> The O<sub>2</sub> adduct is the

dominating species in frozen solutions of porphyrin **1a** (or **1b**) containing 3 equivalents of imidazole. In contrast, a large fraction of  $\text{Co}^{\text{II}}\text{P}\cdot\text{base}$  complex was still present even when using 7-8 equivalents of the weaker base BzI (Figure 7).<sup>20</sup> Moreover, samples containing Im underwent much faster  $\mu$ -peroxo dimer formation<sup>21</sup> as shown by the loss of the EPR signal in measurements performed after 30-50 min of standing at room temperature. For samples containing BzI the signal intensity remained unchanged when the spectra were recorded after 13 h at room temperature. This observation indicates that  $\text{O}_2$  complexes are not present at room temperature (note that EPR spectra are recorded at 77K), which is due to the weaker basicity of BzI. Support for this conclusion is the large reduction in signal intensity ( $\sim 80\%$ ) showing  $\mu$ -peroxo dimer formation observed when **1b** solution containing BzI is kept at around  $-30^\circ\text{C}$  for 3h (lower temperatures strongly favor the formation of  $\text{Co}^{\text{II}}$  porphyrin- $\text{O}_2$  complexes). These results also indicate that for solutions containing Im there must be an appreciable concentration of  $\text{Co}^{\text{II}}$  porphyrin- $\text{O}_2$  complex already at room temperature in the presence of air, which is quickly converted to  $\mu$ -peroxo dimers. Finally, it is worth noting that porphyrin **1a** gave systematically higher amounts of  $\text{O}_2$  complex than **1b** under identical conditions for reasons not yet understood.

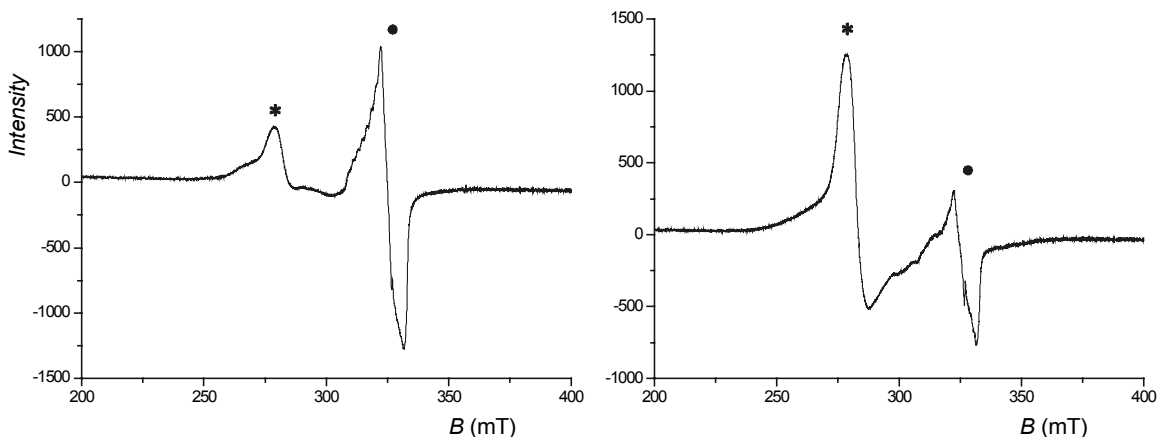


**Figure 7.** EPR spectra of a frozen solution of (left) **1a** ( $1.26 \times 10^{-3}$  M) with 8.0 equiv of benzimidazole in the presence of air; (right) **1b** ( $1.28 \times 10^{-3}$  M) with 7.9 equiv of benzimidazole in the presence of air. In both spectra the signal on the right (\*) at  $g \sim 2.32$  is assigned to  $\text{Co}^{\text{II}}\text{P}\cdot\text{base}$  while the other signal (•) at  $g \sim 2.01$  is assigned to  $\text{Co}^{\text{II}}\text{P}\cdot\text{base}\cdot\text{O}_2$  complex.

Assemblies **1a•2** and **1b•2**, prepared from  $1.26$ - $1.28 \times 10^{-3}$  M porphyrin solutions and 1.7 equiv of calix[4]arene **2**, do not bind  $\text{O}_2$  in the absence of an axial bases (see Figures 5b

and **6b**).<sup>22</sup> However, upon addition of Im or BzI, O<sub>2</sub> complexes were obtained as observed for **1a** and **1b**. These are possibly quaternary complexes formed by one porphyrin unit, one calix[4]arene, one base and one O<sub>2</sub> molecule. The presence of the signal at  $g \sim 2.32$  indicates that conversion to the O<sub>2</sub> complex was not quantitative (Figure 8). The choice of imidazole and benzimidazole as axial bases was dictated by their different molecular dimensions, which can affect their spatial location in complexes **1•2•base**. It was previously shown for analogous ion-pair complexes based on Zn-porphyrins (section 4.2.3) that small nitrogenous ligands such as 4-methylpyridine and 1-MeIm can be encapsulated in the cavity formed between calix[4]arene **2** and porphyrins **1**, while the bulkier caffeine is bound outside on the solvent exposed porphyrin face. A similar behavior is expected for imidazole (encapsulation) and benzimidazole (external complexation). Unfortunately the EPR spectra did not provide any indications about the location of the axial base in the assembly and consequently about the location of O<sub>2</sub>. Furthermore, independently from the base used, no appreciable difference was noted for **1a•2** when compared with the measurements performed with **1a** in the absence of **2**. Slightly larger amounts of O<sub>2</sub> adduct were obtained for **1b•2** compared to **1b** (larger signal for Co<sup>II</sup>P•base•O<sub>2</sub> complex vs Co<sup>II</sup>P•base complex in Figure 8 compared to Figure 7-right).

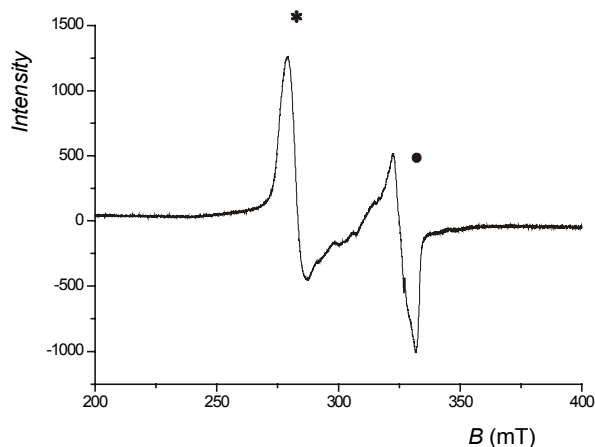


**Figure 8.** EPR spectrum of a frozen solution of **1b•2** (**1b**  $1.28 \times 10^{-3}$  M, 1.7 equiv **2**) with 8.0 equiv of benzimidazole in the presence of air. The signal at  $g \sim 2.32$  (\*) is assigned to Co<sup>II</sup>P•base, the signal at  $g \sim 2.01$  (•) is assigned to Co<sup>II</sup>P•base•O<sub>2</sub> complex.

Surprisingly, when solutions of **1a•2** and **1b•2** containing benzimidazole were left at room temperature for 1-2 h a clear decrease in signal intensity could be observed, thus indicating formation of diamagnetic  $\text{Co}^{\text{III}}$  species. This transformation occurs faster than for **1a** and **1b** under identical conditions. These results contradict the expectation that binding of benzimidazole at the solvent exposed porphyrin face will induce binding of  $\text{O}_2$  within the cavity, preventing the formation of  $\mu$ -peroxo dimers. However, it is important to note that there are other possible oxidative mechanisms leading to EPR-inactive  $\text{Co}^{\text{III}}$  species.<sup>13</sup> One of these may be favored by the calix[4]arene moiety in close proximity to the bound  $\text{O}_2$ .

Thus, these preliminary studies show that binding of  $\text{O}_2$  to self-assembled complexes **1•2** in the presence of an axial base is taking place, but it is hard to describe how calix[4]arene **2** is affecting  $\text{O}_2$  binding. Further structural studies will be necessary to clarify the the complex structure.

#### **5.2.4 Facilitated $\text{O}_2$ transport across supported liquid membranes**

Separation of  $\text{O}_2$  and  $\text{N}_2$  from air is an important process for the production of these two industrially important gases. For large scale preparation of pure gases the method of choice is distillation using cryogenic plants. However, for many industrial applications, especially involving combustion processes, high purity  $\text{O}_2$  is not necessary and  $\text{O}_2$  enriched air can be a valid substitute. In this respect, membrane separation processes may play a crucial role due to the lower costs compared to cryogenic distillation.<sup>2,23</sup> The separation of  $\text{N}_2$  and  $\text{O}_2$  have been achieved using *polymeric membranes*<sup>24</sup> with selective permeability for  $\text{O}_2$ , or *supported liquid membranes*<sup>25,26</sup> in which the liquid phase is a solution containing a selective and reversible  $\text{O}_2$  carrier immobilized in the pores of a thin porous polymer. In the latter case, transport of  $\text{O}_2$  involves chemical binding of  $\text{O}_2$  to the carrier and diffusion limited transport along the concentration gradient created across the membrane, between the feed and the permeate side.<sup>27</sup> Therefore, such membranes are often called *facilitated transport membranes*.<sup>28</sup>

Self-assembled  $\text{O}_2$  carrier solutions were prepared dissolving porphyrins **1**, calix[4]arene **2** and 1-MeIm in water ( $2.0 \times 10^{-3}$  M,  $6.0 \times 10^{-3}$  M, and  $2.0 \times 10^{-2}$  M., respectively). The hydrophilic porous membranes were loaded by immersion in the carrier solutions. The

membranes were then placed in a gas permeation set-up and the feed and the permeate gas streams were analyzed for their content in O<sub>2</sub> and N<sub>2</sub>. Preliminary results of these measurements have been reported elsewhere.<sup>29</sup> Here only one example is reported in which a commercially available membrane (Millipore VMWP) was loaded with a solution containing **1b**, **2**, and 1-MeIm. The feed gas composition was 20% O<sub>2</sub> and 80% N<sub>2</sub>. Facilitated O<sub>2</sub> transport was observed, even though the facilitation factor was only a modest 1.15 (selectivity coefficient 2.3-2.4) with respect to the membrane loaded with only H<sub>2</sub>O (facilitation factor = 1, selectivity = 2, see Figure 9). Decrease in membrane selectivity was observed after 4-6 h indicating possible degradation of the carrier. Enhanced O<sub>2</sub> transport was observed only if all the components necessary for the self-assembled carrier were present.

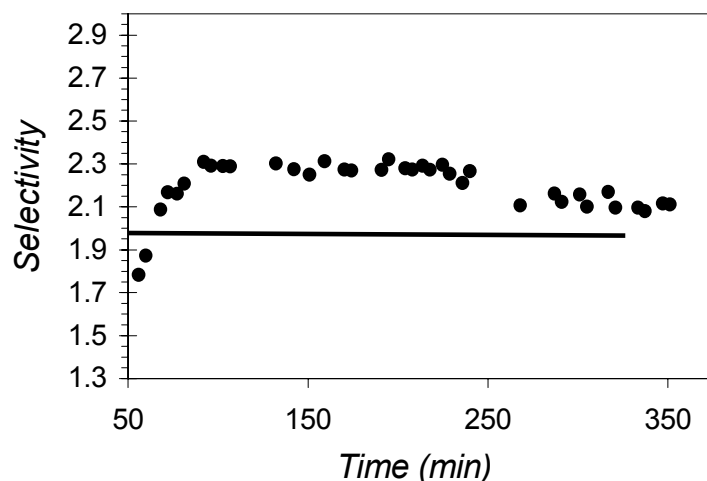


**Figure 9.** Facilitated O<sub>2</sub> transport (dots) observed for a Millipore VMWP membrane loaded with a solution of assembly **1b•2** in water in the presence of 1-MeIm at 10 °C (**1b** =  $2.0 \times 10^{-3}$  M, 3 equiv **2**, 10 equiv of 1-MeIm). The solid line shows the O<sub>2</sub>/N<sub>2</sub> selectivity of the membrane loaded with only H<sub>2</sub>O. Feed gas composition 20% O<sub>2</sub> / 80% N<sub>2</sub>.

### 5.3 Conclusions

Even though the results reported in this Chapter are not optimal, for the application of these carriers in membrane technology, self-assembled complexes **1•2** can be considered a novel class of water-soluble functional models for O<sub>2</sub> binding heme-proteins. A great advantage of these systems is the availability due to the noncovalent synthetic assembly



in their preparation. However, the main drawback is the complexity of the system in which multiple equilibria and species may contribute to the overall response towards changes from the outside (for instance in O<sub>2</sub> concentration). More studies are needed to fully understand the systems and possibly to design a second generation of more efficient self-assembled O<sub>2</sub> carriers.

## 5.4 Experimental part

Mass spectra were measured using a Perkin Elmer/PerSeptive Biosystem Voyager-DE-RP MALDI-TOF mass spectrometer (PerSeptive Biosystem, Inc., Framingham, MA, USA) equipped with delayed extraction. UV-vis measurements were performed on a Varian Cary 3E UV-vis spectrophotometer equipped with a Helma QX optical fiber probe (path length=1.000 cm), using solvents of spectroscopic grade. Calorimetric measurements were carried out using a Microcal VP-ITC microcalorimeter with a cell volume of 1.4115 mL. X-Band EPR spectra were recorded on a Jeol RE2x electron spin resonance spectrometer using DPPH (diphenylpicrylhydrazyl,  $g=2.0036$ ) as a standard. All the EPR measurements were performed in frozen solutions (40:60 MeOH/H<sub>2</sub>O) at 77 K.

Membrane preparation and the sweep gas permeation set-up used to study the facilitated O<sub>2</sub> transport across supported liquid membranes,<sup>29</sup> O<sub>2</sub> binding experiments in solution,<sup>30</sup> synthesis of free base porphyrins **1**<sup>11</sup> and of calix[4]arene **2**<sup>10</sup> have been described in detail elsewhere.

### Preparation of porphyrins **1a** and **1b**

Free base porphyrin **1** was dissolved in deoxygenated MeOH containing 10-20 equiv of Co(Ac)<sub>2</sub>. The solution was stirred 1 h at 40 °C under N<sub>2</sub> (insertion of the metal was followed by UV-vis spectroscopy). Porphyrins **1a** and **1b** (**1b** MALDI-TOF MS:  $m/z$  1898.7 [M-PF<sub>6</sub>]<sup>+</sup>, calculated for [C<sub>80</sub>H<sub>92</sub>N<sub>16</sub>O<sub>8</sub>P<sub>3</sub>F<sub>18</sub>Co]<sup>+</sup> 1898.6) were isolated as hexafluorophosphate salts by precipitation upon addition of NH<sub>4</sub>PF<sub>6</sub>.

## 5.5 References and notes

1. For an overview on the field of natural and biomimetic O<sub>2</sub> carriers see Chapter 2.7 of this thesis.
2. *Oxygen Complexes and Oxygen Activation by Transition Metals*; Martell, A. E.; Sawyer, D. T., Ed.; Plenum Press: New York, 1988.
3. Extensive work has been carried out using membranes containing aqueous solutions of hemoglobin or of bis(histidinato)-cobalt(II) as carriers. See ref 2 and references therein.
4. De Bolfo, J. A.; Smith, T. D.; Boas, J. F.; Pilbrow, J. R. *J. Chem. Soc., Dalton Trans.* **1976**, 1495-1500.
5. Evans, D. F.; Wood, D. *J. Chem. Soc., Dalton Tras.* **1987**, 3099-3101.
6. Zhang, X.; Uffelman, E.; Collman, J. P. U. S. Patent 5384397 A, 1995.
7. Zhang, X.; Uffelman, E. S.; Collman, J. P. U. S. Patent 5274090 A, 1993.
8. For reversible O<sub>2</sub> binding to Fe<sup>II</sup> porphyrins in aqueous media see Komatsu, T.; Hayakawa, S.; Yanagimoto, T.; Kobayakawa, M.; Nakagawa, A.; Tsuchida, E. *Bull. Chem. Soc. Jpn.* **2001**, *74*, 1703-1707. Tsuchida, E.; Komatsu, T.; Arai, K.; Yamada, K.; Nishide, H.; Fuhrhop, J. H. *Langmuir* **1995**, *11*, 1877-1884.
9. Jones, R. D.; Summerville, D. A.; Basolo, F. *Chem. Rev.* **1979**, *79*, 139-179.
10. Fiammengo, R.; Timmerman, P.; Huskens, J.; Versluis, K.; Heck, A. J. R.; Reinhoudt, D. N. *Tetrahedron* **2002**, *58*, 757-764. See also Chapter 3.
11. Fiammengo, R.; Crego-Calama, M.; Timmerman, P.; Reinhoudt, D. N. **2002**, *J. Am. Chem. Soc.* submitted. See also Chapter 7.
12. The presence of an axial base is necessary to enhance the electron density on the Co atom thus increasing the binding ability of Co<sup>II</sup>porphyrins for O<sub>2</sub>.

13. Busch, D. H.; Alcock, N. W. *Chem. Rev.* **1994**, *94*, 585-623.
14. Hambright, P.; Fleischer, E. B. *Inorg. Chem.* **1970**, *9*, 1757-1761.
15. Stynes, H. C.; Ibers, J. A. *J. Am. Chem. Soc.* **1972**, *94*, 5125-5127.
16. Walker, F. A. *J. Am. Chem. Soc.* **1970**, *92*, 4235-4244.
17. It has been observed that the similar 5,10,15,20-tetrakis(*N*-methylpyridinium-4-yl)porphyrinatocobalt(II) can be converted almost quantitatively to the O<sub>2</sub> complex if a solution of the porphyrin in water is bubbled with O<sub>2</sub> for three minutes at r.t. before cooling. See ref 5.
18. Araullo-McAdams, C.; Kadish, K. M. *Inorg. Chem.* **1990**, *29*, 2749-2757.
19. Assignment of the **g** tensor principal axis and determination of the **g** and  $A^{Co}$  matrixes for Co<sup>II</sup>porphyrin-O<sub>2</sub> complex is generally difficult from simple X-band CW EPR spectra and required more sophisticated spectroscopic techniques for accurate determinations. See Van Doorslaer, S.; Schweiger, A. *J. Phys. Chem. B* **2000**, *104*, 2919-2927.
20. The amount of BzI was not further increased since a difference in the spectrum of **1a** was only observed in going from 1 to 3 equiv and not for further additions.
21. Under the experimental conditions used in this Chapter for the EPR spectra,  $\mu$ -peroxo dimer formation is the main cause for the loss of the EPR signal. See ref 5.
22. The measured  $K_{1,2}$  allows for the prediction that 1.7 equiv of calix[4]arene **2** are necessary to obtain higher than 85% of assembly formation at concentrations in the millimolar range used for EPR experiments.
23. Figoli, A.; Sager, W. F. C.; Mulder, M. H. V. *J. Membrane Sci.* **2001**, *181*, 97-110.
24. Lonsdale, H. K. *J. Membr. Sci.* **1982**, *10*, 81-181.
25. Baker, R. W.; Roman, I. C.; Lonsdale, H. K. *J. Membr. Sci.* **1987**, *31*, 15-29.

26. Johnson, B. M.; Baker, R. W.; Matson, S. L.; Smith, K. L.; Roman, I. C.; Tuttle, M. E.; Lonsdale, H. K. *J. Membr. Sci.* **1987**, *31*, 31-67.
27. Mulder, M. H. V. *Basic Principles of Membrane Technology*; Kluwer Academic Publisher: Dordrecht, 1996.
28. The mathematical model for the transport mechanism can be found in refs 2, 26-27.
29. For more details about the O<sub>2</sub> transport results see: Figoli A. *Synthesis of nanostructured mixed matrix membranes for facilitated gas separation*, PhD Thesis (ISBN 90-365-1673-0), University of Twente, 2001, p 139-152.
30. See Experimental part Chapter 6.



# NONCOVALENT SECONDARY INTERACTIONS IN CO(II)SALEN COMPLEXES: O<sub>2</sub> BINDING AND CATALYTIC ACTIVITY IN CYCLOHEXENE OXYGENATION\*

### 6.1 Introduction

The oxygen binding abilities of Co(II)Salen (Salen = bis(salicylidene)ethylenediamine) complexes have long been established and have stimulated research towards reversible O<sub>2</sub> carriers<sup>1,2</sup> and their use as catalysts in oxidation of organic substrates with O<sub>2</sub> as stoichiometric oxidant.<sup>3-7</sup> Variations on the two aromatic rings of the salen ligand have been introduced to investigate the electronic and the steric factors affecting O<sub>2</sub> binding and the reactivity of the metal O<sub>2</sub> complex. However, modification of the salen structure via introduction of *functionalized* diamino bridges has been rarely attempted.<sup>8-10</sup> This is probably as a consequence of the already excellent results obtained by Jacobsen in the enantioselective epoxidation of unfunctionalized alkenes using the easily obtainable (*R,R*)-[*N,N'*-bis(3,5-di-*t*Bu-salicylidene)-1,2-cyclohexanediamine]Mn(III).<sup>11</sup>

Nevertheless, more research in ligand design is of fundamental importance in the field of Salen complexes, as a valuable alternative to metal porphyrins for the development of biomimetic heme-protein models.<sup>12,13</sup> Moreover, recently it has been shown that noncovalent secondary interactions such as metal coordination are very important in order to obtain highly efficient and selective catalysts based on Salen complexes.<sup>14</sup>

---

\* Part of this chapter has been submitted for publication: Fiammengo, R.; Bruinink, C. M.; Crego-Calama, M.; Reinhoudt, D. N. *J. Org. Chem.* **2002**.

In this Chapter the preparation of three novel Co(II)Salen complexes **1-3** bearing (for **1** and **2**) an OH functionalized diamino bridge is reported (Figure 1). The presence of the hydroxyl groups in **1** increases the affinity for oxygen due to hydrogen bonding with the Co-coordinated O<sub>2</sub> (Figure 2).

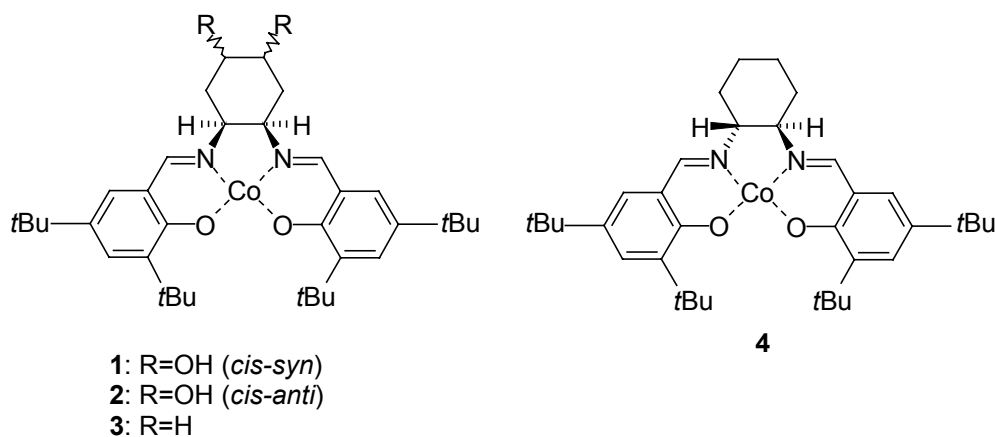


**Figure 1.** Structures of Co(II)Salens **1-4**

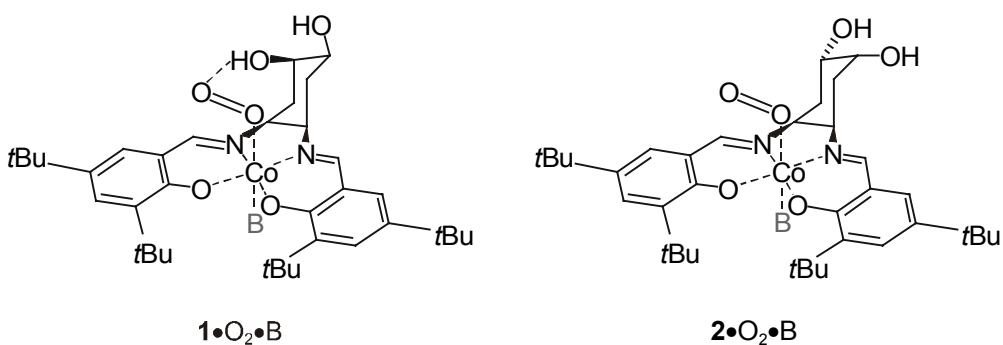


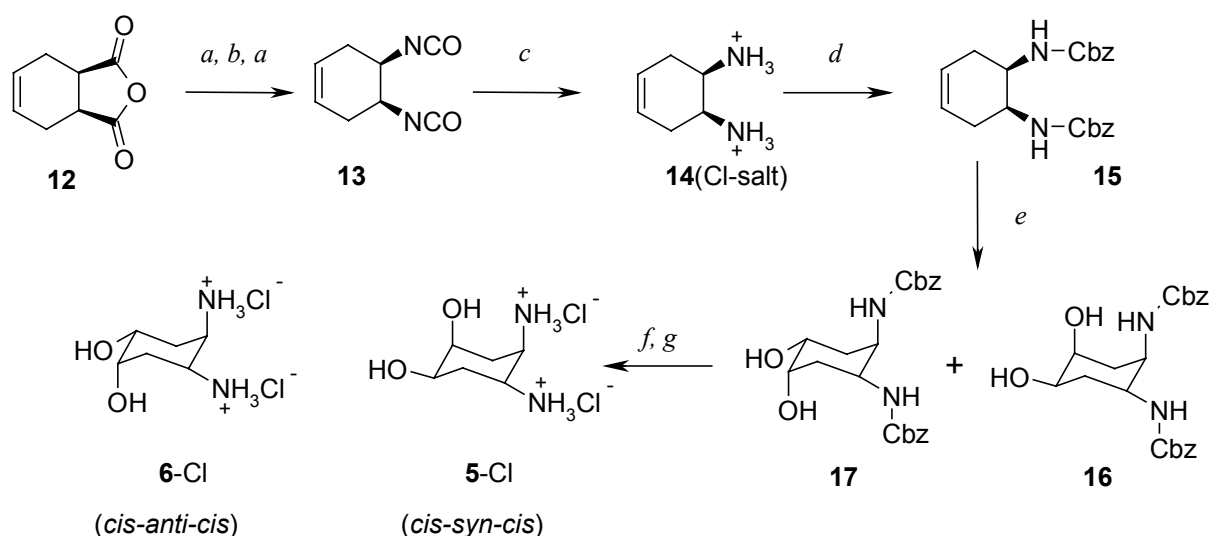
**Figure 2.** Schematic representation of ternary complexes **1•O<sub>2</sub>•B** and **2•O<sub>2</sub>•B** showing hydrogen-bonding stabilization of Co-coordinated O<sub>2</sub> (left). B=base (1-MeIm or propionaldehyde in the text).

To the best of our knowledge, this is the first time that the role of hydrogen bonding as noncovalent secondary interactions in Salen complexes has been considered.<sup>15</sup> This design mimics the hydrogen-bonding interaction operated by the distal His residue in hemoglobin and myoglobin or by Tyr in O<sub>2</sub> avid *Ascaris* hemoglobin.<sup>16,17</sup> Moreover, Co(II)Salen **1-3** and the commercially available **4** have been tested in the aerobic

oxidation of cyclohexene (Scheme 3). Reduced catalytic activity is observed as a consequence of the Co-O<sub>2</sub> complex stabilization.

## 6.2 Results and discussion

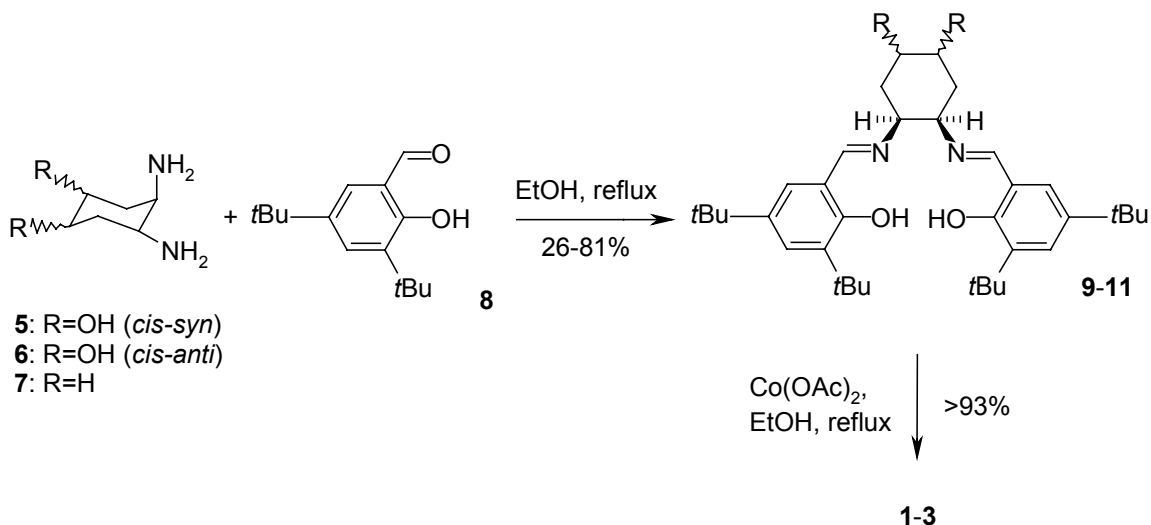
*Synthesis.* Co(II)Salenes **1** and **2** were prepared starting from the two diastereomeric *cis*-1,2-diamino-*cis*-4,5-dihydroxycyclohexanes (**5** and **6** respectively). The corresponding dihydrochloride salts (**5-Cl** and **6-Cl**) were synthesized from *cis*-1,2,3,6-tetraphthalic anhydride **12** following a slightly modified literature procedure (Scheme 1).<sup>18</sup> Catalytic osmylation of Cbz-protected 1,2-diaminocyclohex-4-ene **15** using NMO (4-methylmorpholine-*N*-oxide) as the primary oxidant and DABCO as the ligand afforded a mixture of diastereomeric *cis* diols **16** and **17** in 36:64 ratio (80% yield) at room temperature.<sup>19</sup> Deprotection via catalytic hydrogenation and precipitation with HCl in EtOH afforded the desired salts.



**Scheme 1.** <sup>a</sup> TMS-N<sub>3</sub>, THF, reflux, 3h. <sup>b</sup> SOCl<sub>2</sub>, CCl<sub>4</sub>, cat. DMF, 50°C, 2.5 h. <sup>c</sup> conc. HCl, THF/acetone, rt, 14 h. <sup>d</sup> Cbz-Cl, *N,N*-diisopropyl-*N*-ethylamine, THF/H<sub>2</sub>O, 0°C, 3 h. <sup>e</sup> NMO, OsO<sub>4</sub> (0.02 equiv), DABCO (0.2 equiv) acetone/H<sub>2</sub>O, rt, 72 h. **16** and **17** separation by column chromatography. <sup>f</sup> 10% Pd/C, H<sub>2</sub>, EtOH, rt, 5 h. <sup>g</sup> HCl/EtOH, rt.



Salen ligands **9-11** were prepared by condensation of 3,5-di-*t*-butyl-2-hydroxybenzaldehyde **8** with diamine **5-6** or with *cis*-1,2-diaminocyclohexane **7**, respectively, in refluxing ethanol in moderate to good yields.<sup>20</sup> Subsequent metalation with CoAc<sub>2</sub> afforded Co(II)Salen **1-3** in 93-95% yield (Scheme 2).



Scheme 2

Structural diversity is introduced in Co(II)Salen complexes **1-4** via the 1,2-diaminocyclohexane bridge. The stereochemistry of the two amino groups is (*meso*)-*cis* in **1-3** and (*R,R*)-*trans* in **4**. As a result, **1-3** have non-planar structures, with the cyclohexyl ring being at roughly 90° to the Co(II)-N<sub>2</sub>O<sub>2</sub> plane.<sup>21</sup> Therefore, this spatial arrangement should shield the Co-coordinated O<sub>2</sub>. In contrast, as evident from an earlier X-ray crystal structure,<sup>22</sup> the commercially available Co(II)Salen **4** is roughly planar.

Additionally, two *cis* hydroxyl groups have been introduced on the cyclohexane ring of **1** and **2** in position 4 and 5. The orientation of these two OH groups is either *syn* or *anti* to the two amino groups (see Scheme 1). A CPK model of Co(II)Salen **1** shows that the *syn* arrangement of the *cis*-4,5-hydroxyl groups is necessary for one OH to point directly towards the Co-O<sub>2</sub> moiety, thus adopting the required orientation to form a hydrogen bond with O<sub>2</sub>. No hydrogen bond is possible when the hydroxyl groups are arranged *anti* as in Co(II)Salen **2** and **3** (Figure 2).

*Oxygen binding studies.* Reversible binding of O<sub>2</sub> to Co(II)Salen complexes **1-4** in CH<sub>3</sub>CN or 1:1 toluene/CH<sub>3</sub>CN in the presence of 1-methylimidazole (1-MeIm, 6-7 × 10<sup>-3</sup> M) were studied by following the UV-vis spectral changes (Figures 3 and 4) occurring upon equilibration of the solution with O<sub>2</sub>/N<sub>2</sub> gas mixtures of varying composition (expressed as O<sub>2</sub> partial pressure  $p_{O_2}$ ). The experimental data were treated in terms of 1:1:1 equilibrium<sup>23</sup> between CoL (**2-4**), 1-MeIm and O<sub>2</sub> (eq 1) to evaluate the binding constants,<sup>24</sup>  $K_{O_2}$  (eq 2).



$$K_{O_2} = [\text{CoL}\cdot 1\text{-MeIm}\cdot \text{O}_2] / ([\text{CoL}][1\text{-MeIm}] p_{O_2}) \quad (2)$$

For complexes **2-4**,  $K_{O_2}$  values close to 10 M<sup>-1</sup> Torr<sup>-1</sup> were determined at 10 °C (Table 1) while **1**, under identical conditions, showed much higher O<sub>2</sub> affinity. The complexation is so strong that saturation was obtained already at  $p_{O_2} < 12$  Torr, which precluded the measurement of the binding constant with our experimental set up. Nevertheless, considering **1**•1-MeIm•O<sub>2</sub> > 90% at 12 Torr, a lower limit of 100 M<sup>-1</sup> Torr<sup>-1</sup> can be estimated for  $K_{O_2}$ , one order of magnitude higher than for the diastereomeric complex **2**.

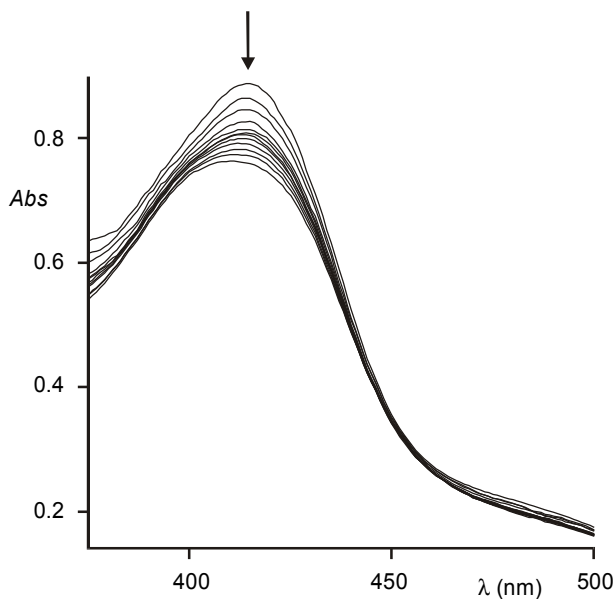


**Figure 3.** Spectral changes as function of increasing  $p_{O_2}$  in equilibrium with a solution of **2** at 10 °C.  $[\mathbf{2}] = 11 \times 10^{-5}$  M, in CH<sub>3</sub>CN,  $[1\text{-MeIm}] = 7 \times 10^{-3}$  M. Max.  $p_{O_2} = 152$  Torr.

This result agrees with the proposed hydrogen bonding stabilization of Co-coordinated O<sub>2</sub> which, according to the three-dimensional arrangement of its hydroxyl groups, is specific for **1**. Moreover, the similar and lower  $K_{O_2}$  determined for **2-4** show that the spatial arrangement of the diamino bridges of these complexes has no appreciable influence on O<sub>2</sub> binding.

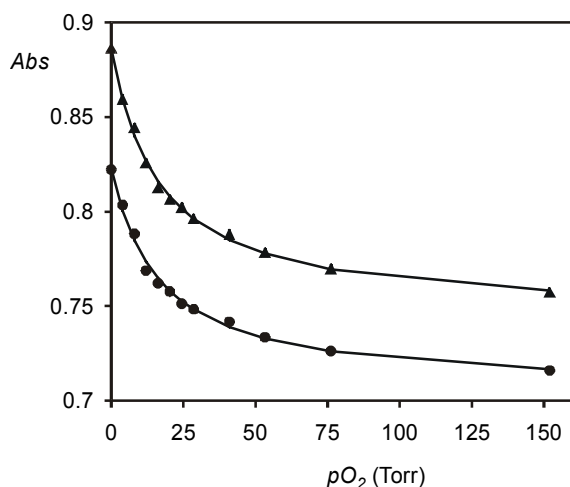


**Figure 4.** Absorbance changes at 416 nm (▲) and at 424 nm (●) as function of the  $pO_2$  in equilibrium with a  $11 \times 10^{-5}$  M solution of **2** in CH<sub>3</sub>CN, [1-MeIm] =  $7 \times 10^{-3}$  M. Solid lines are the best fitting according to a 1:1:1 model (see text).

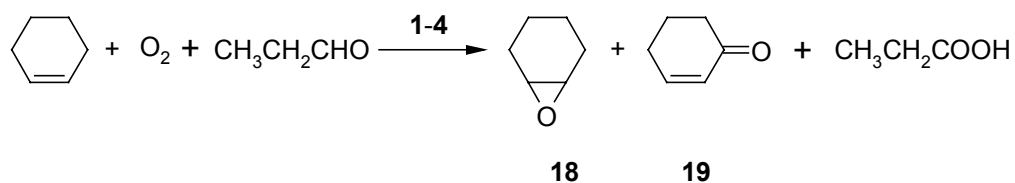
**Table 1.** Formation constants of ternary complexes CoL•1-MeIm•O<sub>2</sub> in CH<sub>3</sub>CN solutions at 10 °C. [CoL] =  $6-10 \times 10^{-5}$  M, [1-MeIm] =  $6-7 \times 10^{-3}$  M.

	$K_{O_2}$ (M <sup>-1</sup> Torr <sup>-1</sup> )
<b>1</b>	$\geq 100^a$
<b>2</b>	8.4
<b>3</b>	13.6
<b>4</b>	$9.5^b$

<sup>a</sup> estimated value (see text). <sup>b</sup> 1:1 toluene/acetonitrile

In the absence of 1-methylimidazole, O<sub>2</sub> binding to **1-4** was neither observed at 10 nor at -10 °C. This result confirms that strong O<sub>2</sub> complexation to **1** is due to secondary interactions (hydrogen bonding) stabilizing the ternary complex **1**•1-MeIm•O<sub>2</sub> and not to alteration of the metal center electronic properties.

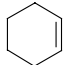
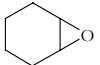
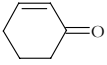
*Oxygenation of cyclohexene.* Co(II) Schiff's base complexes<sup>3</sup> as well as Co(II)porphyrins<sup>25</sup> catalyze the oxidation of organic substrates (e.g. alkenes and alkanes) with O<sub>2</sub> as the bulk oxidant in the presence of reducing agents such as aldehydes. Therefore, oxidation of cyclohexene with O<sub>2</sub> in the presence of propanal (Scheme 3) was chosen as a model reaction to study the relationship between noncovalent secondary interactions stabilizing O<sub>2</sub> binding and the catalytic activity of complexes **1-4**. A mechanistic study of the oxygenation of cyclohexene with Co(II)Salens **1-4** is beyond the scope of this work. However, it has been reported for similar systems that the reaction probably starts with the formation of a CoL•B•O<sub>2</sub> complex (where B = aldehyde)<sup>26</sup> in close analogy with the formation of CoL•1-MeIm•O<sub>2</sub> under the equilibrium conditions reported here.



**Scheme 3**

Complexes **1-4** efficiently catalyze cyclohexene oxidation under mild conditions (20 °C, 1 atmosphere of O<sub>2</sub>, 0.5 mol% of catalyst, propionaldehyde as co-reductant) affording, independently from the catalyst used, two oxygenation products<sup>27</sup> viz. cyclohexene oxide **18** and 2-cyclohexene-1-one **19** in 4.7 ± 0.5 ratio (**18/19**) at 70 % conversion (Figure 5).<sup>28</sup> The constant product selectivity observed for different metal catalyst shows a common catalytic pathway for all the reactions, which probably involves radical chain reactivity, a well-documented pathway for Co complexes catalyzed oxidations.<sup>5,7,29</sup> Nevertheless, different catalysts exhibit distinct reactivities, as evident from the measured induction times (*t*<sub>ind</sub>), initial reaction rate (*r*<sub>i</sub>), and half-life times for cyclohexene conversion (*t*<sub>1/2</sub>) (Table 2). These differences can be related to the catalyst structure and in particular to the hydrogen bonding ability of **1** vs **2-4** and possibly to the steric hindrance around the metal center caused by the orientation of the cyclohexyl ring with respect to the Co(II)-N<sub>2</sub>O<sub>2</sub> plane (coplanar as in **4** vs bent as in **1-3**).

**Table 2.** Catalytic oxidation of cyclohexene with Co(II)Salen **1-4**. Induction times ( $t_{\text{ind}}$ ), initial rates for cyclohexene consumption and product formation ( $r_i$ ) and cyclohexene half-life times ( $t_{1/2}$ ). Typical reaction conditions as in Figure 5.

	$t_{\text{ind}} (\times 10^3 \text{ s})$	$r_i (\times 10^5 \text{ mol l}^{-1} \text{ s}^{-1})$			$t_{1/2} (\times 10^3 \text{ s})$
					
<b>1</b>	8.82	2.33	2.13	0.48	4.79
<b>2</b>	2.73	2.48	2.18	0.65	4.23
<b>3</b>	4.62	2.87	3.15	0.77	3.77
<b>4</b>	0.40	1.07	2.56	0.35	2.58

During  $t_{\text{ind}}$  no oxygenation products were detected in the reaction mixture via gas chromatographic analysis (GC). However, the reaction mixture underwent a series of color changes from brick red to brown and finally green, which is similar to previous observations for similar reactions.<sup>30</sup> The color change to green has been attributed to the formation of Co(III)-hydroperoxide complexes in solution from the starting  $\text{CoL}\cdot\text{B}\cdot\text{O}_2$  complexes via radical reaction with the aldehyde (H-abstraction) during the initiation step. The longest  $t_{\text{ind}}$  (8800 s) is observed for Co(II)Salen **1** and indicates a retarded formation of the Co(III)-hydroperoxide intermediate. Thus, the hydrogen bond reduces the radical reactivity of  $\mathbf{1}\cdot\text{B}\cdot\text{O}_2$  in comparison to complexes  $(\mathbf{2-4})\cdot\text{B}\cdot\text{O}_2$ . The shortest  $t_{\text{ind}}$  (400 s) is observed for **4**, which is consistent with the absence of a hydrogen bond and of steric hindrance that protects the Co-O<sub>2</sub> moiety due to its planar structure. The  $t_{\text{ind}}$  for **2** and **3** are somewhere in between, as expected for complexes without hydrogen bond possibilities but with a nonplanar structure. The relative order of these values remains still unclear. Furthermore, the initial reaction rate ( $r_i$ ) and the half-life time for cyclohexene conversion ( $t_{1/2}$ , the time at which 50% of cyclohexene is converted minus  $t_{\text{ind}}$ ) are different within these series of catalyst **1-4** (Table 2). It is generally accepted that acylperoxy radicals and Co-coordinated acylperoxy complexes are the active oxygen transfer species formed during propagation of the oxidation reaction catalyzed by Co(II)complexes.<sup>7,31,32</sup> Thus, the results reported in Table 2 suggest that Co(II)Salens **1-4** participate to some extent in the oxygen transfer to the substrate, possibly as Co-

coordinated acylperoxy species, and not only in the initiation step. Consequently, hydrogen bonding and steric hindrance also play an important role in stabilizing these intermediate species during the propagation step of the reaction. In fact, **1** is the least reactive catalyst presenting the smallest  $r_i$  and the longest  $t_{1/2}$ , while **4** is the most reactive one having the shortest  $t_{1/2}$ . The  $r_i$  values for **4** are somehow smaller than expected. However, this catalyst also exhibits a slightly different concentration vs time profile when compared to catalysts **1-3**. Actually, the oxidation time course obtained for catalyst **4** resembles an autocatalytic reaction (Figure 6). Probably for this reason the initial rates ( $r_i$ ) for **4** (Table 2) are the smallest in the series while  $t_{1/2}$  is the shortest, indicating higher reactivity.

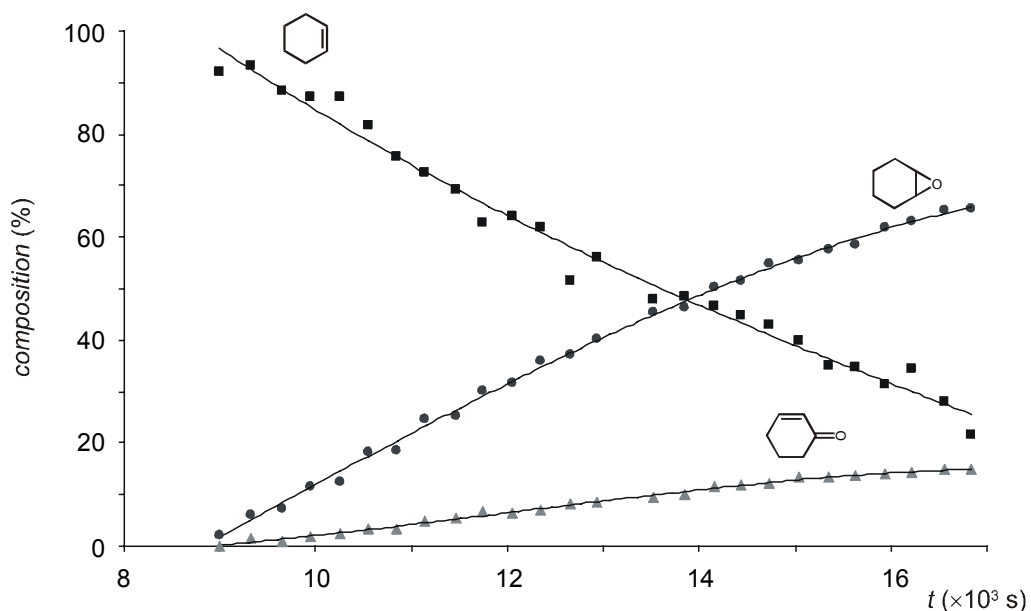


**Figure 5.** Concentration vs time profile for cyclohexene (0.18 M in CH<sub>3</sub>CN) oxidation catalyzed by Co(II)Salen **1** (0.005 equiv). Conditions: 20 °C, O<sub>2</sub> 1 atm, propanal (4 equiv).

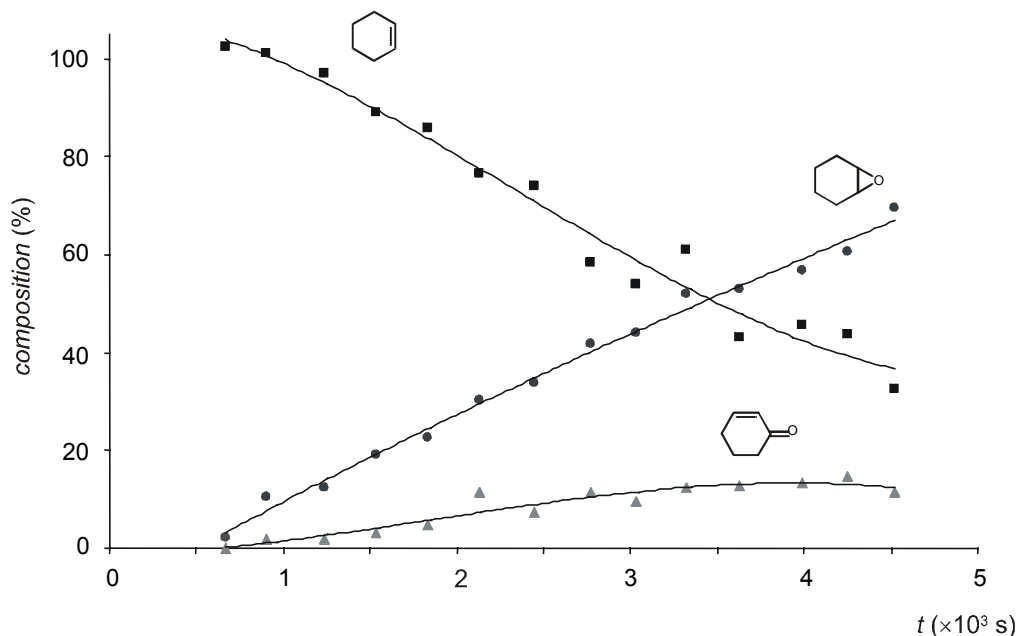


**Figure 6.** Concentration vs time profile for cyclohexene oxidation catalyzed by Co(II)Salen **4**. Conditions as in Figure 5. Note especially the slightly sigmoidal shape for the cyclohexene curve.

### 6.3 Conclusions

O<sub>2</sub> affinity studies on novel Co(II)Salen complexes **1-3** (and on commercially available **4**) have shown that noncovalent secondary interactions and especially hydrogen bonding largely increase O<sub>2</sub> binding (**1** vs **2-4**). The observed enhanced O<sub>2</sub> binding for **1** is also reflected in the lower catalytic reactivity in the cyclohexene oxidation. The simple variations introduced on the salen ligand skeleton, and in particular on the diamino bridge, show substantial control over the binding properties of Co(II)Salen complexes by secondary interactions. These results might allow introduction of an alternative model to the heavily exploited field of biomimetic superstructured porphyrins.

### 6.4 Experimental part

<sup>1</sup>H NMR and <sup>13</sup>C NMR spectra were performed on a Varian Unity INOVA (300 MHz) or a Varian Unity 400 WB NMR spectrometer. <sup>1</sup>H NMR chemical shift values (300 MHz) are expressed in ppm relative to residual CHD<sub>2</sub>OD ( $\delta$  3.30) or CHCl<sub>3</sub> ( $\delta$  7.26). <sup>13</sup>C NMR chemical shift values (100 MHz) are expressed in ppm relative to residual CD<sub>3</sub>OD ( $\delta$

49.0) or CDCl<sub>3</sub> ( $\delta$  76.9). Infrared spectra were recorded on a FT-IR Perkin Elmer Spectrum BX spectrometer using KBr pellets. Elemental analyses were carried out using a 1106 Carlo-Erba Strumentazione element analyzer. MS FAB spectra were measured on a Finnigan MAT 90 spectrometer with m-nitrobenzylalcohol (NBA) as the matrix. GC spectra were recorded on a Varian 3400 gas chromatograph equipped with a flame ionization detector (FID), using a capillary column (30 m, 0.25  $\mu$ m film thickness) with DB-5MS stationary phase (for temperature program, response factor determination see Supplementary Informations).

### General procedure for the synthesis of Salenes 9 and 10

3,5-di-*t*-butyl-2-hydroxybenzaldehyde **8** (280 mg, 1.2 mmol) was added to a solution of *cis*-1,2-diamino-*cis*-4,5-dihydroxycyclohexane dihydrochloride salt **5-Cl**<sup>18</sup> (or **6-Cl**)<sup>18</sup> (120 mg, 0.55 mmol) and NaHCO<sub>3</sub> (100 mg, 1.2 mmol) in 10 ml of EtOH at room temperature. The reaction mixture was stirred for 1 hour at 75 °C, and the solvent was removed under vacuum. The product was extracted from the solid residue with CHCl<sub>3</sub> and recrystallized from CH<sub>3</sub>OH.

### (1*R*,2*S*,3*R*,4*S*)-[*N,N'*-bis(3,5-di-*t*Bu-salicylidene)-4,5-dihydroxy-1,2-cyclohexanediamine **10**

Yield: 26%. <sup>1</sup>H NMR (400 MHz, CDCl<sub>3</sub>):  $\delta$  (ppm) 12.88 (bs, 2H), 8.26 (s, 2H), 7.27 (d, 2H,  $J=2.2$  Hz), 6.96 (d, 2H,  $J=2.2$  Hz), 3.95-3.86 (m, 2H), 3.59-3.52 (m, 2H), 2.56 (bs, 2H), 2.35-2.25 (m, 2H), 1.98-1.90 (m, 2H), 1.28 (s, 18H), 1.18 (s, 18H). <sup>13</sup>C NMR (100 MHz, CDCl<sub>3</sub>):  $\delta$  (ppm) 166.59, 158.08, 140.38, 137.01, 127.62, 126.40, 117.86, 69.96, 67.90, 35.23, 34.30, 31.64, 29.59. IR: (cm<sup>-1</sup>) 3369, 2958, 2910, 2870, 1629, 1467, 1439, 1391, 1362, 1274, 1251, 1203, 1173, 1100, 1039, 968, 773. FAB-MS:  $m/z$  578.3 ([M]<sup>+</sup>, calcd 578.4). Anal. calcd for C<sub>36</sub>H<sub>54</sub>N<sub>2</sub>O<sub>4</sub>: %C 74.70, %H 9.40, %N 4.84; found: %C 74.25, %H 9.50, %N 4.75.



**(1*R*,2*S*,3*S*,4*R*)-[*N,N'*-bis(3,5-di-*t*Bu-salicylidene)-4,5-dihydroxy-1,2-cyclohexanediamine 9**

Yield: 65% yield. <sup>1</sup>H NMR (400 MHz, CDCl<sub>3</sub>): δ (ppm) 13.46 (bs, 2H), 8.40 (s, 2H), 7.37 (d, 2H, *J*=2.3 Hz), 7.07 (d, 2H, *J*=2.3 Hz), 4.38-4.31 (m, 2H), 3.90-3.80 (m, 2H), 2.25 (bs, 2H), 2.21-2.10 (m, 4H), 1.40 (s, 18H), 1.29 (s, 18H). <sup>13</sup>C NMR (100 MHz, CDCl<sub>3</sub>): δ (ppm) 166.64, 158.22, 140.28, 136.82, 127.34, 126.31, 118.01, 68.71, 35.22, 34.31, 34.01, 31.67, 29.64. IR: (cm<sup>-1</sup>) 3422, 2957, 2909, 2871, 1628, 1459, 1439, 1390, 1362, 1274, 1250, 1202, 1174, 1088, 1027. FAB-MS: *m/z* 578.3 ([M]<sup>+</sup>, calcd 578.4). Anal. calcd for C<sub>36</sub>H<sub>54</sub>N<sub>2</sub>O<sub>4</sub>: %C 74.70, %H 9.40, %N 4.84; found: %C 73.99, %H 9.52, %N 4.76.

**Preparation of (1*R*,2*S*)-[*N,N'*-bis(3,5-di-*t*Bu-salicylidene)-1,2-cyclohexanediamine 11**

3,5-di-*t*-butyl-2-hydroxybenzaldehyde **8** (490 mg, 2.1 mmol) was added to a solution of *cis*-1,2-diaminocyclohexane **7** (120 μl, 1.0 mmol) in 20 ml of EtOH at room temperature. The reaction mixture was stirred for 1 hour at 75 °C, and gradually cooled down to room temperature to allow precipitation of the product. The bright yellow solid was then filtrated and washed several times with cold CH<sub>3</sub>OH. Yield: 81% (445 mg, 0.81 mmol).

<sup>1</sup>H NMR (400 MHz, CDCl<sub>3</sub>): δ (ppm) 13.77 (bs, 2H), 8.37 (s, 2H), 7.36 (d, 2H, *J*=2.3 Hz), 7.07 (d, 2H, *J*=2.3 Hz), 3.63-3.57 (m, 2H), 2.09-1.92 (m, 2H), 1.82-1.73 (m, 2H), 1.67-1.55 (m, 2H), 1.42 (s, 18H), 1.29 (s, 18H). <sup>13</sup>C NMR (100 MHz, CDCl<sub>3</sub>): δ (ppm) 165.41, 158.40, 140.00, 136.80, 127.03, 126.17, 118.15, 69.53, 35.24, 34.30, 31.70, 30.65, 29.67, 22.94. IR: (cm<sup>-1</sup>) 2997, 2955, 2864, 1630, 1598, 1459, 1441, 1390, 1362, 1273, 1251, 1204, 1174, 1134, 1083, 989, 879, 853, 827, 773. FAB-MS: *m/z* 546.3 ([M]<sup>+</sup>, calcd 546.4), 547.3. Anal. calcd for C<sub>36</sub>H<sub>54</sub>N<sub>2</sub>O<sub>2</sub>: %C 79.07, %H 9.95, %N 5.12; found: %C 78.99, %H 10.13, %N 5.25.

**General procedure for the synthesis of Co(II)Salen 1-3**

Salens **9-11** (1 equiv) were dissolved under nitrogen in degassed EtOH (typically 0.7 mmol in 10 ml). A Co(Ac)<sub>2</sub>·4H<sub>2</sub>O solution in degassed EtOH (1.5 equiv in 5 ml) was then added causing an immediate color change from bright yellow to deep red. The reaction mixture was heated to reflux for 1 hour under nitrogen and dried in vacuo. The product

was extracted from the solid residue with  $\text{CHCl}_3$ , dried under vacuum, and washed with  $\text{CH}_3\text{OH}$  affording **1-3** as brick red/dark red solids which were always stored under nitrogen at  $-30\text{ }^\circ\text{C}$ .

**Co(II)Salen 1** Yield: 97%. FAB-MS:  $m/z$  635.3 ( $[\text{M}]^+$ , calcd. 635.3). Anal. calcd for  $\text{C}_{36}\text{H}_{52}\text{N}_2\text{O}_4\text{Co}$ : %C 68.01, %H 8.24, %N 4.41; found: %C 67.74, %H 8.36, %N 4.35.

**Co(II)Salen 2** Yield: 100%. FAB-MS:  $m/z$  635.3 ( $[\text{M}]^+$ , calcd. 635.3). Anal. calcd for  $\text{C}_{36}\text{H}_{52}\text{N}_2\text{O}_4\text{Co}$ : %C 68.01, %H 8.24, %N 4.41; found: %C 67.60, %H 8.51, %N 4.26.

**Co(II)Salen 3** Yield: 93%. FAB-MS:  $m/z$  603.3 ( $[\text{M}]^+$ , calcd. 603.3). Anal. calcd for  $\text{C}_{36}\text{H}_{52}\text{N}_2\text{O}_2\text{Co}$ : %C 71.62, %H 8.68, %N 4.64; found: %C 72.03, %H 8.45, %N 4.80.

### Oxygen binding measurements

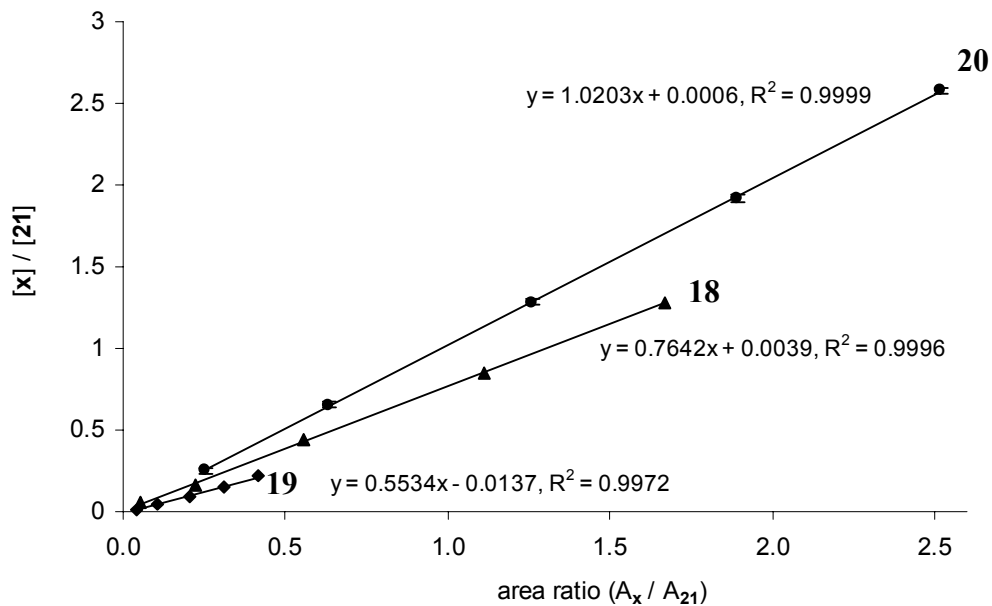
$\text{O}_2$  affinities were measured spectrophotometrically under equilibrium conditions with a Varian Cary 3E UV-vis spectrophotometer equipped with a Helma QX optical fiber probe (path length = 1.000 cm), using solvents of spectroscopic grade. Solutions of Co(II)Salenes **1-4** ( $6\text{-}10 \times 10^{-5}$  M) in  $\text{CH}_3\text{CN}$  containing 1-Melm ( $6\text{-}7 \times 10^{-3}$  M) were prepared under nitrogen using degassed solvent. The solutions were transferred to a measuring chamber thermostated at  $10\text{ }^\circ\text{C}$  and equipped with the UV-vis optical probe.  $\text{O}_2$  content in the gas layer in equilibrium with the solution in the chamber was varied using the flow method.<sup>33</sup>  $p\text{O}_2$  was varied between 3.9 and 152 Torr.

### General procedure for the catalytic oxidation of cyclohexene

In a an external-cooling jacketed reactor at  $20\text{ }^\circ\text{C}$  with vigorous stirring, a freshly prepared solution of Co(II)Salen (**1-4**, 0.005 equiv respect to cyclohexene) and 1,2-dichlorobenzene as the internal standard (200  $\mu\text{l}$ ) in  $\text{CH}_3\text{CN}$  (25 ml) was equilibrated (2-5 min) with  $\text{O}_2$  (1 atm). Propanal (1.4 ml, 20 mmol) and cyclohexene (500  $\mu\text{l}$ , 5.0 mmol) were then added simultaneously to start the reaction. The reaction course was monitored via GC analysis: 50  $\mu\text{l}$  samples were withdrawn from the reaction mixture and diluted

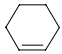
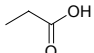
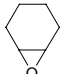
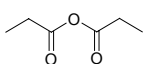
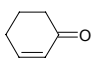
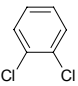
with 250  $\mu\text{l}$  of  $\text{CH}_2\text{Cl}_2$  before injection. The detected products were epoxide 18, unsaturated ketone 19, propionic acid and traces of propionaldehyde.

### GC analysis of the catalytic oxidation of cyclohexene



**Figure 7.** Response factors for 18-20

**Table 3.** Retention times ( $t$ ) for analytical samples of compounds present in the cyclohexene oxidation reaction mixture

		$t$ (min)
	<b>20</b>	1.8
		1.9-2.4
	<b>18</b>	3.5
		4.3
	<b>19</b>	4.6
	<b>21</b>	6.0

GC method: injector 200 °C; detector 280 °C; column: 50 °C (hold 0.5 min), ramp 7 °C/min to 75 °C (hold 0.1 min), ramp 25 °C/min to 120 °C.

The retention times observed for compounds possibly present in the reaction mixture are summarized in Table 3 (determined using commercially available samples). Response factors were determined for products **18** and **19** and for cyclohexene **20** using 1,2-dichlorobenzene as internal standard (Figure 7).

## 6.5 References and notes

1. For an X-ray structure of a 1:1 O<sub>2</sub>-Co(II)Salen complex carrying 1-Melm as an axial base see: Avdeef, A.; Schaefer, W. P. *J. Am. Chem. Soc.* **1976**, *98*, 5153-5159.
2. For review articles see: Jones, R. D.; Summerville, D. A.; Basolo, F. *Chem. Rev.* **1979**, *79*, 139-179 and Niederhoffer, E. C.; Timmons, J. H.; Martell, A. E. *Chem. Rev.* **1984**, *84*, 137-203. For more recent works see: Miyokawa, K.; Kinoshita, S.; Etoh, T.; Wakita, H. *Bull. Chem. Soc. Jpn.* **1992**, *65*, 3374-3377. Bhattacharya, S.; Mandal, S. S. *J. Chem. Soc., Chem. Commun.* **1995**, 2489-2490. Krebs, J. F.; Borovik, A. S. *Chem. Commun.* **1998**, 553-554. Nishide, H.; Mizuma, H.; Tsuchida, E.; McBreen, J. *Bull. Chem. Soc. Jpn.* **1999**, *72*, 1123-1127. Sharma, A. C.; Borovik, A. S. *J. Am. Chem. Soc.* **2000**, *122*, 8946-8955.
3. For review articles see: Mukayama, T.; Yamada, T. *Bull. Chem. Soc. Jpn.* **1995**, *68*, 17-35. Bailey, C. L.; Drago, R. S. *Coord. Chem. Rev.* **1987**, *79*, 321-332.
4. Bernardo, K.; Leppard, S.; Robert, A.; Commenges, G.; Dahan, F.; Meunier, B. *Inorg. Chem.* **1996**, *35*, 387-396.
5. Rhodes, B.; Rowling, S.; Tidswell, P.; Woodward, S.; Brown, S. M. *J. Mol. Catal. A* **1997**, *116*, 375-384.
6. Kureshi, R. I.; Khan, N. H.; Abdi, S. H. R.; Bhatt, A. K.; Iyer, P. *J. Mol. Catal.* **1997**, *121*, 25-31.
7. Kholdeeva, O. A.; Vanina, M. P. *React. Kinet. Catal. Lett.* **2001**, *73*, 83-89.

8. Zanello, P.; Cini, R.; Cinquantini, A.; Orioli, P. L. *J. Chem. Soc., Dalton Trans.* **1983**, 2159-2166.
9. Corden, B. B.; Drago, R. S.; Perito, R. P. *J. Am. Chem. Soc.* **1985**, *107*, 2903-2907.
10. Blaauw, R.; Kingma, I. E.; Laan, J. H.; van der Baan, J. L.; Balt, S.; de Bolster, M. W. G.; Klumpp, G. W.; Smeets, W. J. J.; Spek, A. L. *J. Chem. Soc., Perkin 1* **2000**, 1199-1210.
11. Jacobsen, E. N. *Catalytic Asymmetric Synthesis*; Ojima, I., Ed.; VCH: New York, 1993; pp 159-199.
12. For covalent superstructured porphyrins as model systems for heme-proteins, see: Collman, J. P.; Fu, L. *Acc. Chem. Res.* **1999**, *32*, 455-463. Collman, J. P. *Inorg. Chem.* **1997**, *36*, 5145-5155. Momentau, M.; Reed, C. A. *Chem. Rev.* **1994**, *94*, 659-698. For supramolecular modified porphyrins see: Weiss, J. *J. Incl. Phenom.* **2001**, *40*, 1-22. Robertson, A.; Shinkai, S. *Coord. Chem. Rev.* **2000**, *205*, 157-199. Tani, F.; Matsu-ura, M.; Nakayama, S.; Ichimura, M.; Nakamura, N.; Naruta, Y. *J. Am. Chem. Soc.* **2001**, *123*, 1133-1142. Gazeau, S.; Pècaut, J.; Marchon, J.-C. *Chem. Commun.* **2001**, 1644-1645. Starnes, S. D.; Rudkevich, D. M.; Rebek, J., Jr. *J. Am. Chem. Soc.* **2001**, *123*, 4659-4669.
13. For Co(II) Schiff base "lacunar complexes" as biomimetic O<sub>2</sub> carriers: Busch, D. H.; Alcock, N. W. *Chem. Rev.* **1994**, *94*, 585-623. Rybak-Akimova, E. V.; Marek, K.; Masarwa, M.; Busch, D. H. *Inorg. Chim. Acta* **1998**, *270*, 151-161. See also ref 2.
14. Cooperative bimetallic mechanism in epoxide ring-opening reaction catalyzed by Co(III)Salen and Cr(III)Salen complexes: Jacobsen, E. N. *Acc. Chem. Res.* **2000**, *33*, 421-431. Ready, J. M.; Jacobsen, E. N. *J. Am. Chem. Soc.* **2001**, *123*, 2687-2688. Ready, J. M.; Jacobsen, E. N. *Angew. Chem. Int. Ed.* **2002**, *41*, 1374-1377. Supramolecular metallocleft catalysts (UO<sub>2</sub>Salophen): van Axel Castelli V.; Dalla Cort, A.; Mandolini, L.; Reinhoudt, D. N.; Schiaffino, L. *Chem. Eur. J.* **2000**, *6*, 1193-1198. van Axel Castelli, V.; Dalla Cort, A.; Mandolini, L. *J. Am. Chem. Soc.*

- 1998**, *120*, 12688-12689.
15. Hydrogen bond stabilization of the Co-coordinated O<sub>2</sub> has been considered for a Co(II) Schiff base complex obtained from salicyl aldehyde and L-Serine. However no binding studies have been performed to quantify the interaction, see: Punniyamurthy, T.; Bhatia, B.; Reddy, M. M.; Maikap, G. C.; Iqbal, J. *Tetrahedron* **1997**, *53*, 7649-7670.
  16. Goldberg, D. E. *Chem. Rev.* **1999**, *99*, 3371-3378.
  17. Hydrogen-bonding interactions and reactivity of coordinated O<sub>2</sub> in natural and biomimetic porphyrin systems: Harris, D. L.; Loew, G. H. *J. Am. Chem. Soc.* **1994**, *116*, 11671-11674. Chang, C. K.; Avilés, G.; Bag, N. *J. Am. Chem. Soc.* **1994**, *116*, 12127-12128.
  18. Witiak, D. T.; Rotella, D. P.; Filippi, J. A.; Gallucci, J. *J. Med. Chem.* **1987**, *30*, 1327-1336.
  19. No further attempt to increase the diastereoselectivity of the osmylation reaction was made.
  20. Judged from NMR spectra condensation of diamino diols **5-6** with aldehyde **8** was quantitative. Poor crystallization from methanol lowered the yield in isolated products **9-10** in comparison to **11**.
  21. van Doorn, A. R.; Schaafstra, R.; Bos, M.; Harkema, S.; van Eerden, J.; Verboom, W.; Reinhoudt, D. N. *J. Org. Chem.* **1991**, *56*, 6083-6084.
  22. Leung, W.-H.; Chan, E. Y. Y.; Chow, E. K. F.; Williams, I. D.; Peng, S.-M. *J. Chem. Soc., Dalton Trans.* **1996**, 1229-1236.
  23. Binding of O<sub>2</sub> has often been considered as a 1:1 equilibrium between O<sub>2</sub> and CoL•B. Experimentally, it is required that [B] be high enough to have CoL•B as the predominant species in solution before O<sub>2</sub> addition. This condition is difficult to achieve with complexes **1-4** in CH<sub>3</sub>CN. For instance, binding constants of < 10 M<sup>-1</sup>

- for pyridine to CoL complexes similar to **3** and **4** in CHCl<sub>3</sub> are reported, see ref 24.
24. O<sub>2</sub> binding constants for Co(II)Salen complexes similar to **3** and **4** have been reported for pyridine and DMF solutions at 20 °C. However, [O<sub>2</sub>] = 1 M was assumed as standard state and therefore the values are not directly comparable with our results. See: Cesarotti, E.; Gullotti, M.; Pasini, A.; Ugo, R. *J. Chem. Soc., Dalton Trans.* **1977**, 757-763.
  25. Mandal, A. K.; Iqbal, J. *Tetrahedron* **1997**, *53*, 7641-7648.
  26. Kalra, S. J. S.; Punniyamurthy, T.; Iqbal, J. *Tetrahedron Lett.* **1994**, *35*, 4847-4850.
  27. 2-Cyclohexen-1-ol (product of allylic oxidation) was not detected by GC in all the cases reported here.
  28. GC analysis showed that conversion of up to 98% could be reached by extension of the reaction time (overnight). A control experiment was carried out using the same reaction conditions in the absence of catalyst. No oxidation of the cyclohexene or aldehyde was observed.
  29. Sheldon, R. A.; Kochi, J. K. *Metal-Catalyzed Oxydations of Organic Compounds*; Academic Press: New York, 1981.
  30. Hamilton, D. E.; Drago, R. S.; Zombeck, A. *J. Am. Chem. Soc.* **1987**, *109*, 374-379.
  31. Mastrorilli, P.; Nobile, C. F.; Suranna, G. P.; Lopez, L. *Tetrahedron* **1995**, *51*, 7943-7950.
  32. Nam, W.; Kim, H. J.; Kim, S. H.; Ho, R. Y. N.; Valentine, J. S. *Inorg. Chem.* **1996**, *35*, 1045-1049.
  33. Collman, J. P.; Brauman, J. I.; Doxsee, K. M.; Halbert, T. R.; Hayes, S. E.; Suslick, K. S. *J. Am. Chem. Soc.* **1978**, *100*, 2761-2766.

### RECOGNITION OF CAFFEINE IN AQUEOUS SOLUTIONS\*

#### 7.1 Introduction

Caffeine is probably one of the most widely used drugs in the world. It is a natural constituent of tea, coffee, guarana paste, cola nuts, and cacao beans. It is also added to many popular soft drinks and is a component of pharmacological preparations and over-the-counter medications including analgesics (where caffeine acts as an adjuvant), diet aids, and cold/flu remedies. In all its consumable forms caffeine is present in aqueous solutions or mixtures. Recently, three synthetic systems that recognize caffeine in non polar solvents ( $\text{CHCl}_3$ ,  $\text{CH}_2\text{Cl}_2$ ) have been reported.<sup>1-3</sup> These receptors bind caffeine mainly via hydrogen-bonding interactions. However, for applications in sensor and/or separation technology, it is of major interest to control and direct molecular interactions between caffeine and synthetic receptors in water.

In aqueous solution, the interaction of caffeine with polyphenols, which are present in coffee and especially in tealeaves, has been studied.<sup>4-7</sup> Additionally, flat aromatic molecules such as ethidium bromide (DNA intercalator) form weak complexes ( $K_a \sim 10$ - $200 \text{ M}^{-1}$ ) with caffeine predominantly via aspecific hydrophobic interactions.<sup>8</sup> For theophylline complexation (see Table 5) more sophisticated target-binding RNAs (aptamers)<sup>9</sup> and combinatorial techniques have been used. This system binds theophylline in aqueous solution very tightly ( $K_a = 3.1 \times 10^6 \text{ M}^{-1}$ ) and selectively in comparison to caffeine ( $K_a = 286 \text{ M}^{-1}$ ).<sup>10</sup> Attempts to obtain caffeine selective systems have been reported in the field of molecularly imprinted polymers.<sup>11-13</sup> However, none of these has a

---

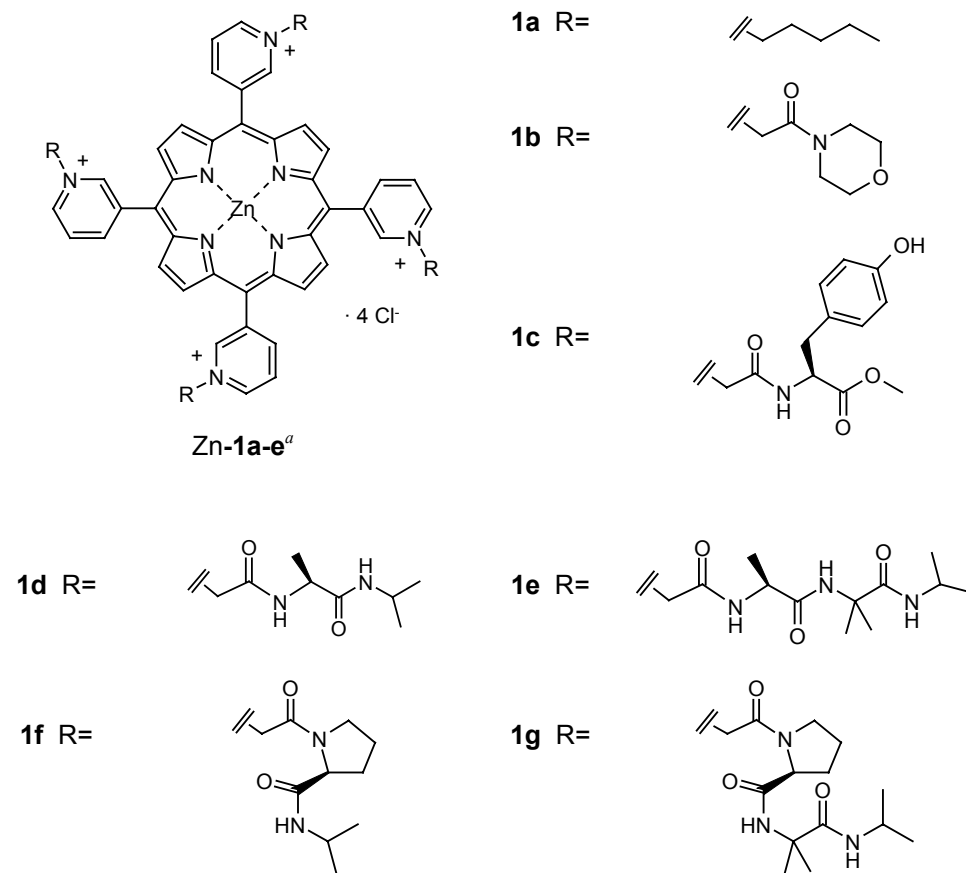
\* This work has been submitted for publication: Fiammengo, R.; Crego-Calama, M.; Timmerman, P.; Reinhoudt, D. N. *J. Am. Chem. Soc.* **2002**.



simple and easily accessible molecular structure that recognizes caffeine in aqueous solutions.

In this chapter a series of novel receptors that bind caffeine in aqueous solutions, viz. water-soluble peptide-porphyrin conjugates **Zn-1** (Chart 1) are reported.<sup>14-16</sup> Remarkably, the association constants of complexes between **Zn-1** and caffeine ( $K_a \sim 6000 \text{ M}^{-1}$  for **Zn-1a-d** and **Zn-1f**, Table 1) are up to 20 times higher than the RNA based system<sup>10</sup> and only 5-6 times lower than the highest binding constant measured with an artificial receptor in non polar organic solvents.<sup>1</sup>

Chart 1



<sup>a</sup> **Zn-1b** has  $\text{PF}_6^-$  as counterion.

The design of these water-soluble receptors for caffeine combines the flat aromatic surface of a porphyrin, to favor hydrophobic interactions, with a Lewis-acidic metal center for ligand coordination. The four alkyl groups on the pyridine nitrogens bear polar functionalities to increase the water solubility of the system. Moreover, they can also influence the binding ability. In fact, due to the non-symmetrical substitution of the pyridyl rings (nitrogen atom in position 3) the alkyl chains are oriented at an angle with respect to the porphyrin plane, providing a somewhat shielded recognition site.<sup>17</sup> The alkyl groups used in this work are aminoacid or dipeptide moieties as well as simple hydrocarbon chains or amides derived from morpholine. The sensing system possesses a built-in transduction mechanism to monitor the complexation of caffeine, *viz.* the intrinsic UV-vis activity of the porphyrin core.

Using this system, complexation of caffeine and a number of structurally related molecules was studied in buffered aqueous solution (sodium carbonate buffer pH = 9.6 or sodium oxalate buffer pH = 3.7).<sup>18</sup> The binding mechanism was also investigated using isothermal titration microcalorimetry (ITC) and NMR spectroscopy.

## 7.2 Results and discussion

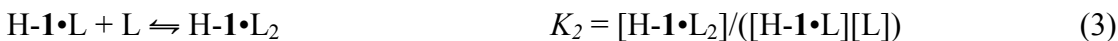
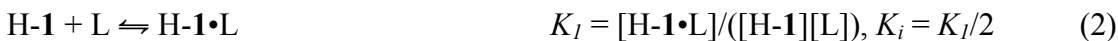
### 7.2.1 Synthesis.

Porphyrin Zn-1 were prepared following known literature procedures.<sup>19,20</sup> Alkylation of commercially available 5,10,15,20-tetra(3-pyridyl)porphyrin with pentylbromide in DMF (Zn-1a)<sup>19</sup> or with the appropriate chloroacetyl amide derivative in CH<sub>3</sub>CN afforded receptors Zn-1b-g.<sup>20</sup> Chloroacetamido amino acid or dipeptide amides used in the alkylation reactions were prepared by solution-phase peptide chemistry starting from Boc-amino acids (EDC/HOBt coupling reactions).

### 7.2.2 Caffeine binding studies

Binding of caffeine to water-soluble receptors **1** can be expressed in terms of the equilibria<sup>21,22</sup> described by equations 1 or 2 and 3 (depending whether the porphyrin is metalated (Zn-1) or free-base (H-1)) where  $K_i$  is the intrinsic binding constant accounting for the presence of two degenerate binding sites. The replacement of a water molecule

coordinated to the Zn by an added ligand (eq. 1) has been already reported for several other water-soluble porphyrins.<sup>23-26</sup>



For the free-base porphyrins reported here it is assumed that there are two available binding sites corresponding to the two porphyrin faces (eq. 2-3).<sup>27</sup> Investigation of the binding phenomenon using different experimental techniques (UV spectroscopy and microcalorimetry) in different concentration ranges (vide infra), support this model.

Unfortunately, comparison of the binding properties of receptors **1** with other previously reported systems proved to be difficult. In fact, several reports have considered the complexation of neutral guests with the planar, symmetrical 5,10,15,20-tetrakis(1-methylpyridinium-4-yl)porphyrin. Generally a 1:1 stoichiometry has been assumed based on the occurrence of isosbestic points during spectrophotometric titrations.<sup>16,28-30</sup> However, a detailed analysis by several research groups has shown that neither their presence nor their absence has any decisive value in diagnosing the number of species in the mixture.<sup>31</sup>

Controversial opinions have been expressed about the coordination mode of nitrogenous bases to 5,10,15,20-tetrakis-(*N*-alkylpyridinium-4-yl)Zn-porphyrinate in water. It has been proposed that the interaction of ligand heteroatoms with the Zn atom is not strong enough to lead to axial coordination and that face-to-face association dominates the binding.<sup>30</sup> Other groups have treated the binding of pyridine and 1-methylimidazole according to a water-exchanging equilibrium (eq. 1).<sup>25,32,33</sup> Association constants  $K_a = 3800 \text{ M}^{-1}$  and  $4900 \text{ M}^{-1}$  were reported for the two ligands, respectively.<sup>32</sup> However, the magnitudes of these  $K_a$ s were not consistent with the binding of nitrogenous bases to water soluble Zn-porphyrins ( $14\text{-}29 \text{ M}^{-1}$  for pyridine<sup>25,33</sup> and  $36\text{-}69 \text{ M}^{-1}$  for imidazole<sup>25</sup>) reported by other groups.

*UV-vis spectroscopy studies.* The binding of caffeine to receptors **1** was evaluated by monitoring the UV-vis intensity variations occurring in the Soret band region (between 400 and 480 nm) as a function of increasing guest concentration (see Tables 1 and 3). Bathochromic shifts between 4 and 5 nm upon complexation were observed for all

receptors, except Zn-1c (described later in more detail). The largest relative changes in molar absorptivity were between 36 and 43% ( $\Delta\epsilon < 0$ ). The spectral changes, showing well defined isosbestic points in all cases, were fitted according to eq. 1 for metalated receptors Zn-1 or to eq. 2-3 for free-base porphyrins.

**Table 1.** Binding constants of caffeine to porphyrins Zn-1 in aqueous solutions (sodium carbonate buffer,  $I = 0.008$  M, pH = 9.6), obtained by UV-vis and ITC titrations.

Host	$K_a (\times 10^3 \text{ M}^{-1})$
Zn-1a	$6.2 \pm 0.1 (5.15 \pm 0.04)^c$
Zn-1b <sup>a</sup>	$6.5 \pm 0.1$
Zn-1c	$4.28 \pm 0.08 (6.09 \pm 0.07)^b$
Zn-1d	$5.66 \pm 0.05 (6.72 \pm 0.08)^c$
Zn-1e	$3.26 \pm 0.05 (2.75 \pm 0.04)^c$
Zn-1f	$6.43 \pm 0.08 (6.06 \pm 0.06)^b$
Zn-1g	$2.83 \pm 0.02$

<sup>a</sup> PF<sub>6</sub><sup>-</sup> as counterion. <sup>b</sup> Sodium oxalate buffer,  $I = 0.008$  M, pH = 3.7. <sup>c</sup> Data obtained via ITC, sodium carbonate buffer  $I = 0.11$  M, pH = 10.3.

From the  $K_a$  values (Table 1) it is clear that caffeine complexation is influenced by the *N*-alkyl chain length. For receptors Zn-1a-d and Zn-1f bearing short alkyl chains (5-8 atoms) the  $K_a$  value is roughly two times higher than for receptors Zn-1e and Zn-1g bearing longer chains (11 atoms). Therefore longer chains are hindering, to some extent, the binding of caffeine. It should be noted that receptors 1, even though soluble in water, bear chains that are to some extent hydrophobic to promote the formation of a hydrophobic binding site. However, chain hydrophobicity can also cause stronger interaction with the porphyrin core, thus disfavoring the binding process.

<sup>1</sup>H NMR spectrometry studies. Structural analysis of receptors Zn-1 by <sup>1</sup>H NMR also support the interaction of the longer peptidic chains with the porphyrin platform (Figures 1,2).<sup>34</sup>

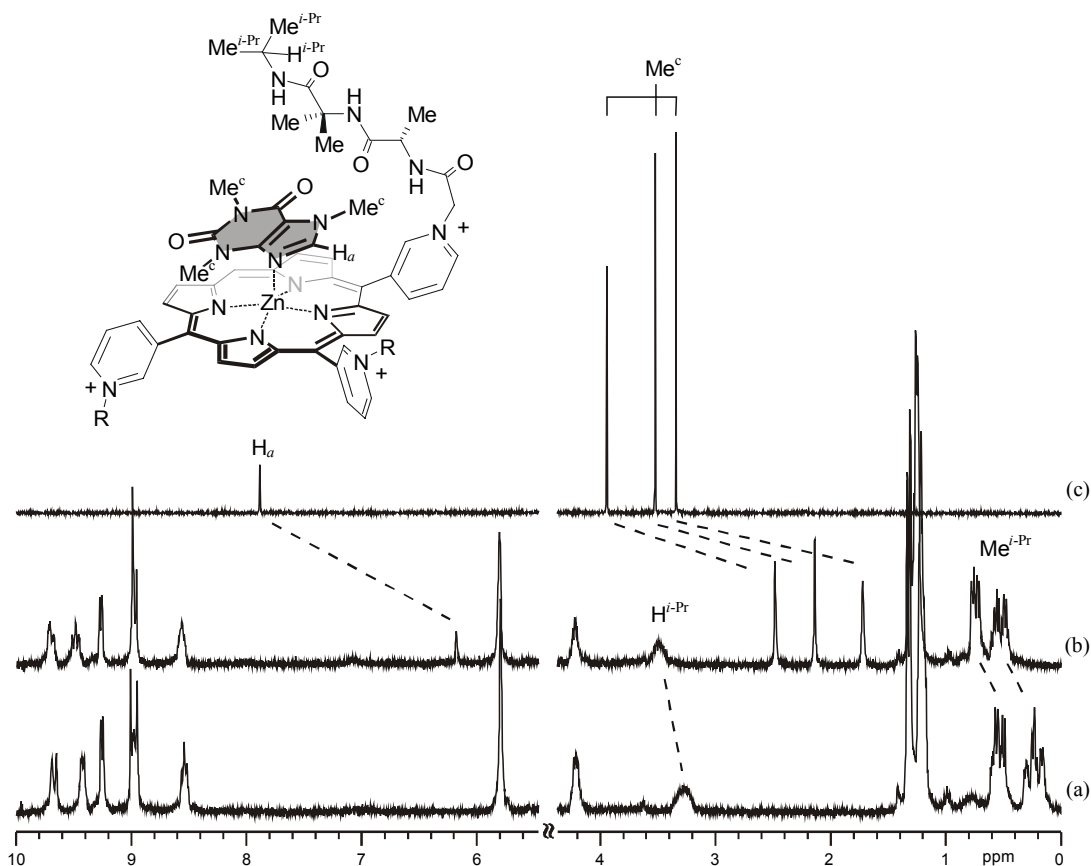


**Figure 1.** Binding of caffeine to receptor **Zn-1e** in D<sub>2</sub>O solution (1.7 mM). Top: schematic representation of the complex **Zn-1e**•caffeine (only one peptide arm is shown for clarity). Bottom: <sup>1</sup>H NMR spectra of **Zn-1e** (a); **Zn-1e** + 1.1 equiv of caffeine (b); caffeine (c).

In the absence of a guest, the spectra of receptors **Zn-1e** (Figure 1a) and **Zn-1g** in D<sub>2</sub>O show an upfield shift for the *i*-Pr group protons when compared with receptors **Zn-1d** and **Zn-1f**. In fact, receptors **Zn-1d** and **Zn-1f** exhibit signals at  $\delta$  3.75 ppm H<sup>*i*-Pr</sup> and  $\delta$  0.98 ppm Me<sup>*i*-Pr</sup> (Figure 2a), indicating no particular interaction with the porphyrin core. In contrast, the signals of the *i*-Pr groups of receptors **Zn-1e** and **Zn-1g** are observed at  $\delta$  3.29 ppm H<sup>*i*-Pr</sup>,  $\delta$  0.12-0.33 and 0.46-0.63 ppm Me<sup>*i*-Pr</sup> for **Zn-1e** and at  $\delta$  3.31 ppm H<sup>*i*-Pr</sup>,  $\delta$  0.04-0.38 and 0.44-0.68 ppm Me<sup>*i*-Pr</sup> for **Zn-1g**. This suggests that the long chains of receptor **Zn-1e** and **Zn-1g** are positioned above or below the porphyrin plane in the shielding region caused by the macrocycle ring current.

Upon addition of 1-2 equivalents of caffeine to a solution of receptor **Zn-1e** (or **Zn-1g**) in D<sub>2</sub>O the *i*-Pr group signals shifted downfield ( $\Delta\delta$  0.2 ppm H<sup>*i*-Pr</sup> and 0.2 and 0.3 ppm for the two Me<sup>*i*-Pr</sup>, Figure 1b) while no effect was observed for the shorter chains of receptors

Zn-**1d** (Figure 2b) and Zn-**1f**. Therefore it is likely that the side chains in receptors Zn-**1e** and Zn-**1g** are folded back over the porphyrin plane and are displaced upon caffeine complexation. On the contrary, the shorter alkyl chains of receptors Zn-**1d** and Zn-**1f** do not hinder the complexation of caffeine. Furthermore, caffeine signals also undergo large upfield shifts between 1 and 2 ppm for proton  $H_a$  on C-8 (see Figures 1b, 2b) and between 0.9 and 1.7 ppm for the three methyl groups ( $Me^c$ ) upon complexation with all receptors **1** (metalated or not).

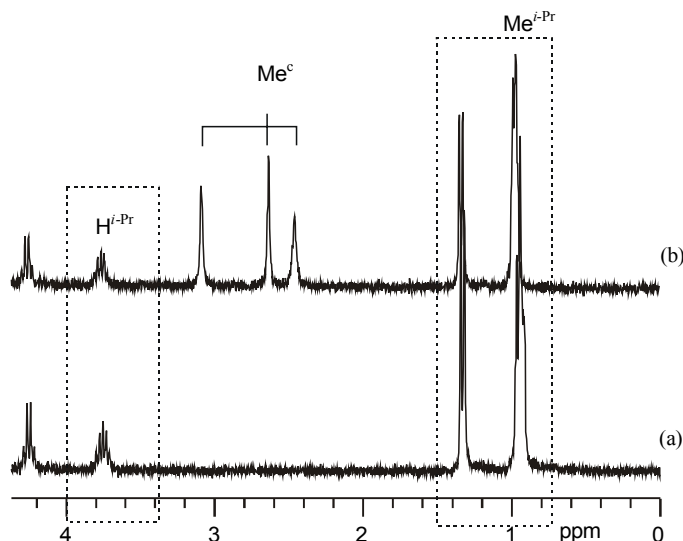


**Figure 2.** Binding of caffeine to receptor Zn-**1d** in  $D_2O$  solution (1.7 mM). The signals for the *i-Pr* groups of the receptor are not shifted (see text). Signals for caffeine  $Me^c$  are upfield shifted when compared to their position in the absence of receptor, confirming complexation. (a) Zn-**1d**; (b) Zn-**1d** + 2.4 equiv of caffeine.

*ITC studies.* ITC experiments also confirm the influence of the chain length on caffeine complexation (Table 1). The enthalpograms, *i.e.* the evolved heat per added mole of caffeine during the calorimetric titration, were fitted to 1:1 model and good agreement with the binding constants obtained via UV titrations was found. The same trend is observed with the  $K_a$  for Zn-**1d** approximately two times higher than the  $K_a$  for Zn-**1e**.

Thermodynamic parameters for caffeine binding to porphyrins **1** can be extracted from the ITC experiments (Table 2). In general, large negative enthalpy and entropy contributions are observed for the complexation of caffeine. The large negative enthalpy change associated with the formation of the complex is consistent with a substantial contribution of hydrophobic and stacking interactions to the binding process.

**Table 2.** Thermodynamic parameters for caffeine binding to porphyrin Zn-1 in aqueous solutions determined via ITC (sodium carbonate buffer,  $I = 0.11$  M, pH = 10.3). For  $K_a$  values see Table 1.

Host	$\Delta H^\circ$ (kJ mol <sup>-1</sup> )	$\Delta S^\circ$ (J mol <sup>-1</sup> K <sup>-1</sup> )
Zn-1a	-36.7 ± 0.1	-52.2 ± 0.3
Zn-1d	-34.5 ± 0.2	-42.5 ± 0.8
Zn-1e	-39.3 ± 0.2	-65.9 ± 0.8

Negative entropic contributions have also been observed by Mizutani and coworkers for binding of amine and amino esters to Zn-porphyrin receptors and have been analyzed in terms of induced-fit type complexes.<sup>35</sup> Conformational restrictions upon complex formation and/or receptor reorganization (as observed from NMR measurements for Zn-1e and Zn-1g) cause entropy losses ( $\Delta S^\circ < 0$ ) which are only partially compensated by the entropic gain from desolvation. Accordingly, the long chain receptor Zn-1e has a significantly more negative  $\Delta S^\circ$  value (-65.9 J mol<sup>-1</sup> K<sup>-1</sup>) than Zn-1d (-42.5 J mol<sup>-1</sup> K<sup>-1</sup>), which agrees with the necessity of displacing the longer alkyl chains of Zn-1e from the porphyrin faces. Even though the binding strength of Zn-1a is similar to that of the other short chain receptors ( $K_a \sim 6000$  M<sup>-1</sup>), the thermodynamic parameters are not comparable due to the quite different nature of the *N*-substituents and their influence on the solvation of the receptor.

*Free-base porphyrin receptors.* To gain more information about the binding mode and to assess the role of the Zn atom, UV and ITC studies on metal free receptors 1c and 1d were performed (Figures 3 and 4). UV titration curves for the complexation of caffeine were fitted to 1:1 and 2:1 caffeine to receptor stoichiometry. Despite the presence of isosbestic points, better fits were obtained using the 2:1 binding model, although the differences are too small to discard the possibility of 1:1 stoichiometry. On the other hand, fitting to a 2:1 model gave better agreement between the UV and ITC measurements.<sup>36</sup>

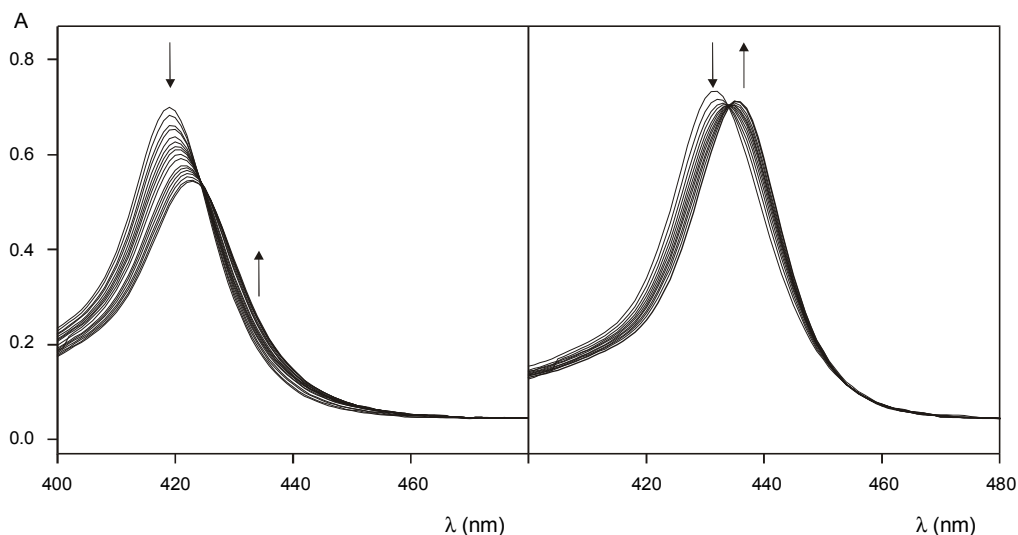


**Figure 3.** Changes in the UV-vis absorption spectra of receptors free-base-**1d** (left) and Zn-**1d** (right) upon addition of caffeine. [Porphyrin]  $\sim$  2.5  $\mu$ M in carbonate buffered solution ( $I = 0.008$  M, pH = 9.6).

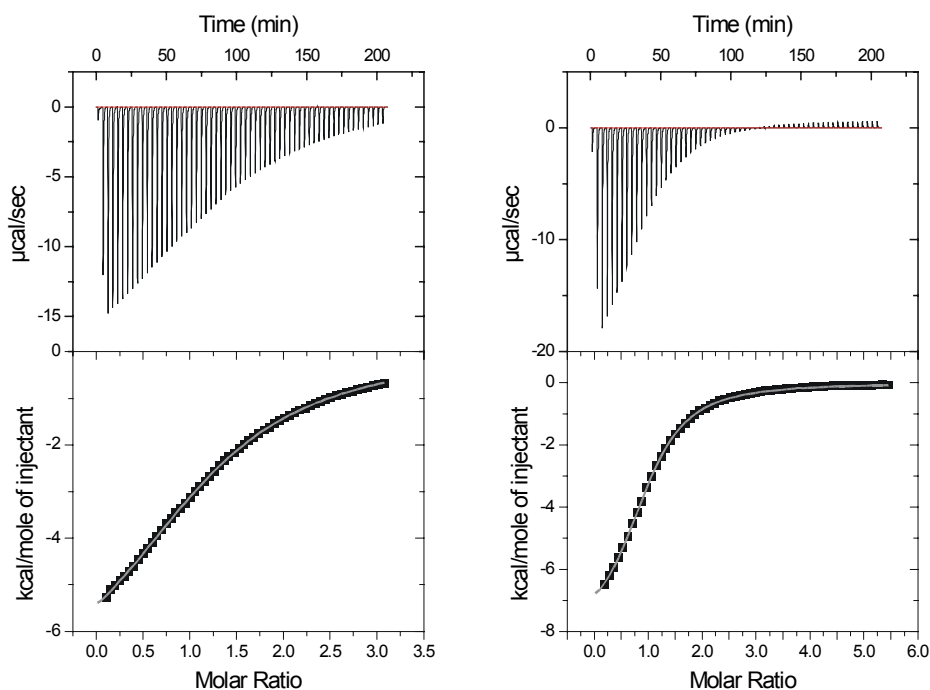


**Figure 4.** Microcalorimetric titrations of receptors free-base-**1d** (left) and Zn-**1d** (right) with caffeine. [Porphyrin]  $\sim$  1 mM in carbonate buffered solution ( $I = 0.11$  M, pH = 10.3).

Binding of caffeine  $K_i$  (Table 3) to the free base receptors (taking into account the presence of two degenerate binding sites) is around four times weaker than for the corresponding metalated hosts. For example, considering both the UV and the ITC data,



Zn-**1d** and free-base **1d** bind caffeine with  $K_a \sim 6100 \text{ M}^{-1}$  and  $K_a \sim 1600 \text{ M}^{-1}$ , respectively.

**Table 3.** Binding constants for caffeine to free-base porphyrins **1** in aqueous solutions

	Host	$K_1 (\times 10^3 \text{ M}^{-1})^a$	$K_2 (\times 10^3 \text{ M}^{-1})$
UV <sup>b</sup>	<b>1c</b>	1.4	0.41
UV <sup>b</sup>	<b>1d</b>	1.5	0.37
ITC <sup>c,d</sup>	<b>1d</b>	1.8	0.52

<sup>a</sup>  $K_i = K_i/2$ . For definitions of  $K_1$  and  $K_2$  see eq. 2, 3. <sup>b</sup> Error margin  $\pm 10\%$ . Sodium carbonate buffer,  $I = 0.008 \text{ M}$ ,  $\text{pH} = 9.6$ . <sup>c</sup> Sodium carbonate buffer  $I = 0.11 \text{ M}$ ,  $\text{pH} = 10.3$ . <sup>d</sup> Thermodynamic parameters:  $\Delta H^\circ_i = -27.7 \pm 0.1 \text{ kJ mol}^{-1}$ ,  $\Delta S^\circ_i = -30.8 \pm 0.8 \text{ J mol}^{-1} \text{ K}^{-1}$  and  $\Delta H^\circ_2 = -13.2 \pm 0.2 \text{ kJ mol}^{-1}$ ,  $\Delta S^\circ_2 = 7.8 \pm 0.8 \text{ J mol}^{-1} \text{ K}^{-1}$ .

Comparison of the thermodynamic parameters for metal-free **1d** ( $\Delta H^\circ_i = -27.7 \text{ kJ mol}^{-1}$  and  $\Delta S^\circ_i = -30.8 \text{ J mol}^{-1} \text{ K}^{-1}$ ) and Zn-**1d** ( $\Delta H^\circ = -34.5 \text{ kJ mol}^{-1}$  and  $\Delta S^\circ = -42.5 \text{ J mol}^{-1} \text{ K}^{-1}$ ) shows that the difference between the two receptors in the binding process is mostly due to enthalpy. Thus, the more negative enthalpic contribution (which overrules a more negative entropic contribution) for Zn-**1d** suggests a direct interaction of the guest with the Zn center. Caffeine can coordinate to the Zn center via the imidazole nitrogen N-9 (see structure Table 5).<sup>37</sup> However, the methyl group at N-3 prevents a good perpendicular arrangement with respect to the porphyrin plane (the effect is partially compensated by a position of the Zn atom above the porphyrin plane, towards the axial ligand<sup>24</sup>). Therefore, caffeine likely binds to receptor Zn-**1** in a tilted way, with an angle smaller than  $90^\circ$  between the molecular planes of caffeine and porphyrin. Support for this proposed complex structure is corroborated by a report of complex  $[\text{Rh}_2(\text{acetato})_4(\text{caffeine})_2]$  in which binding of the two caffeine moieties at an angle different from the optimal does not prevent metal coordination at nitrogen N-9.<sup>38</sup>

Additional evidence arises from various modes for the binding of bicyclic nucleobases such as adenine and guanine (structurally similar to caffeine) to metalloporphyrins reported in the literature. In some cases direct metal coordination<sup>39-41</sup> was invoked,

whereas others used only hydrophobic interactions.<sup>42</sup> The experiments reported here show that the presence of Zn is an important factor for enhanced binding affinity of caffeine.

*Tyr-substituted porphyrin Zn-1c.* Tyr moieties were introduced affording receptor **Zn-1c** to possibly enhance the binding of caffeine through stacking with the phenol units. However, the Tyr-based chains are long (10 atoms) and hydrophobic enough to be positioned on top of the porphyrin plane,<sup>43</sup> which may hinder caffeine binding like the chains of **Zn-1e** and **Zn-1g**.

<sup>1</sup>H NMR spectra of **Zn-1c** and free-base **1c** in D<sub>2</sub>O confirm the folding of the peptide chains towards the porphyrin core, as shown by the upfield shifted signals for the four aromatic protons of the phenol rings (6.78 and 6.18 ppm compared to 7.07 and 6.66 ppm for the spectrum recorded in CD<sub>3</sub>OD).<sup>44</sup> Moreover, different from the non-ionizable side chains of **Zn-1e** and **Zn-1g**, the phenol OH moiety can be deprotonated<sup>45</sup> and a CPK model suggests that the phenolate moiety could coordinate intramolecularly to the Zn.<sup>46</sup>

This hypothesis was verified by studying the UV-vis spectrum of the receptor under different conditions. The UV-vis spectrum of **Zn-1c** in carbonate buffered solution (pH = 9.6) showed a 7 nm red shifted Soret (in comparison to **Zn-1d** and **Zn-1f**) and a quite marked hypochromicity which was not caused by aggregation (Figure 5). When dissolved in an oxalate buffer or in pure water (pH = 3.7 and ~7 respectively) these effects were not observed and the spectrum closely resembles that of the other receptors. Metal-free **1c** had a much smaller response to the basic pH ( $\Delta\lambda_{\text{max}} = 0$  nm and only a modest hypochromicity, Figure 5).

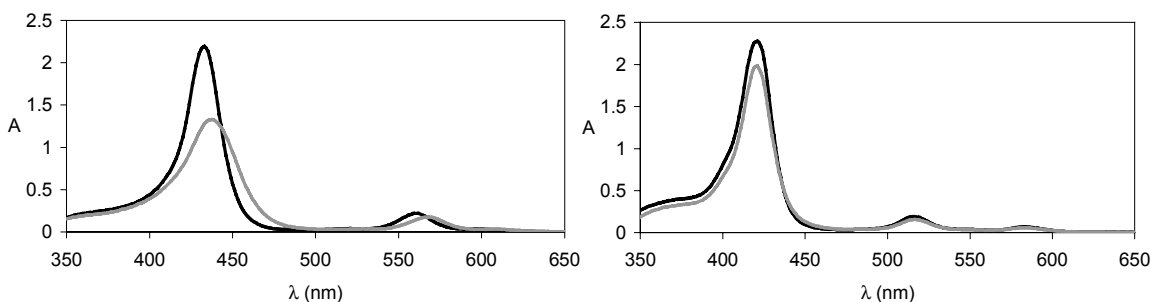


**Figure 5.** UV-vis spectra for receptors **Zn-1c** (left) and metal-free-**1c** (right) at pH 7 (black traces) and at pH 9.6 (gray traces).

The intramolecular coordination of the Tyr moiety to the Zn is also expected to lower the caffeine binding because of competition for the metal center (although only at basic pH). Binding of caffeine to receptor Zn-1c in basic solutions is observed with  $K_a = 4280 \text{ M}^{-1}$ . The binding strength is indeed reduced by the competitive effect played by the phenolate moieties, since at pH 3.7, where the amount of phenolate form is negligible, stronger binding ( $K_a = 6090 \text{ M}^{-1}$ ) is observed.

The data also show that receptor Zn-1c binds caffeine two times stronger than receptors Zn-1e and Zn-1g, which have substituents with comparable chain length (see Table 1). This result may indicate stabilizing interactions between the Tyr phenol rings and the electron deficient caffeine  $\pi$ -system.

### 7.2.3 Selectivity towards other ligands structurally related to caffeine

*1-Methylimidazole (1-MeIm)*. Imidazole-based ligands, resembling the 5-membered ring of caffeine,<sup>47</sup> are known to coordinate to metal porphyrins in aqueous solution.<sup>25,33,48</sup> Binding of 1-methylimidazole to receptors **1** was studied by UV-vis spectroscopy through the spectral changes in the Q-band region induced during the titrations (500-630 nm, see Figure 6). The results (Table 4) show that the binding mechanism is substantially different from that observed in the case of caffeine and predominantly involves metal coordination. A division between receptors bearing short or long chains, similar to what was observed for caffeine binding, can also be made in case of 1-MeIm binding. However, the effect of the chain length on the binding strength is in opposite direction. All short chain receptors (Zn-1a, Zn-1b, Zn-1d and Zn-1f) show similar binding constants ( $K_a \sim 50 \text{ M}^{-1}$ ) while Zn-1e and Zn-1g bind 1-MeIm three times stronger ( $K_a \sim 150 \text{ M}^{-1}$ ). Coordination of 1-methylimidazole to the Zn atom takes place perpendicular to the porphyrin plane. This indicates that the ligand is small enough that no reorganization of the alkyl chains of Zn-1e and Zn-1g is necessary to accommodate it. Moreover the higher stability of the complexes obtained with Zn-1e and Zn-1g (with respect to the short chain receptors) is probably due to the hydrophobic pocket created by the peptidic chains on the porphyrin plane.

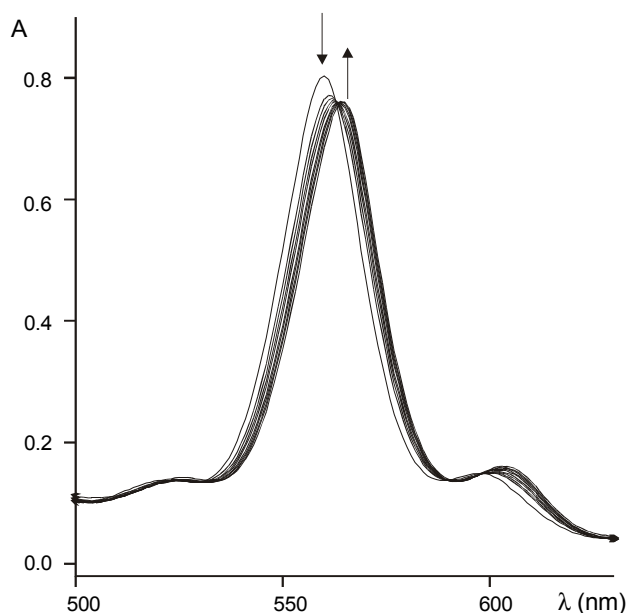


**Figure 6.** Changes in the UV-vis absorption spectra of Zn-1e upon addition of 1-methylimidazole. [Porphyrin]  $\sim$ 40  $\mu$ M in carbonate buffered solution ( $I = 0.008$  M, pH = 9.6).

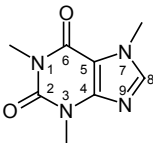
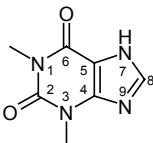
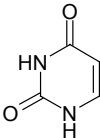
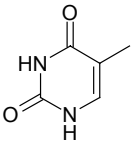
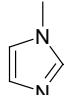
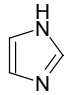
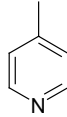
**Table 4.** Binding constants for 1-methylimidazole to porphyrin Zn-1 in aqueous solution (sodium carbonate buffer,  $I = 0.008$ M, pH = 9.6) from UV-vis titrations.

Host	$K_a$ ( $M^{-1}$ )
Zn-1a	$51 \pm 2$
Zn-1b	$45 \pm 2$
Zn-1d	$58 \pm 2$
<b>1d</b>	<1
Zn-1e	$151 \pm 2$
Zn-1f	$57 \pm 1$
Zn-1g	$165 \pm 3$

Metal-free Zn-1d did not show any appreciable binding of 1-MeIm (no significant changes of the spectrum were observed during the titration), confirming that metal coordination is the driving force for complex formation.

*Other ligands.* Investigation of the binding of ligands other than 1-MeIm was undertaken using only receptor Zn-1e as the model system (Table 5).

**Table 5.** Binding constants for different ligands to porphyrin Zn-1e in aqueous solution (sodium carbonate buffer,  $I = 8$  mM, pH = 9.6)

Guest		$K_a$ ( $M^{-1}$ )
caffeine		$(3.26 \pm 0.05) \times 10^3$
theophylline		$(2.52 \pm 0.05) \times 10^3$
uracil		$< 5$
thymine		$< 5$
1-methylimidazole		$(1.51 \pm 0.02) \times 10^2$
imidazole		$(1.56 \pm 0.02) \times 10^2$
4-methylpyridine		$(3.5 \pm 0.1) \times 10^1$

Imidazole coordinates to Zn-1e with the same strength as 1-methylimidazole ( $K_a = 156 M^{-1}$ , 20 times weaker than caffeine) while 4-methylpyridine is bound with a significantly smaller affinity ( $K_a = 35 M^{-1}$ ). These observations clearly confirm that hydrophobic or  $\pi$ -stacking interactions play an important role in stabilizing the caffeine complex with Zn-1e in addition to metal coordination. The interactions of Zn-1e with guest molecules that lack the nitrogen donor atom and resemble the six-member ring of caffeine (like uracil or thymine) were also studied. These molecules might also be able to associate to

Zn-1e if the binding mode is predominantly  $\pi$ -stacking. Interestingly, UV-vis titrations did not show any appreciable binding ( $< 5 \text{ M}^{-1}$ ). Therefore, strong binding is favored by the bicyclic structure of caffeine, supporting the involvement of hydrophobic interactions. The structurally closely related theophylline (which lacks only the N-7 methyl group of caffeine) also shows complexation by tetracationic porphyrin Zn-1e indicating a similar binding mode. However, it is interesting to note that in view of the small structural difference between the two molecules, the binding strength is distinctly lower.

### 7.3 Conclusions and outlook

Although receptors Zn-1, and especially Zn-1c, Zn-1e and Zn-1g, are not yet suitable for practical use (sensors), the results reported in this chapter show for the first time recognition of caffeine in aqueous solution and provide a detailed view of the binding process from several experimental techniques. The data show that even porphyrin Zn-1a bearing simple alkyl chains binds caffeine. However, the use of amino acid or peptide chains allows the introduction of additional interactions. In particular, if the chains on the pyridyl rings are longer than 10 atoms (Zn-1c, Zn-1e and Zn-1g) interaction with the porphyrin surface and therefore influence on the recognition site become possible. The balance of the various contributions to binding is very subtle and involves competition for the hydrophobic surface (Zn-1e and Zn-1g) and additional stabilizing stacking interactions (Zn-1c).

Influence of the alkyl chains on guest recognition has also been shown for a much smaller guest such as 1-methylimidazole, which binds to porphyrins Zn-1 via a different mechanism. In fact, the longer chain receptors showed enhanced binding for 1-methylimidazole.

The present work also shows that influence on the recognition abilities of our synthetic receptors can be achieved even though only very simple porphyrin-peptide conjugates are used (one or two aminoacids with thus far relatively small differences in the side chain nature). Much more complex porphyrin-peptide conjugates bearing chains as long as 20 amino acids have been reported so far in the literature for the mimic of heme-protein.<sup>49</sup> The present approach is expected to have great potential for the preparation of novel

water-soluble receptors, the affinity of which may be tailored by the proper choice of peptidic moieties.

## 7.4 Experimental part

### 7.4.1 General information and instrumentation

All reagents used were purchased from Aldrich or Acros Organics and used without further purification. All the reactions were performed under nitrogen atmosphere.  $^1\text{H}$  NMR and  $^{13}\text{C}$  NMR spectra were performed on a Varian Unity INOVA (300 MHz) or a Varian Unity 400 WB NMR spectrometer.  $^1\text{H}$  NMR chemical shift values (300 MHz) are expressed in ppm ( $\delta$ ) relative to residual  $\text{CHD}_2\text{OD}$  ( $\delta$  3.30),  $\text{CHD}_2\text{CN}$  ( $\delta$  1.93), or  $\text{CHCl}_3$  ( $\delta$  7.26).  $^{13}\text{C}$  NMR chemical shift values (100 MHz) are expressed in ppm ( $\delta$ ) relative to residual  $\text{CD}_3\text{OD}$  ( $\delta$  49.0) or  $\text{CD}_3\text{CN}$  ( $\delta$  1.3). UV-vis measurements were performed on a Varian Cary 3E UV-vis spectrophotometer equipped with a Helma QX optical fiber probe (path length = 1.000 cm), using solvents of spectroscopic grade. Mass spectra were measured using a Perkin Elmer/PerSeptive Biosystem Voyager-DE-RP MALDI-TOF mass spectrometer (PerSeptive Biosystem, Inc., Framingham, MA, USA) equipped with delayed extraction. A 337nm UV Nitrogen laser producing 2 ns pulses was used and the mass spectra were obtained in the linear and reflectron mode.

### 7.4.2 Buffers

Carbonate buffer ( $I = 0.11$  M, pH = 10.3) was prepared dissolving dry  $\text{Na}_2\text{CO}_3$  (723 mg) and dry  $\text{NaHCO}_3$  (573 mg) in distilled water (250 ml). The buffer was used as such or eventually diluted to obtain the desired ionic strength.

Oxalate buffer ( $I = 0.008$  M, pH = 3.7) was prepared adding oxalic acid (683 mg) to a NaOH solution (8.2 ml, 1 M) and diluting to 100 ml.

### 7.4.3 Binding studies

*Dilution experiments:* Proof that the receptors used in this study were in their monomeric form was obtained by recording the UV-vis spectra of the receptor over a range of concentrations ( $1.0\text{-}9.0 \times 10^{-6}$  M, in the presence of the buffer) for a total of 7-12

experimental observations. Plot of the absorbances vs concentrations were always linear (correlation > 0.995) indicating no aggregation under the measuring conditions ([porphyrins] between  $2.4$  and  $4.8 \times 10^{-6}$  M).

Aggregation was also absent at higher porphyrin concentrations ( $2.8 \times 10^{-3}$  M) as proved for receptor Zn-**1e** by a microcalorimetric (ITC) experiment. A solution of Zn-**1e** in water (in the microburette) was added in aliquots to the sample cell containing initially only water. The resulting enthalpogram, *i.e.* the evolved heat per added mole of **1e** is featureless and only shows a small constant endothermic effect which is attributed to dilution of the porphyrin solution.

*UV-Vis:* Binding of guests to receptor **1** was evaluated by monitoring the spectral variation upon addition of guest solution either in the Soret band region (400-480 nm) or in the Q-band region (500-630 nm) of the porphyrin spectra. Changes in the Q-band region were monitored in cases where preliminary measurements indicated a smaller binding constant. For these measurements the concentration of receptors **1** was 10-20 times higher than for the titrations monitored in the Soret band region (see text for typical values). In all cases the titration covers the 20%-80% interval of complex formation. Each titration consisted of 13 to 20 data points. The experimental spectral changes were fitted to a 1:1 binding model using a nonlinear least-squares fitting procedure considering simultaneously 6 different wavelengths (model written with program Scientist<sup>®</sup>, MicroMath<sup>®</sup>). In the case of 2:1 binding, the data were fitted also using a nonlinear least-squares fitting procedure considering simultaneously 2 different wavelengths (model written with program Microsoft<sup>®</sup> Excel).

*Microcalorimetry (ITC):* Calorimetric measurements were carried out using a Microcal VP-ITC microcalorimeter with a cell volume of 1.4115 mL. Aliquots of a 16.8 mM caffeine solution in sodium carbonate buffer ( $I = 0.11$  M, pH = 10.3) contained in the buret were added to the receptor solution (in the same buffer) contained in the calorimetric cell (receptor concentration 0.7-1.6 mM). Data were fitted to a 1:1 model for metalated receptors and to a 1:2 (receptor/guest) model in the case of free base receptor **1d**. Fittings of the experimental data to the appropriate complexation model were obtained using Origin<sup>®</sup> implemented with the calorimetric set up provided by Microcal Inc.



#### 7.4.4 Synthesis

*Preparation of N-chloroacetyl derivatives of amino acid amides/esters and dipeptide amides.* Amino acid amides and dipeptide amides were prepared by standard solution-phase peptide chemistry.

*Couplings:* A mixture of Boc amino acids (1.0 equiv), EDC (1.1 equiv), HOBt (1.0 equiv) and DIEA (1.0 equiv) in CH<sub>2</sub>Cl<sub>2</sub> (or CH<sub>3</sub>CN) under N<sub>2</sub> was stirred at 0 °C for 5-10 minutes. A solution of the desired amino compound (1.1 equiv) and DIEA (1.2 equiv) in CH<sub>2</sub>Cl<sub>2</sub> (or CH<sub>3</sub>CN) was added and the reaction mixture was allowed to warm up to r.t. The final concentration of the Boc-amino acid in the mixture was between 0.1 and 0.3 M. The reaction course was monitored by TLC (silica gel, CHCl<sub>3</sub>/CH<sub>3</sub>CH<sub>2</sub>OH 9:1). After disappearance of the Boc-amino acid, the reaction mixture was diluted (~10 times) with EtOAc and washed with citric acid (0.5 M), NaHCO<sub>3</sub> (5%), and brine. The organic layer was then dried over Na<sub>2</sub>SO<sub>4</sub> and the solvent removed under vacuum. Yields were between 75 and 90%.

*Boc- deprotection:* TFA/CH<sub>2</sub>Cl<sub>2</sub> 1:1, 30 min. to 1h under N<sub>2</sub>.

*Chloroacetylation:* Chloroacetyl chloride (1.0 equiv) was reacted with the desired amino compound under biphasic conditions (CH<sub>2</sub>Cl<sub>2</sub>/saturated aqueous Na<sub>2</sub>CO<sub>3</sub>) at 0 °C for 45-60 minutes. The reaction mixture was then treated as the other coupling reaction mixtures. Yields were between 65 and 90%.

*Preparation of tetracationic porphyrin receptors (I).* The synthesis of porphyrins Zn-**1a** and Zn-**1b** has been published previously.<sup>19,20</sup> Receptors Zn-**1c-g** have been prepared under the same conditions reported for Zn-**1b** with a slightly modified workup procedure. The alkylation reaction mixture was dried under vacuum and the solid residue was triturated and washed extensively with ether and CH<sub>2</sub>Cl<sub>2</sub>. Then the product was extracted by dissolution with the minimum amount of CH<sub>3</sub>CN. The solution was evaporated and the residue redissolved in CH<sub>3</sub>OH. ZnAc<sub>2</sub> (~10 equiv) was added and the reaction mixture was stirred at 40 °C for 1h. The excess ZnAc<sub>2</sub> was removed via reverse-phase chromatography (stationary phase RP-8, eluent: from H<sub>2</sub>O to 1:1 H<sub>2</sub>O/CH<sub>3</sub>CN/0.1% TFA mixture.) The eluted solution was first concentrated under vacuum and then lyophilized. The solid residue was redissolved in H<sub>2</sub>O/CH<sub>3</sub>CN 1:1 and transformed in the

tetrachloride salt by ion-exchange column (DOWEX 1-X8, 50-100 mesh, Cl-form). Receptors **Zn-1** were obtained as solids after concentration and lyophilization. Combined yields for alkylation and metallation ranged between 70 and 85%. (Free-base receptors **1c** and **1d** were prepared in analogous manner, the reverse phase and ion exchange columns following directly the alkylation step).

Due to the hygroscopic nature of the chloride salts, satisfactory elemental analyses were not obtained. However, purity of the compounds was confirmed by analytical HPLC.

**5,10,15,20-tetrakis(*N*-(AcetylTyr-OMe)pyridinium-3-yl) porphyrin (1c).** Prepared from 5,10,15,20-tetra(3-pyridyl)porphyrin and chloroacetyl-Tyr-OMe.

Metal Free-**1c**:  $^1\text{H NMR}$  ( $\text{CD}_3\text{CN}$ )  $\delta$  9.46 (s, 4H), 9.33 (d,  $J=7.9$  Hz, 4H), 9.12 (d,  $J=6.1$  Hz, 4H), 9.04 (s, 8H), 8.54 (m, 4H), 7.62 (d,  $J=7.4$  Hz, 4H), 7.15 (bs, 4H) 7.05 (m, 8H), 6.65 (m, 8H), 5.60 (AB system, 8H), 4.76 (m, 4H), 3.66 (m, 12H), 3.09 (dd,  $J=14.0, 4.9$  Hz, 4H), 2.96 (dd,  $J=14.0, 7.5$  Hz, 4H), -3.07 (s, 2H).

UV-vis ( $\text{H}_2\text{O}$ ) 421, 516, 546, 583. MALDI-TOF MS:  $m/z$  1667.5  $[\text{M-Cl}]^+$  (calculated for  $[\text{C}_{88}\text{H}_{82}\text{N}_{12}\text{O}_{16}\text{Cl}_3]^+$  1667.5).

**Zn-1c**:  $^1\text{H NMR}$  ( $\text{CD}_3\text{OD}$ )  $\delta$  9.79 (bm, 4H), 9.40 (bm, 4H), 9.32 (d,  $J=6.3$  Hz, 4H), 9.10 (m, 8H), 8.57 (t,  $J=7$  Hz, 4H), 7.07 (m, 8H), 6.66 (m, 8H), 5.79 (AB system, 8H), 3.71 (m, 12H), 3.17 (dd,  $J=13.9, 5.5$  Hz, 4H), 2.97 (dd,  $J=13.9, 8.8$  Hz, 4H).  $^1\text{H NMR}$  ( $\text{D}_2\text{O}$ )  $\delta$  9.33 (m, 8H), 9.08 (bm, 4H), 8.83 (m, 8H), 8.45 (bm, 4H), 6.78 (m, 8H), 6.18 (m, 8H), 5.58 (m, 8H), 3.59 (m, 12H), 2.91 (bm, 4H), 2.60 (bm, 4H). UV-vis ( $\text{H}_2\text{O}$ ) 433, 520, 560, 598; MALDI-TOF MS:  $m/z$  1729.5  $[\text{M-Cl}]^+$  (calculated for  $[\text{C}_{88}\text{H}_{80}\text{N}_{12}\text{O}_{16}\text{Cl}_3\text{Zn}]^+$  1729.4).

**5,10,15,20-tetrakis(*N*-(AcetylAla-NH-*i*-Pr)pyridinium-3-yl) porphyrin (1d).** Prepared from 5,10,15,20-tetra(3-pyridyl)porphyrin and chloroacetyl-Ala-NH-*i*-Pr.

Metal Free-**1d**:  $^1\text{H NMR}$  ( $\text{CD}_3\text{OD}$ )  $\delta$  10.02 (m, 4H), 9.50 (m, 8H), 9.20 (bs, 8H), 8.65 (m, 4H), 5.88 (m, 8H), 4.41 (m, 4H), 3.93 (m, 4H), 1.43 (m, 12H), 1.19-1.08 (m, 24H).

UV-vis ( $\text{H}_2\text{O}$ ) 420, 515, 544, 580. MALDI-TOF MS:  $m/z$  1409.8  $[\text{M-Cl}]^+$  (calculated for  $[\text{C}_{72}\text{H}_{86}\text{N}_{16}\text{O}_8\text{Cl}_3]^+$  1407.6).

**Zn-1d:**  $^1\text{H}$  NMR ( $\text{CD}_3\text{CN}$ )  $\delta$  9.54 (m, 4H), 9.24 (m, 4H), 9.15 (m, 4H), 8.95 (s, 8H), 8.40 (m, 4H), 8.25 (m, 4H), 7.05 (m, 4H), 5.68 (AB system, 8H), 4.38 (m, 4H), 3.90 (m, 4H), 1.34 (d,  $J=7.1$  Hz, 12H), 1.02 (m, 24H).  $^1\text{H}$  NMR ( $\text{D}_2\text{O}$ )  $\delta$  9.68 (bs, 4H), 9.40 (bm, 4H), 9.23 (d,  $J=6.3$  Hz, 4H), 8.97 (m, 8H), 8.52 (m, 4H), 5.77 (s, 8H), 4.25 (m, 4H), 3.75 (sept,  $J=6.5$  Hz, 4H), 1.33 (d,  $J=7.2$  Hz, 12H), 0.95 (m, 24H).  $^{13}\text{C}$  NMR ( $\text{CD}_3\text{CN}$ )  $\delta$  165.02, 151.40, 150.18, 149.01, 145.96, 143.51, 133.70, 127.21, 114.00, 63.29, 51.01, 42.65, 22.47, 18.84. IR (KBr): 3314, 3101, 2984, 1679, 1545, 1458, 1207, 1140, 843, 801, 724. UV-vis ( $\text{CH}_3\text{OH}$ ) 433, 519, 559, 597, 638. MALDI-TOF MS:  $m/z$  1470.8  $[\text{M}-\text{Cl}]^+$  (calculated for  $[\text{C}_{72}\text{H}_{84}\text{N}_{16}\text{O}_8\text{Cl}_3\text{Zn}]^+$  1469.5).

**[5,10,15,20-tetrakis(*N*-(AcetylAlaAib-NH-*i*-Pr)pyridinium-3-yl)porphyrinato]zinc(II) (1e).** Prepared from 5,10,15,20-tetra(3-pyridyl)porphyrin and chloroacetyl-AlaAib-NH-*i*-Pr.

$^1\text{H}$  NMR ( $\text{D}_2\text{O}$ )  $\delta$  9.68 (m, 4H), 9.42 (m, 4H), 9.26 (d,  $J=6.2$  Hz, 4H), 8.98 (m, 8H), 8.54 (m, 4H), 5.80 (s, 8H), 4.21 (m, 4H), 3.29 (bm, 4H), 1.33 (d,  $J=7.2$  Hz, 12H), 1.22 (m, 24H), 0.63-0.46 (m, 12H), 0.33-0.12 (m, 12H). UV-vis ( $\text{CH}_3\text{OH}$ ) 432, 519, 560, 597, 640. MALDI-TOF MS:  $m/z$  1809.4  $[\text{M}-\text{Cl}]^+$  (calculated for  $[\text{C}_{88}\text{H}_{112}\text{N}_{20}\text{O}_{12}\text{Cl}_3\text{Zn}]^+$  1809.7).

**[5,10,15,20-tetrakis(*N*-(AcetylPro-NH-*i*-Pr)pyridinium-3-yl)porphyrinato]zinc(II) (1f).** Prepared from 5,10,15,20-tetra(3-pyridyl)porphyrin and chloroacetyl-Pro-NH-*i*-Pr.

$^1\text{H}$  NMR ( $\text{D}_2\text{O}$ )  $\delta$  9.66 (m, 4H), 9.40 (m, 4H), 9.20 (m, 4H), 9.06-8.75 (m, 8H), 8.52 (m, 4H), 5.94 (bs, 8H), 4.38 (m, 4H), 3.85-3.55 (m, 12 H), 2.24 (bm, 4H), 2.09-1.80 (bm, 12H), 0.98 (m, 24H). ( $\text{CH}_3\text{OH}$ ) 432, 519, 561, 597, 640. MALDI-TOF MS:  $m/z$  1574.6  $[\text{M}-\text{Cl}]^+$  (calculated for  $[\text{C}_{80}\text{H}_{92}\text{N}_{16}\text{O}_8\text{Cl}_3\text{Zn}]^+$  1573.6).

**[5,10,15,20-tetrakis(*N*-(AcetylProAib-NH-*i*-Pr)pyridinium-3-yl)porphyrinato]zinc(II) (1g).** Prepared from 5,10,15,20-tetra(3-pyridyl)porphyrin and chloroacetyl-ProAib-NH-*i*-Pr.

$^1\text{H}$  NMR ( $\text{D}_2\text{O}$ )  $\delta$  9.68 (m, 4H), 9.44 (m, 4H), 9.23 (m, 4H), 8.99 (m, 8H), 8.55 (m, 4H), 5.97 (s, 8H), 4.37 (bm, 4H), 3.71 (bm, 8H), 3.31 (bm, 4H), 2.24 (m, 4H), 2.01 (m, 8H),

1.86 (m, 4H), 1.25 (m, 24H), 0.68-0.44 (m, 12H), 0.38-0.04 (m, 12H). (CH<sub>3</sub>OH) 433, 520, 558, 597, 638. MALDI-TOF MS: m/z 1913.9 [M-Cl]<sup>+</sup> (calculated for [C<sub>9</sub>H<sub>120</sub>N<sub>20</sub>O<sub>12</sub>Cl<sub>3</sub>Zn]<sup>+</sup> 1913.8).

## 7.5 References and notes

1. Waldvogel, S. R.; Fröhlich, R.; Schalley, C. A. *Angew. Chem., Int. Ed.* **2000**, *39*, 2472-2475.
2. Goswami, S.; Mahapatra, A. K.; Mukherjee, R. *J. Chem. Soc., Perkin Trans. 1* **2001**, 2717-2726.
3. Ballester, P.; Barceló, M. A.; Costa, A.; Deyà, P. M.; Morey, J.; Orell, M.; Hunter, C. A. *Tetrahedron Lett.* **2000**, *41*, 3849-3853.
4. Charlton, A. J.; Davis, A. L.; Jones, D. P.; Lewis, J. R.; Davies, A. P.; Haslam, E.; Williamson, M. P. *J. Chem. Soc., Perkin Trans. 2* **2000**, 317-322.
5. Martin, R.; Lilley, T. H.; Falshaw, C. P.; Halsam, E.; Begley, M. J.; Magnolato, D. *Phytochemistry* **1986**, *26*, 273-279.
6. Martin, R.; Lilley, T. H.; Bailey, N. A.; Falshaw, C. P.; Haslam, E.; Magnolato, D.; Begley, M. J. *J. Chem. Soc., Chem. Commun.* **1986**, 105-106.
7. Gaffney, S. H.; Martin, R.; Lilley, T. H.; Haslam, E.; Magnolato, D. *J. Chem. Soc., Chem. Commun.* **1986**, 107-109.
8. Zdunek, M.; Piosik, J.; Kapuscinski, J. *Biophys. Chem.* **2000**, *84*, 77-85.
9. Frauendorf, C.; Jäschke, A. *Bioorgan. Med. Chem.* **2001**, *9*, 2521-2524.
10. Jenison, R. D.; Gill, S. C.; Pardi, A.; Polisky, B. *Science* **1994**, *263*, 1425-1428. The values are reported as dissociation constants  $K_d = 1/K_a$ .
11. Villamena, F. A.; De La Cruz, A. A. *J. Appl. Polym. Sci.* **2001**, *82*, 195-205.

12. Kobayashi, T.; Murawaki, Y.; Reddy, P. S.; Abe, M.; Fujii, N. *Anal. Chim. Acta* **2001**, *435*, 141-149.
13. Carter, S. R.; Rimmer, S. *Adv. Mater.* **2002**, *14*, 667-670.
14. For recent reviews about porphyrin receptors see: (a) Weiss, J. *J. Incl. Phenom.* **2001**, *40*, 1-22. (b) Robertson, A.; Shinkai, S. *Coord. Chem. Rev.* **2000**, *205*, 157-199. (c) Ogoshi, H.; Mizutani, T. *Curr. Opin. Chem. Biol.* **1999**, *3*, 736-739. (d) Ogoshi, H.; Mizutani, T. *Acc. Chem. Res.* **1998**, *31*, 81-89.
15. For other water soluble receptors based on cationic (*N*-alkyl)pyridyl porphyrins see: (a) Sirish, M.; Chertkov, V. A.; Schneider, H.-J. *Chem. Eur. J.* **2002**, *5*, 1181-1188. (b) Schneider, H.-J.; Tianjun, L.; Sirish, M.; Malinovski, V. *Tetrahedron* **2002**, *58*, 779-786. (c) Sirish, M.; Schneider, H.-J. *J. Am. Chem. Soc.* **2000**, *122*, 5881-5882.
16. Sirish M.; Schneider, H.-J. *Chem. Commun.* **2000**, 23-24.
17. A statistical mixture of atropoisomers is expected to be present in solution. In this case the  $\alpha\alpha\alpha\beta$  isomer, the most abundant one, together with the  $\alpha\alpha\alpha\alpha$  isomer should account for 62.5% of the mixture. NMR measurements did not provide any indications about isomer distribution. Changes induced by complexation seem to occur but are also difficult to be quantified. See Mizutani, T.; Horiguchi, T.; Koyama, H.; Uratani, I.; Ogoshi, H. *Bull. Chem. Soc. Jpn.* **1998**, *71*, 413-418.
18. A basic buffer was chosen to allow comparison of the data obtained for caffeine with the one obtained for more basic guests (Tables 4 and 5) without having to consider protonation equilibria (see Rekharsky, M. V.; Nakamura, A.; Hembury, G. A.; Inoue, Y. *Bull. Chem. Soc. Jpn.* **2001**, *74*, 449-457). Furthermore, as shown for receptor Zn-**1f** in Table 1, there is not any appreciable effect on caffeine binding if the acidic oxalate buffer is used (with the exception of Zn-**1c** due to the ionization equilibrium involving the Tyr OH group).
19. Mizutani, T.; Horiguchi, T.; Koyama, H.; Uratani, I.; Ogoshi, H. *Bull. Chem. Soc. Jpn.* **1998**, *71*, 413-418.

20. Fiammengo, R.; Timmerman, P.; Huskens, J.; Versluis, K.; Heck, A. J. R.; Reinhoudt, D. N. *Tetrahedron* **2002**, *58*, 757-764.
21. Caffeine is known to dimerize or self-aggregate in aqueous solutions, but the association constants are very small ( $5\text{-}8\text{ M}^{-1}$ ) and do not affect the binding process in our experiments. See Horman, I.; Dreux, B. *Helv. Chim. Acta* **1984**, *67*, 754-764 and Charlton, A. J.; Davis, A. L.; Jones, D. P.; Lewis, J. R.; Davies, A. P.; Haslam, E.; Williamson, M. P. *J. Chem. Soc., Perkin Trans. 2* **2000**, 317-322)
22. Porphyrins concentration in the UV experiments is between  $2.4$  and  $4.8 \times 10^{-6}$  M and preliminary dilution experiments showed no aggregation in the range  $1.0\text{-}9.0 \times 10^{-6}$  M. Study of the binding equilibria by ITC required much higher porphyrins concentration ( $1.2\text{-}1.8 \times 10^{-3}$  M). Aggregation was also not observed in these conditions as proven directly by a microcalorimetric experiment on porphyrin Zn-1e (see experimental part).
23. Imai, H.; Misawa, K.; Munakata, H.; Uemori, Y. *Chem. Lett.* **2001**, 688-689.
24. Weiss, J. *J. Incl. Phenom.* **2001**, *40*, 1-22.
25. Imai, H.; Munakata, H.; Takahashi, A.; Nakagawa, S.; Ihara, Y.; Uemori, Y. *J. Chem. Soc., Perkin Trans. 2* **1999**, 2565-2568.
26. Stacking of a second caffeine molecule on the distal porphyrin face (the one not occupied by coordination of the first molecule) has not been considered since the  $K_a$ s obtained from measurements in different concentration ranges (UV and ITC) were in good agreement.
27. For an example in which the occurrence of 2:1 complexes is considered see ref. 36.
28. Liu, T.; Schneider, H.-J. *Angew. Chem., Int. Ed.* **2002**, *41*, 1368-1370.
29. Jasuja, R.; Jameson, D. M.; Nishijo, C. K.; Larsen, R. W. *J. Chem. Phys. B* **1997**, *101*, 1444-1450.

30. Schneider, H.-J.; Wang, M. *J. Org. Chem.* **1994**, *59*, 7464-7462.
31. Connors, K. A. *Binding Constants*; John Wiley & Sons., Inc.: Canada, 1987; pp 141-187.
32. D' Souza, F.; Deviprasad, G. R.; Zandler, M. E. *J. Chem. Soc., Dalton Trans.* **1997**, 3699-3703.
33. Mizutani, T.; Wada, K.; Kitagawa, S. *J. Am. Chem. Soc.* **1999**, *121*, 11425-11431.
34. The signals have a complex multiplicity pattern, which agrees with the presence of different conformational isomers interconverting slowly on the NMR chemical shift time scale at room temperature.
35. Mizutani, T.; Wada, K.; Kitagawa, S. *J. Org. Chem.* **2000**, *65*, 6097-6106.
36. This is not surprising since ITC measurements performed at concentrations 500-1000 times higher than UV measurements have a higher contribution coming from the existence of 2:1 species.
37. Aoki, K.; Yamazaki, H. *J. Chem. Soc., Chem. Commun.* **1980**, 186-188.
38. The two caffeine molecules are found asymmetrically reclined between the two dirhodium-diacetate planes in order to accommodate base stacking. See Aoki, K.; Yamazaki, H. *J. Chem. Soc., Chem. Commun.* **1980**, 186-188.
39. Kuroda, Y.; Hatakeyama, H.; Inakoshi, N.; Ogoshi, H. *Tetrahedron Lett.* **1993**, *34*, 8285-8288.
40. Ogoshi, H.; Hatakeyama, H.; Kotani, J.; Kawashima, A.; Kuroda, Y. *J. Am. Chem. Soc.* **1991**, *113*, 8181-8183.
41. Ogoshi, H.; Hatakeyama, H.; Yamamura, K.; Kuroda, Y. *Chem. Lett.* **1990**, 51-54.
42. Pasternack, R. F.; Gibbs, E. J.; Gaudemer, A.; Antebi, A.; Bassner, S.; De Poy, L.; Turner, D. H.; Williams, A.; Laplace, F.; Lansard, M. H.; Merienne, C.; Perrée-

- Fauvet, M. *J. Am. Chem. Soc.* **1985**, *107*, 8179-8186.
43. Stacking interactions between the Tyr phenol moiety and tetracationic 5,10,15,20-*tetrakis*-(*N*-methylpyridinium-4-yl)porphyrinato zinc(II) chloride salt give stabilization to the porphyrin - Tyr complex in aqueous solution. See: (a) Mikros, E.; Gaudamer, A.; Pasternack, R. *Inorg. Chim. Acta* **1988**, *153*, 199-200. (b) Verchère-Bèaur, C.; Mikros, E.; Perrée-Fauvet, M.; Gaudamer, A. *J. Inorg. Biochem.* **1990**, *40*, 127-139.
44. The difference observed between Zn-**1c** and metal-free **1c** is = 0.1 ppm.
45. The pK<sub>a</sub> value for the Tyr side chain is around 10.07 as reported in *Handbook of Chemistry and Physics*, 58<sup>th</sup> Ed.; CRC Press Inc.: Cleveland, Ohio, 1977; p. C-767. No mention is made about the ionic strength under which this value was measured.
46. Similar intramolecular coordination has been shown for pyridyl appended Zn-tetraphenyl porphyrins in non-polar solvents, see: Walker, F. A.; Benson, M. *J. Am. Chem. Soc.* **1980**, *102*, 5530-5538.
47. From electronic considerations imidazole and 1-methylimidazole should be better ligands than caffeine due to increased basicity.
48. Cramer, R. E.; Ho, D. M.; van Doorne, W.; Ibers, J. A.; Norton, T.; Kashiwagi, M. *Inorg. Chem.* **1981**, *20*, 2457-2461.
49. Lombardi, A.; Natri, F.; Pavone, V. *Chem. Rev.* **2001**, *101*, 3165-3189.





## Summary

This Ph.D. thesis describes the preparation, characterization, and study of supramolecular systems for the mimicry of heme-protein binding sites.

A general introduction about the recent development of supramolecular chemistry is outlined in Chapter 1. Special attention is given to the preparation of *functional systems* and in particular to self-assembled structures with biomimetic functions due to their relevance in the elucidation of the properties of natural biological systems.

In Chapter 2 the recent literature concerning the study of self-assembled model systems (obtained from synthetic subunits) with biomimetic functions is reviewed. Only examples in which the self-assembly process takes place in solution are considered and the contributions are grouped by biomimetic function. In sections 2.2 - 2.6 examples of electron and energy transfer processes, enzyme mimics, allosteric systems, and artificial molecular machines are described. The second part of the chapter (section 2.7) is more directly connected with the central part of this thesis viz. the preparation of self-assembled synthetic analogues of O<sub>2</sub> binding heme-proteins. This section focuses on the most important biochemical aspects of O<sub>2</sub> binding heme-proteins and gives an overview of the synthetic models obtained via “classical” covalent synthesis.

In Chapter 3 the preparation of noncovalent calix[4]arene capped porphyrins in polar solvents via ionic interactions is described. The preparation of a superstructured porphyrin architecture via noncovalent synthesis is the first necessary step towards the mimicry of O<sub>2</sub> binding heme proteins. Tetracationic zinc(II) *meso*-tetrakis(*N*-alkylpyridinium-3-yl) porphyrins and anionic 25,26,27,28-tetrakis(2-ethoxyethoxy)-calix[4]arene tetrasulfonate are the building blocks synthesized for this purpose. These building blocks self-assemble due to ionic interactions in solvents such as methanol, DMSO, 1,3-dimethyl-3,4,5,6-tetrahydropyrimidin-2(1*H*)-one, and mixtures containing as much as  $x_{water} = 45\%$  (molar fraction of water). The systems (structural mimics of heme-

proteins) have been studied with UV-vis,  $^1\text{H}$  NMR, and mass spectrometry (ESI-TOF). The thermodynamic parameters associated with the assembly process have been determined via variable temperature experiments and, when possible, via isothermal titration microcalorimetry (ITC). The assemblies described in this chapter are remarkably stable under a variety of conditions (formation constant  $\sim 10^6$ - $10^7$   $\text{M}^{-1}$  in neat solvents,  $\sim 10^5$   $\text{M}^{-1}$  in the presence of salts).

Self-assembly in polar solvents is just the first step towards the development of heme-protein model systems via noncovalent synthesis. Therefore, the preparation of water-soluble systems is definitely a major advance considering the biological relevance of water. Its achievement requires not only water-soluble building blocks but also that the assemblies remain water-soluble once they are formed. Thus Chapter 4 deals with water-soluble structural mimics of heme-proteins. In the design of the porphyrin-based building block the short peptides attached to the macrocycle are responsible for the relatively large water solubility of the assemblies (concentrations up to 2-5 mM). Formation of ternary complexes upon addition of nitrogenous base ligands has been observed. These ligands coordinate to the metal center of the assembly, and the structure of the complexes is directed by the sterical requirements of the base used. Small bases such as 4-methyl pyridine are complexed preferentially inside the hydrophobic cavity of the assemblies while larger molecules such as caffeine are bound outside the cavity at the solvent exposed porphyrin face.

The “inert” zinc porphyrins have been replaced by cobalt porphyrins (able to bind  $\text{O}_2$ ) to afford the functional models of heme-proteins described in Chapter 5. This chapter deals with the self-assembly of tetracationic cobalt(II) porphyrins and tetraanionic calix[4]arenes to prepare water soluble  $\text{O}_2$  binding heme-protein models. The  $\text{O}_2$  binding ability has been tested using UV-vis and electron paramagnetic resonance (EPR) spectroscopy. Even though the complex nature of these systems (due to the presence of multiple equilibria) prevents a full description of the situation in solution, they have been tested in membranes for  $\text{O}_2/\text{N}_2$  separation. A modest but significant facilitated  $\text{O}_2$  transport (facilitation factor = 1.15, selectivity coefficient = 2.3-2.4) is observed for membrane loaded with the self-assembled systems with respect to the membrane loaded with only  $\text{H}_2\text{O}$  (facilitation factor = 1.0, selectivity = 2.0).

Other organic ligands besides porphyrins can be used for the preparation of O<sub>2</sub> binding metal complexes, among them Salen (*bis*(sallylidene)ethylenediamine) ligands. The supramolecular design of novel cobalt(II) Salen complexes able to stabilize the Co-coordinated O<sub>2</sub> via hydrogen-bonding is the topic of Chapter 6. This design mimics the hydrogen-bonding interaction operated by the distal His residue in hemoglobin and myoglobin or by Tyr in O<sub>2</sub> avid *Ascaris* hemoglobin. The affinity for O<sub>2</sub> is increased ten times in comparison to systems lacking such interaction. These Co(II)Salen complexes have also been tested in relation to their catalytic activity in the oxidation of cyclohexene with the aim of studying the relation existing between stabilization of the Co-O<sub>2</sub> moiety and reactivity. The more thermodynamically stable Co-O<sub>2</sub> complexes yield lower reactivity.

During the studies on water-soluble porphyrin systems (Chapter 4), the much higher coordination strength of caffeine compared to other nitrogenous bases was noticed and led to the study of these cationic porphyrins (and some novel derivatives) as potential sensors for caffeine, the results of which are reported in Chapter 7. The remarkable affinity observed for caffeine in water ( $K_a \sim 6000 \text{ M}^{-1}$ ) is due to a combination of metal coordination and stacking interactions. The results reported in this chapter show for the first time recognition of caffeine in aqueous solution and provide a detailed view of the binding process from several experimental techniques. The use of amino acid or peptide chains (of appropriate length) allows the introduction of additional interactions, which can be used to influence the recognition site. The intrinsic UV-vis activity of the porphyrin core and the relevance of working directly in aqueous solution are interesting features in view of sensing applications.



## Samenvatting

Dit proefschrift beschrijft de synthese, karakterisatie en bestudering van supramoleculaire systemen voor het nabootsen van de heem-proteïnen bindingsplaatsen.

Een algemene inleiding over de recente ontwikkelingen in de supramoleculaire chemie is uiteengezet in hoofdstuk 1. Speciale aandacht is besteed aan de synthese van *functionele systemen*, met name aan zelf-assemblerende structuren met biomimetische functionaliteiten, die relevant zijn in de opheldering van de eigenschappen van natuurlijke biologische systemen.

In hoofdstuk 2 is een overzicht gegeven van de recente literatuur betreffende de bestudering van zelf-assemblerende model systemen (verkregen uit synthetische sub-eenheden) met biomimetische functionaliteiten. Alleen voorbeelden van systemen die zelf-assembleren in oplossing zijn in beschouwing genomen en gerangschikt naar biomimetische functie. In de paragrafen 2.2 – 2.6 zijn voorbeelden beschreven van elektron-energie overdrachtsprocessen, enzym nabootsingen, allosterische systemen en kunstmatige moleculaire machines. Het tweede gedeelte van dit hoofdstuk (paragraaf 2.7) is meer direct verbonden met het centrale gedeelte van dit proefschrift, te weten de synthese van zelf-assemblerende synthetische analogen van O<sub>2</sub> bindende heem-proteïnen. Deze paragraaf richt zich op de meest belangrijke biochemische aspecten van O<sub>2</sub> bindende heem-proteïnen en geeft een overzicht van synthetische modellen verkregen via “klassieke” covalente synthese.

In hoofdstuk 3 is de synthese beschreven van niet-covalente calix[4]areen-porfyrine complexen via ionische interacties in polaire oplosmiddelen. De synthese van een suprastructurele porfyrine architectuur via niet-covalente synthese is de eerste noodzakelijke stap richting de nabootsing van O<sub>2</sub> bindende heem-proteïnen. Tetracationische zink(II) *meso*-tertrakis(*N*-alkylpyridinium-3-yl) porfyrines en anionische 25,26,27,28-tetrakis(2-ethoxyethoxy)-calix[4]areen tetrasulfonaat zijn de

gesynthetiseerde bouwstenen voor dit doel. Deze bouwstenen zelf-assembleren als gevolg van ionische interacties in oplosmiddelen zoals methanol, DMSO, 1,3-dimethyl-3,4,5,6-tetrahydropyrimidin-2(1*H*)-on en mengsels die zoveel als  $x_{\text{water}} = 45\%$  (molfractie water) bevatten. De systemen (structurele nabootsingen van heem-proteïnen) zijn bestudeerd met UV-vis,  $^1\text{H}$  NMR en massa spectroscopie (ESI-TOF). De thermodynamische parameters van het zelf-assemblerende proces zijn bepaald met variabele temperatuur experimenten en waar mogelijk met behulp van isothermische titratie microcalorimetrie (ITC). De assemblages beschreven in dit hoofdstuk zijn opmerkelijk stabiel onder een verscheidenheid aan condities (vormingsconstante  $\sim 10^6$ - $10^7 \text{ M}^{-1}$  in pure oplosmiddelen,  $\sim 10^5 \text{ M}^{-1}$  in aanwezigheid van zouten).

Zelf-assemblage in polaire oplossingen is slechts de eerste stap naar de ontwikkeling van heem-proteïnen model systemen via niet-covalente synthese. De synthese van water-oplosbare systemen is daarom absoluut de belangrijkste vooruitgang gezien de biologische relevantie van water. Succes vereist niet alleen water-oplosbare bouwstenen, maar ook dat de assemblages na vorming oplosbaar blijven in water. Hoofdstuk 4 behandelt de water-oplosbare structurele nabootsingen van heem-proteïnen. In het ontwerp van de porfyriene bouwstenen zijn de korte peptiden verantwoordelijk voor de relatief grote oplosbaarheid van de assemblages (concentraties tot 2-5 mM). Vorming van driedelige complexen is waargenomen bij toevoeging van stikstofhoudende basische liganden. Deze liganden coördineren aan het metaal centrum van de assemblage en de structuur van de complexen wordt bepaald door de sterische eigenschappen van de gebruikte base. Kleine basen zoals 4-methyl pyridine worden bij voorkeur gecomplexeerd binnenin de hydrofobe holte van de assemblages terwijl grotere basen zoals cafeïne aan de buitenkant van de holte aan het oplosmiddel blootgestelde porfyriene worden gebonden.

De “inerte” zink porfyrienes zijn vervangen door kobalt porfyrienes (in staat om  $\text{O}_2$  te binden) om de functionele modellen van heem-proteïnen te verschaffen is beschreven in hoofdstuk 5. Dit hoofdstuk behandelt de zelf-assemblage van tetracationische kobalt(II) porfyrienes met tetraanionische calix[4]arenen voor de synthese van water oplosbare  $\text{O}_2$  bindende heem-proteïnen modellen. De  $\text{O}_2$  binding bekwaamheid is getest met gebruikmaking van UV-vis en elektron paramagnetische resonantie spectroscopie (EPR).

Hoewel de complexe oorsprong van deze systemen in oplossing (als gevolg van meerdere evenwichten) een volledige beschrijving van de situatie verhindert, zijn zij getest in membranen voor O<sub>2</sub>/N<sub>2</sub> scheiding. Een bescheiden maar significante gefaciliteerde O<sub>2</sub> transport (faciliteitsfactor = 1.15, selectiviteitscoëfficiënt = 2.3-2.4) is waargenomen voor een membraan “geladen” met de zelf-assemblerende systemen in vergelijking met de membranen met enkel H<sub>2</sub>O (faciliteitsfactor = 1.0, selectiviteit = 2.0).

Andere organische liganden naast porfyrienes kunnen gebruikt worden voor de synthese van O<sub>2</sub> bindende metaal complexen, waaronder Salen (*bis*(salylydene)ethylenediamine) liganden. Hoofdstuk 6 beschrijft het supramoleculaire ontwerp van nieuwe kobalt(II) Salen complexen die in staat zijn de Co-O<sub>2</sub> via waterstof-binding te stabiliseren. Dit ontwerp bootst de waterstof-bindende interactie na van de distal His residu in hemoglobine and myoglobine of van Tyr in O<sub>2</sub> avid Ascaris hemoglobine. De affiniteit voor O<sub>2</sub> is 10 keer groter in vergelijking met systemen die deze interactie missen. Deze Co(II) Salen complexen zijn ook getest met betrekking tot hun katalytische activiteit in de oxidatie van cyclohexeen met als doel de relatie tussen stabilisatie van de Co-O<sub>2</sub> eenheid en reactiviteit te bestuderen. De meer thermodynamisch stabiele Co-O<sub>2</sub> complexen vertonen een lagere reactiviteit.

Tijdens de studies aan water-oplosbare porfyriene systemen (hoofdstuk 4) is een veel hogere coördinatie sterkte van cafeïne in vergelijking met andere stikstofhoudende basen waargenomen. Deze cationische porfyrienes (en enkele nieuwe derivaten) zijn daarom bestudeerd als mogelijke sensoren voor cafeïne en de resultaten zijn beschreven in hoofdstuk 7. De waargenomen merkwaardige affiniteit voor cafeïne in water ( $K_a \sim 6000 M^{-1}$ ) is te danken aan een combinatie van metaal coördinatie en stapelings interacties. De resultaten beschreven in dit hoofdstuk laten voor de eerste keer de herkenning van cafeïne in waterige oplossing zien en verschaffen een gedetailleerde kijk van het bindingsproces met een aantal experimentele technieken. Het gebruik van aminozuren of peptide ketens (van geschikte lengte) maakt de introductie van bijkomende interacties mogelijk, die gebruikt kunnen worden om de herkenningsplaats te beïnvloeden. De intrinsieke UV-vis activiteit van de porfyriene kern en de relevantie van het direct werken in waterige oplossingen zijn interessante eigenschappen met het oog op sensor toepassingen.





## Acknowledgements

The work described in this thesis would not have been possible without the contributions of many friends and colleagues from the University of Twente and from other research groups in The Netherlands.

First of all I would like to thank my promotor David Reinhoudt for giving me the possibility of working in a very stimulating research group with all the freedom I could ever desire. David, you gave me the opportunity of presenting my work in conferences all around the world and you always stimulate me in writing publications. From you I have learned that being able to communicate the results is as important as carrying out a careful scientific investigation. Thank you for all of this.

I would like to thank my daily supervisors Mercedes Crego-Calama and Peter Timmerman.

Dear Merce you have started to supervise me after more than two years the project was started. Nevertheless, you manage to catch up very soon and to give me very precious suggestions during the long talks we had in the lab. You had also the “honor” (or the pain) to go through the correction of the largest part of my writings, including this thesis. I really appreciate the way you did it. You always stimulated me in being clear and simple in my explanations and, as I told you already many times, I always liked the final result. Muchisimas gracias also for your friendship.

Dear Peter I would like to thank you very much for your supervision during more than half of my Ph.D. project. Thank you for being always available for work (and no work) discussions. I appreciated your enthusiasm.

Special thanks to Jurriaan Huskens and Prof. Feike de Jong for the help in developing the mathematical models that describe the chemical equilibria in the systems object of my studies.

The work described in Chapter 5 has been performed partially at the University of Leiden and I would like to thank Prof. Jan Reedijk and Mr. Ge van Albada for all what they have taught me about EPR spectroscopy and for helpful discussions. The membrane-related part of this work has been carried out in collaboration with the Membrane Technology group (University of Twente) of Prof. Matthias Wessling. I would like to thank him for the many clarifying discussions we had about the membrane permeation experiments and I want to extend my acknowledgement to Alberto Figoli with who I shared the work in the lab. Alberto grazie anche per la tua amicizia al di fuori delle lunghe ore di lavoro.

Prof. Albert Heck and Kees Versluis from the University of Utrecht are gratefully acknowledged for the mass spectrometry measurements reported in Chapter 3.

Special thanks goes to the students that have worked on this project trying some of my ideas but also putting their valuable original contribution: Christiaan Bruinink, Dennis Rots, Kamil Wojciechowski, Davy Martin. You all did an excellent work and it was a real pleasure to collaborate with you!

I would like to thank Richard Egberink for the work he has carried out as part of the project and especially for always being present and helpful with computer-stuff, safety issues, and synthetic discussions.

Joop Toevank, Irene Wolbers, Marc Brower, and Marcel de Bruine thank you for all your help throughout the years. You really did (and Marcel still do) a great job to fulfill the request of such a large group of chemists. Thanks also to Hanny Visser, Tieme Stevens, Roel Fokkens and Annemarie Montanaro-Christenhusz for their indispensable analysis work.

Carla Weber-van der Ploeg, I have to thank you so much for all the help you gave me with the administrative duties, especially in this last period before the “Promotie”.

Becky, Mrinal being Americans you had to play a very important role: proofreaders of my concept thesis! You did it in an excellent way and your suggestions helped me to improve the overall quality of this thesis. Thank you.

One of the nicest things of this four years in Enschede has been the possibility of working in an incredibly stimulating international atmosphere. With many of the people I also had the occasion of enjoy the free time in Enschede. I would like to thank you all and I already apologize if I forget somebody. Niels, Arianna, Kjeld, Jasper, Leonard, Maria, Francesca Cardullo, Jessica, Xue-Mei, Kazu, Tsutomu, Piotr, Anja, Lourdes, Olga, Miguel, Juanjo, Mattijs, Paolo, Monica, Emiel, Stefano, Petra, Barbara, Romina, Mario, Susanna, Lorenza, Micol, and Luca, I consider myself lucky to have friends like you.

Francesca grazie per essermi stata amica in questi anni, per essere stata spesso a sentire le mie elucubrazioni e le mie boiate, per quando ero nervoso con il mondo intero e per quando le cose andavano bene.

Tommaso e Marta, thanks for being my paranimfen but especially for all the time we spent together. Tommaso sei un vero amico, e da te ho cercato di imparare a essere puntuale, disponibile e...sportivo.

Da ultimi vorrei ringraziare voi mamma, papà e Lucio per essermi sempre stati vicino durante questi anni e avere sostenuto le mie scelte anche se mi hanno portato lontano da voi.

*Grazie di cuore a tutti,*

*Roberto*



## The author

Roberto Fiammengo was born in Torino (Italy) on September 19, 1971. In 1990 he obtained his diploma with specialization in industrial chemistry at the Technical Highschool "E. Fermi" in Mantova (Italy). In June 1997 he graduated full marks in Chemistry at the University of Padova (Italy). During his undergraduate training period at the Department of Organic Chemistry he worked on asymmetric oxidations mediated by titanium complexes and on stereoselective Diels-Alder reactions under the supervision of Prof. F. di Furia and Prof. G. Licini. His M.Sc. thesis is entitled "*(-)-trans*-benzo[*e*]-1,4-dithiine-*S,S'*-dioxide: a new C<sub>2</sub> symmetry dienophile". From July 1997 to October 1997 he continued the work on stereoselective oxidations and from November 1997 to August 1998 he worked on the derivatization of tetrasubstituted  $\alpha$ -amino acids, under the supervision of Prof. G. Modena (Dep. of Organic Chemistry, University of Padova) in collaboration with DSM (Geleen, The Netherlands). In September 1998 he joined the group of Supramolecular Chemistry and Technology (SMCT) at the University of Twente as a Ph.D. candidate under the supervision of Prof. dr. ir. D. N. Reinhoudt. The research performed during the period 1998-2002 is described in this thesis. Currently he is working as a post-doc in the group of Prof. P. Scrimin (Dep. of Organic Chemistry, University of Padova) on synthetic models of metallonucleases.